Republic of Iraq

Ministry of Higher Education and Scientific Research

University of Anbar

College of Engineering

Civil Engineering Department

Studying Nano Clay Production and Its Effect on Some Characteristics of SCC

A Thesis

Submitted to the Civil Engineering Department of the

College of Engineering of Anbar University

In Partial Fulfillment of the Requirements

For the Degree of Master of Science

In Civil Engineering

By

Nibras Younis Rasheed Al-Ani

(B.Sc., Civil Engineering, 2001)

Supervised by

Prof. Dr. Ibrahim A. AL-Jumaily

Asst. Prof. Dr. Nahla N. Hilal

April 2021, A.D.   **Sha'ban 1442, A.H.**
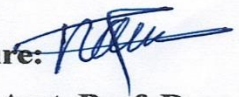
Supervisor's Certification

We certify that this thesis entitled " **Studying Nano Clay Production and Its Effect on Some Characteristics of SCC** " was prepared by (**Nibras Younis Rasheed Al-Ani**) under our supervision at the Department Civil Engineering, University of Anbar, in partial fulfillment of the requirements for the degree of Master of Science in Civil Engineering.

Signature: 2. Aljumaily

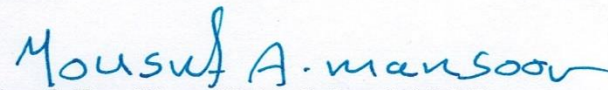Name: Prof. Dr.

Ibrahim A. Al-Jumaily

Date: 4/ 6 / 2021

Signature:

Name: Asst. Prof. Dr.

Nahla N. Hilal

Date: 4/ 6 / 2021

In view of the available recommendation, I forward this thesis for debate by the examining committee.

Signature: Mousuf A. mansoor

Name: Asst. Prof. Dr. Yousif Abdulwahid Mansoor

(Head of Civil Engineering Department)

Date: 8 / 6 / 2021

Linguistic Certification

This is to certify that I have read this thesis entitled " **Studying Nano Clay Production and Its Effect on Some Characteristics of SCC** " which was prepared by **(Nibras Younis Rasheed Al-Ani)** and corrected most grammatical mistakes, I found therefore this thesis is qualified for debate.

Signature:

Name: Dr. Duraid Muayed Abd

Date: 7/6/ 2021

Signature:

Name: Asst. Prof. Dr. Yousif Abdulwahid Mansoor

(Head of Civil Engineering Department)

Date: 8 /6 /2021

Examining Committee Certification

We certify that we have read this thesis entitled " **Studying Nano Clay Production and Its Effect on Some Characteristics of SCC** " examining committee we examined the student **(Nibras Younis Rasheed Al-Ani)** in its content and that, in our opinion, it meets the standard of a thesis for the degree of Master of Science in Civil Engineering (Material Engineering).

Signature:

Name: Prof. Dr. Abbas Salim
Abbas Al-Ameeri
Date: 7 / 6 / 2021
(Chairman)

Signature:

Name: Asst. Prof. Dr. Ameer
Abdulrahman Hilal
Date: 7/ 6 / 2021
(Member)

Signature:

Name: Asst. Prof. Dr. Mahmoud
Khashaa Al-Ani
Date: 07/ 06/ 2021
(Member)

Signature:

Name: Prof. Dr. Ibrahim
A. Al-Jumaily
Date: 4/ 6 / 2021
(Member and supervisor)

Signature:

Name: Asst. Prof. Dr. Nahla N. Hilal
Date: 4/ 6 / 2021
(Member and supervisor)

(Approval of the College of Engineering)

Signature: Mousul A. Mansoor

Name: Asst. Prof. Dr. Yousif
Abdulwahid Mansoor
(Head of civil Engineering Department)
Date: 8 / 6/ 2021

Signature:

Name: Asst. Prof. Dr. Ameer
Abdulrahman Hilal
(Dean of The College of Engineering)
Date: 8/ 6 / 2021

بسم الله الرحمن الرحيم

اقْرَأْ بِاسْمِ رَبِّكَ الَّذِي خَلَقَ * خَلَقَ الْإِنْسَانَ مِنْ عَلَقٍ * اقْرَأْ وَرَبُّكَ

الْأَكْرَمُ * الَّذِي عَلَّمَ بِالْقَلَمِ * عَلَّمَ الْإِنْسَانَ مَا لَمْ يَعْلَمْ

صدق الله العظيم

سورة العلق
الاية (١ – ٥)

*To my **father's pure soul** that he left my life a few days ago.*

ACKNOWLEDGMENTS

Abstract

The work aimed to prepare Nano clay (NC) from local Iraqi natural Kaolin clay, which was calcined at 700°C for 2 hours, then grinded for 40 hours using ultrafine grinding (Ball milling). Several techniques were used to characterize NC comprising particle size analyzers (PSA), specific surface areas (SSA), X-ray diffraction (XRD), X-ray fluorescence (XRF), scanning electron microscopy (SEM), and Energy-Dispersive X-Ray Spectroscopy (EDX).

The study was conducted by using three different ratios of NC (2%, 4%, and 6%) as partial cement replacements along with the use of quicklime (QLP) with (50,75 and 100) kg, which was prepared in the laboratory by burning Limestone at a temperature of 700 °C for two hours and combined QLP proportions with 4% NC. This depend on the results of fresh Nano clay tests for the self-compacting concrete mixes.

Studying the effect of NC on the characteristics of SCC was performed based on three parameters. Firstly, the workability properties included the slump flow, V-funnel flow time, L-box, sieve segregation resistance, and fresh density. Secondly, the hardened properties were investigated at ages 7, 28, 56, 90 and 120 days, which include mechanical properties (compressive, splitting tensile and flexural strengths as well as modulus of elasticity), and the physical properties (Ultra Pulse Velocity (UPV), the harden density, the volume of permeable pores (Voids) and water absorption). Finally, the durability characteristics were examined, which include the effect of high-temperature treatment at (200, 400, 600, 800) °C at ages 56, 90 and 120 days, as well as resistance to sulfate attack through successive cycles of drying and wetting of 5%, 10% and 20% $MgSO_4$ for a period of 30, 60 and 90 days and comparing the results with those of specimens stored at the same ages in ordinary curing water at ages 56, 90, and 120 days.

The results revealed that the fresh properties decreased with increasing the content of NC. The hardened and durability properties gradually increased with increasing the content of NC and QLP in SCC mixtures. Furthermore, the addition of NC alone has

more significant effect on SCC specimens produced than reference SCC (SCC0) and QLP addition.

The best value was obtained at SCC 6%NC. The results showed that the compressive strength of the SCC with 6% NC were higher than SCC0 by 28.5%, 23.6%, 19.5%, 19% and 18.4% at 7, 28, 56, 90 and 120 days curing ages, respectively. The splitting tensile strength values of SCC 6%NC was higher than reference SCC by about 16.8%, 17.1%, 16% and 12.4% at 28, 56, 90 and 120 days curing ages, respectively. The flexural strength of 6%NC was higher than SCC0 by about 22.6, 25.4, 27.4, 26.5% at 28, 56, 90 and 120 days, respectively. Furthermore, the modulus of elasticity of 6%NC was higher than SCC0 by about 26.1at 90 days curing ages.

The SCC6% NC mixture achieved the gain maximum in compressive strength from the control mixture (SCC0) under the influence of 200 °C by 6.23%, 6.49%, 6.34%, while it achieved the loss minimum in compressive strength from the control mixture (SCC0) under the influence of 800 °C by 64.39%, 61.02%, and 55.8% at ages 56, 90, and 120 days, respectively.

The SCC6% NC mix achieved the minimum loss in compressive strengths than its control mix (SCC0) through immersion in 5%, 10%, and 20% MgSO4 solutions for 30, 60, and 90 days. The strength loss ratio for 6% of NC mixed in SCCs at 30 days of sulfate immersion was lower than that of control mix (SCC0) by 39.43%, 31.43% and 27.1% at 5%, 10% and 20% MgSO4 respectively. At 60 days of sulfate immersion, the strength loss ratio was lower than SCC0 by 34.6%, 30% and 29.5% at 5%, 10% and 20% MgSO4 respectively. Finally, the strength loss ratio at 90 days of sulfate immersion was lower than SCC0 by 56.7%, 44.5% and 40.4 % at 5%, 10% and 20% MgSO4 respectively.

 Also, the combined addition of NC and QLP has noticeable values for the hardened and durability properties. Furthermore, it was found that using 4% NC with 100 kg QLP could provide satisfactory improvement to workability, hardened and durability properties.

Table of Contents

CHAPTER ONE: INTRODUCTION

CHAPTER TWO: LITERATURE REVIEW

**CHAPTER THREE: RESERCH METHODOLOGY
AND MATERIALS CHARACTERIZATION**

CHAPTER FIVE: CONCLUSIONS AND RECOMMENDATIONS

List of Tables

List of Figures

List of Abbreviations

Abbreviation	Description
AFm	Mono sulfa aluminate.
Al_2O_3	Aluminium oxide.
$Al_2O_3\ 2SiO_2$	Aluminosilicate
AlO_6	Aluminum monoxide.
API	Accelerated Pozzolanic Index.
ASTM	American Society for Testing and Materials.
BET	Brunauer-Emmett-Teller analyzer.
BJH	Barrett, Joyner, Halenda analyzer.
QLP	Quicklime.
BS EN	British Standard European Norm
C_2ASH_8	Gehlenite hydrate.
C_2S	Di Calcium Silicate.
C_3A	Tricalcium Aluminate
C_3ASH_6	Hydrogarnet.
C_3S	Tri Calcium Silicate.
C_4AF	Tetra Calcium Alumina-Ferrite.
$CaCO_3$	Calcite.
C-A-H	Calcium Aluminates Hydrate.
CaO	Calcium Oxide.
CH	Calcium Hydroxide
CO_2	Carbon Dioxide
C-S-H	Calcium Silicate Hydrate
DSC	Differential Scanning Calorimetry.
EDS or EDX	Energy-Dispersive X-Ray Spectroscopy.
EFNARG	European Self-Compacting Concrete Guidelines.
Fe_2O_3	Ferric oxide .
GGBFS	Ground Granulated Blast-Furnace Slag.
H_2SiO_4	Monosilicic acid.
H_2So_4	Sulphuric acid
HRWRA	High Range Water-Decreasing Mixture.
ITZ	Interfacial Transition Zone.
K	Kaolin.
K_2O	Potassium oxide.
LP	Limestone.
$Mg(OH)_2$	Magnesium hydroxide.
MgO	Magnesium oxide.
$MgSO_4$	Magnesium sulfate
MK	Metakaolin.

M-S-H	Magnesium silicate hydrate
NC	Nano clay.
NPS	Nanoparticles.
PH	Power of Hydrogen.
PSA	Particle Size Analyzers.
SCC	Self - Compacting Concrete.
SCCs	Self - Compacting Concrete samples .
SEM	Scanning Electron Microscopy.
SFD	Slump Flow Diameter.
SI	Segregated Index.
SiO_4	Monosilicate.
SP	Superplasticizer.
SR	Segregation Ratio
SRC	Sulfate Resisting Cement.
SSA	Special Surface Area.
SSD	Samples Saturated Dry.
TiO_2	Titanium dioxide.
UHPC	Ultra-High Performance Concrete.
UPV	Ultrasonic Pulse Velocity.
VAM	Viscosity Modify Admixture.
VS,VF	Viscosity Slump and V-Funnel Flow
XRD	X-Ray Diffraction.
XRF	X-Ray Fluorescence.

List of Symbols

Symbol	Description
a	Distance From The Line Break Failure to The Nearest Support (Flexural Test).
A, B,C and D	Dry, Full Saturated , Saturated Submerged and Apparent Masses (Porosity Test).
A_{cube}	Cross-Sectional Area of Cube.
b_{pr} , d_{pr} , L_{pr}	Width, Depth and Net Length of a Prism (Flexural Test).
°C	Degree Celsius.
cm	Centimeter.
d	is the spacing between crystal planes (d spacing) (the Bragg angle)
d1 and d2	Diameters of Slump Flow Test.
D_{cy} , L_{cy}	Diameter and Length of The Cylinder (Splitting Tensile Test)
$D_{fresh.}$	Fresh Density of Concrete .
E	Chord Modulus of Elasticity.
f_{cu}	Compressive Strength of Concrete.
f_r	Flexural Strength.
f_{SP}	Splitting Tensile Strength.
g	Gram.
GPa	Gaga Pascale.
H1,H2	Depth of concrete (L-box Test)
hr	Hour.
J	Joule
kg	Kilo Gram.
km	Kilo Meter.
kN	Kilo Newton.
L	Path Length of Sample.
m	Meter.
M_{pass}	Passed Materials Mass (Segregation Test).
M_{total}	Initial SCC Mass (Segregation Test).
m_0	Mass of The Dry Sample by Degrees 110 ℃ (Burning Test)
m_b	Mass of The Burning Sample at Degrees (200,400,600,800) ℃ (Burning Test)
M_c	Mass of Concrete
min	Minute
mm	Mile meter.
MPa	Mage Pascale.
N	Newton.
nm	Nano meter.

P	Maximum Applied Load.
P_o	Porosity.
R^2	Regression Factor.
rpm	Revolutions per minute.
S_1	Stress Corresponding to a Longitudinal Strain of 50×10^{-6} (Modules of Elasticity Test).
S_2	Stress Corresponding to 40% of The Ultimate Stress (Modules of Elasticity Test).
sec	Second.
T	Transit Time (UPV Test)
T_{500}	Slump Flow Time
t_v	Time of the V-funnel Flow
V	Ultrasonic Pulse Velocity Value
V_c	Volume of Concrete
V_{Cube}	Volume of Cube.
V_m	Volume of Casting Mould
V_o	Volume of Permeable Pore Space (Voids).
W	Water Absorption.
W_c	Weight of Fresh Concrete.
ϵ_2	Longitudinal Strain Corresponding to The S_2 Stress (Modules of Elasticity Test).
θ	is the angle between the crystal plane and the diffracted beam (the Bragg angle)
λ	the wave length of the incident-beam X-ray(the Bragg angle)
μm	Micrometer.
μs	Micro second .
ρ	Dry Density.

CHAPTER ONE

INTRODUCTION

Chapter One

Introduction

1.1. Background

Nanoscience is the study of phenomena and manipulation of materials at atomic, molecular and macromolecular scales, where properties differ significantly from those at a larger scale **[1]**.

The ability to investigate, calculate, manipulate, and produce materials at the nanometer scale is known as nanotechnology. A nanometer (nm) is a SI unit of length 10^{-9} or one billionth of a meter **[2]**. A nanomaterial is an item with at least one nanometer-scale dimension (approximately 1 to 100 nm). To prevent single atoms or very small groups of atoms from being known as a nanoparticle, the size range is usually set to a minimum of 1 nm. As a result, nanoscience and nanotechnology deal with 1nm atom clusters in at least one dimension**[3]**.

The important segment of widespread acceptance of nanotechnology provides improvement for system reliability, extends functionality beyond conventional applications, and reduces cost, size, and energy consumption. Incorporating nanotechnology in the field of materials facilitates increasing materials durability and provides materials with ultra-high performance. It also allows for more effective use of natural resources and the attainment of necessary material properties with minimal effort **[4]** . Nanotechnology is primarily characterised as manipulating materials at the nanoscale of $(10^{-9}$ m) to generate novel properties. In the field of nanotechnology, there are two basic methods to produce Nanoparticles: the first is the "Top-down" method, which deconstructs large structures into nanoscale components which it used in this research. The second method is the "bottom-up" method, also known as "molecular nanotechnology," which was pioneered by Drexler et al. **[5]** and in which materials are constructed from their atom components. Using the two methods, several breakthroughs in nanotechnology research could be made in the future **[6]**.

1.2. Research Problem

The current research problem focuses on three main aspects: CO_2 emission from cement production, the presence of large quantities of natural waste materials such as kaolin and limestone rocks and absence of using locally made Nano clay from Iraqi kaolin in concrete including self-compacting concrete mixtures (SCC). Globally, cement is the third largest producer of carbon dioxide emissions to the atmosphere from the decomposition of calcium carbonate oxidation after fossil fuels and deforestation/other land-use changes. Total emissions of CO2 from the global cement industry is estimated to be about 5-8% from the total amount of CO2 in the atmosphere [7].

One of the main drawbacks of SCC is containing a large amount of binder. According to ACI 237R Standards for SCC, the quantity of cement recommended is between (386-475 kg/m3), while the quantity that recommended by EFNRAC recommendations is (400-600 kg/m3) This means that SCC needs high cement quantity to achieve the desired fresh properties. Therefore, the production of SCC with high quantities of cement leads to the emission of carbon dioxide, which in turn leads to environmental pollution [8].

The potential of applied science to boost the performance of concrete and to steer to the event of novel, property, advanced cement based composites with distinctive mechanical, thermal, and electrical properties is promising and many new opportunities are expected to rise in the coming years. Nano alternative cement materials particles can accelerate cement hydration due to their high activity. Similarly, the incorporation of nano-particles can fill pores more effectively to enhance the overall strength and durability. Thus, nanoparticles can lead to the production of a new generation of cement composites with enhanced strength, and durability. The introduction of these novel materials into the public sphere through civil infrastructure can necessitate associate analysis and understanding of the impact that they will wear the surroundings and human health [9].

As mentioned previous, where cement is one of the causes of the emission of carbon dioxide. Therefore, it is considered that incorporating of mineral materials in concrete

is the most straightforward way to reduce the amount of cement. Thereby reducing the emission of carbon dioxide and provides means of ecological and economic disposal for millions of tons of waste of natural and industrial products **[10]**.

1.3. Nano clay (NC)

Clay minerals generally have a one-dimensional layer structure with a thickness of 0.7nm for 1:1 (one - layer from silicate and aluminate) and 1nm for 2:1(two - layers from silicate and one – layer from aluminate) and appear in many surface forms such as planar and interlayer. They are easy to connect with on the external and internal surfaces and can be changed by ion exchange, adsorption, and grafting processes. They have also a plasticity behaviour and harden on drying and firing **[11]**. Nano clay particles are widely produced by mechanical methods using high-energy ball milling, with high pozzolanic reactivity and a flaky, elongated, small, and platy particle shape that can provide a needle action mechanism (the influence of bridging) **[12, 13, 14]**.

1.4. Applications of Nanomaterial in Concrete

Increase on research endeavors of nanotechnology includes many disciplines, including sustainable construction in civil and environmental engineering. Tremendous achievements have been reported on adoption of nanotechnology in sustainable building, but there are more to explore than achieved. Some of the advancements on the adoption of nanotechnology in sustainable construction include enhancing rheology, strength, and durability properties of concrete, which have been depends on its constituent's nanoscopic characteristics.

Concrete is composed at least three phases: a binding phase (cement matrix paste), a particulate phase (aggregates), and interfacial transition zone phase (ITZ). The particulate phase of ordinary strength concrete is much stronger than the binding phase. As a result, the cement matrix has a significant effect on mechanical properties of concrete. The addition of nano fine particles can improve the properties of concrete due to increased surface area and reactivity by filling the nanopores of cement paste **[15]**.

B.Birgisson et al. **[16]** listed the following advances of technological concrete that are most likely to result from the use of nanotechnology:

3

- Development of high-performance cement and concrete products based on mechanical and durability properties.
- Development of sustainable concrete materials and structures for various adverse environments, reducing energy consumption during cement processing, and improving protection.
- Development of novel concrete materials through nanotechnology-based innovative processing of cement and cement paste.
- Advanced characterisation and simulation of concrete at the nano, micro, meso, and macroscales to develop the fundamental multi-scale models for concrete.

1.5. Self - Compacting Concrete (SCC)

Due to the architectural development of the construction industry, there is a high demand for large and complex structures, which often results in complicated casting conditions. Self-compacting concrete (SCC) can describe as a concrete that can compact itself mainly by its own weight without vibration. It is very fluid, so it can go around obstructions and fill all the nooks without the possibility of mortar or other concrete materials separating. There is no entrapped air or rock pockets. This form of concrete doesn't need to be compacted, time and effort saving, labour, and energy saving as will **[17].**

1.6. Nano clay and Self- Compacting Concrete

SCC with Nano clay has an improved compressive, splitting, flexural strength, and durability properties like sulfate attack, fire, freeze-thaw, chloride penetration resistance, shrinkage and a higher density microstructure. On the other side, Nano clay can decrease the workability, porosity, permeability, and water absorption. This improvement is due to Nano clay particles work as nano fillers, nucleation sites, and reactive pozzolan in facilitating hydration and enhancing material properties **[18]**.

1.7. Aim and Objectives

The research aims to transform natural kaolin clay into Nano clay using a combination of ball milling and drying processes to produce high purity of Nano clay particles at scale less than 100 nm consistently. After that, investigate the effect of mixing the

prepared NC on the fresh, mechanical, and durability properties of self –compacting concrete with quicklime(QLP) using sulfate resistant cement (SRC).

To achieve this aim, the following objectives were formulated:

1. Prepares Nano clay particles from Iraqi kaolin by a top-down approach using ultrafine grinding (ball milling).
2. Characterisse the raw material (kaolin clay).
3. Characterisse the prepared Nano clay (NC).
4. Study the effect of using 2, 4, 6 % NC as a partial replacement by cement weight on enhancing or reducing fresh, hardened and durability properties for the SCC mixture.
5. Study the effect of using (50, 75, 100) kg of quicklime (QLP), which was corresponded to (16, 23.4, and 29%) QLP as a partial replacement by cement weight on fresh, hardened and durability properties for the SCC mixture.

1.8. Thesis Outline

The thesis is organised into five chapters as follows:

➢ **Chapter One:** an overview and general information on the subject of this study and states the problem, aim and objectives.

➢ **Chapter Two:** explores the relevant previous studies and their outcomes that laid the groundwork for the current study.

➢ **Chapter Three:** gives a detailed description of the used materials, experimental methods and employed tools to achieve the aim of this study.

➢ **Chapter Four:** analyses and explains the findings of experimental investigation, mainly including the effect of the prepared Nano clay on the performance of SCC mixtures

➢ **Chapter Five:** presents the conclusions drawn from the experimental analysis and recommendations for future work.

CHAPTER TWO

LITERATURE REVIEW

Chapter Two

Literature Review

2.1. Introduction

Nanotechnology is the term used to cover the design, construction and utilization of functional structures with at least one characteristic dimension measured in nanometers. Such materials and systems can be designed to exhibit novel and significantly improved physical, chemical and biological properties, phenomena and processes as a result of the limited size of their constituent particles or molecules. the reason for such interesting and very useful behavior is that when characteristic structural features are intermediate in extent between isolated atoms and bulk macroscopic materials; i.e., in the range of about 10^{-9} m to 10^{-7}m (1 to 100 nm), the objects may display physical attributes substantially different from those displayed by either atoms or bulk materials. Ultimately this can lead to new technological opportunities as well as new challenges [19]. The change in the surface/volume ratio of materials is shown in Figure (2-1).
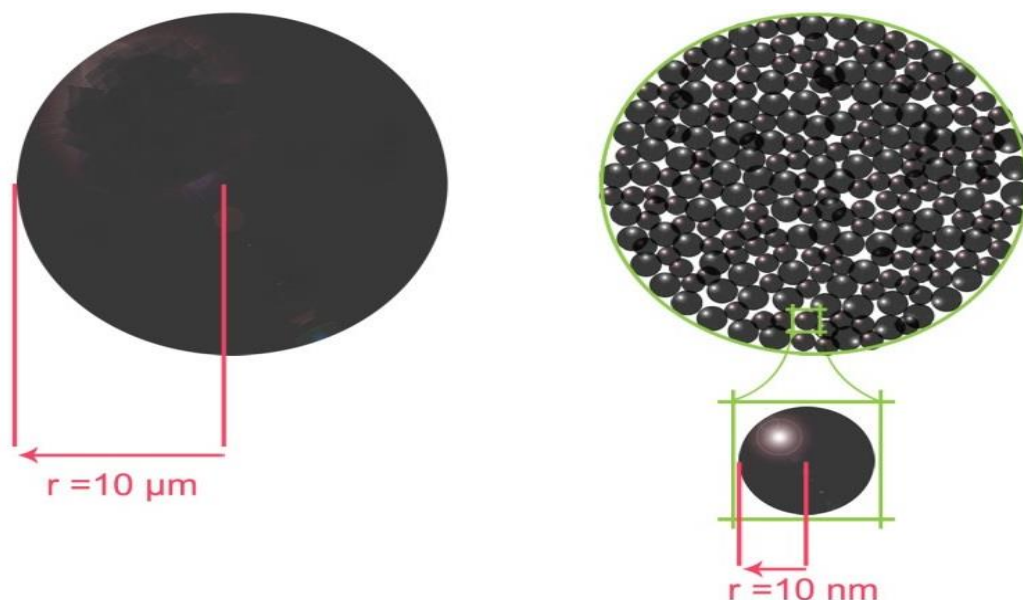
Figure (2-1): Representation of change in the ratio surface/volume between a bulk microsphere and the same microsphere composed by nanoparticles(NPs) [20].

2.2. Production Methods of Nanomaterial

Methods for manufacturing nanomaterials can usually be classified into top-down and bottom-up methods, as shown in Figure (2-2). A top-down method is an easy method to fabricate sculpture from large marble block. Whereas, the bottom-up techniques function in the opposite direction: starting from the atomic or molecular precursors, the nanomaterial, such as a nano-coating, is obtained and gradually assembled until the desired structure is formed **[3]**. The classification of top-down methods is shown in Table (2-1).
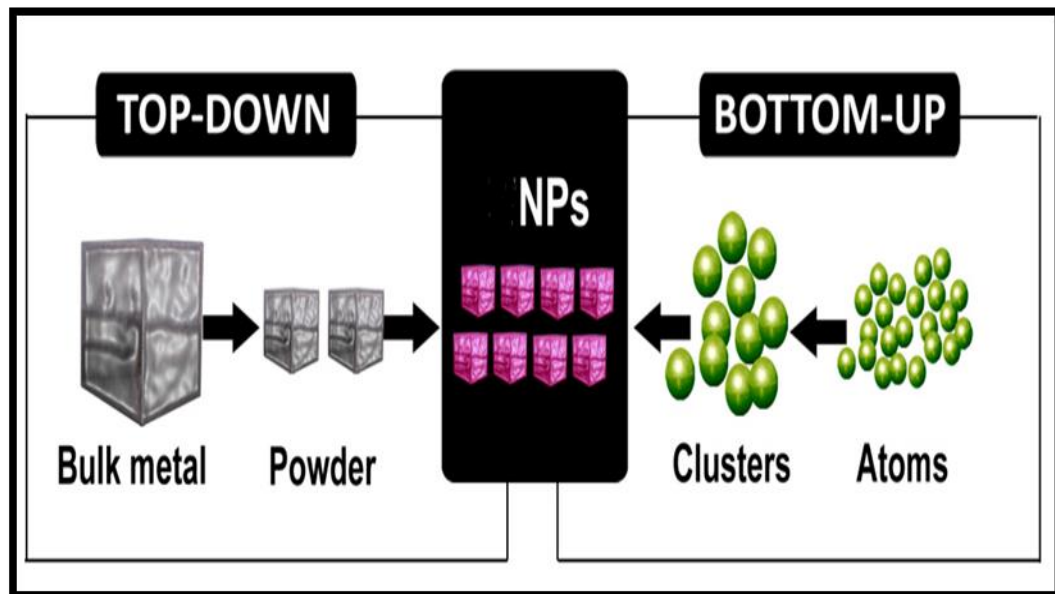
Figure(2-2): Illustration of the "top-down" and "bottom-up" approaches [20].

Table(2-1): Organization of top-down methods [21].

No	Top-down fabrication methods	Comments
1	Mechanical Energy	Mechanical methods employ a physical process that does not involve chemical change (a reaction).
2	Thermal Fabrication Methods	The thermal method employs a physical process (heating) that does not initiate chemical change (a reaction).
3	High Energy Fabrication Methods	High-energy sources such as arcs, solar flux, and plasmas are commonly used to produce nanomaterials from the top-down. These are not labelled as thermal methods because the origin of the heat is not conventional.
4	Chemical Fabrication Methods	The methods that use chemical transformation during a production process.
5	Lithographic Fabrication Methods	Lithography is the means of making printed circuits and computer boards for several decades now.
6	Natural Fabrication Methods	Most of these natural processes are quite familiar, and there is no need to allocate any more time or space.

2.2.1. Mechanical Energy Methods

Mechanical energy methods are utilizing for ease, less expensive and less time consuming fabrication of functional structural in bulk quantity. For such category, ball milling method is the simplest production method. Further, ball milling method uses kinetic energy of medium grinding to produces nanomaterials.

The other mechanical energy methods are compaction and consolidation in which nanomaterials are "put back together", and improved their properties. It is possible to make metallic alloys this way. Industry uses many top-down mechanical methods **[22]**. Table (2-2) shows the classification forms of producing top-down mechanical energy.

Table(2-2): Top-down mechanical energy production methods [22].

No	Method	Comments
1	Ball Milling	Production of nanoparticles by mechanical attrition to produce grain size ≤5nm. High-energy ball milling uses steel balls to transfer kinetic energy by the impact on the sample. High polydisperse products and contamination are problems.
2	Rolling / Beating	Traditional mechanical methods minimise material thickness and refine the structure. Gold can be beaten into a 50nm thick film.
3	Extrusion.Drawing	High-pressure of forcing materials in a plastic phase through a die to form high-aspect-ratio parts like wires. Bi-metal forced through nanopore alumina is an analogous process at the nanoscale and can be considered a thermal-mechanical process.
4	Mechanical Machining, Polishing, Grinding, And Ultra Microtome	Also known as conventional machining; the resolution limit;5µm. Other techniques analogous to mechanical machining perform the same function with laser beams, focused ion beams, and plasmas.
5	Compaction Consolidation	Metal powder ball milled and compacted. Powders are considered bulk materials; therefore, powders' compaction to form bulk material is not considered a bottom-up method.
6	Atomisation	Conversion of a liquid into aerosol particles by forcing through a nozzle at high pressure.

2.2.2. Ball Milling

Ball milling is a method for grinding the fine powder and manufacturing submicron or nano-structured powder materials and used for grinding all kinds of materials. Ball milling was first accomplished by J. Benjamin in 1966.Throughout the years, it has proved to be an effective and simple technique to produce nano-crystalline powders and the possibility of obtaining the large quantity of materials **[23]**. Ball milling is one of the most important mechanical top-down methods, a technique that can produce nano-scale materials by mechanical attrition. In ball milling, the kinetic energy of a grinding medium (e.g., stainless steel ball bearings, zirconia and porcelain) is transferred to coarse-grained metal, ceramic, or polymeric sample materials with the

a direct purpose of size reduction. During the ball milling process, severe plastic deformation of the sample material initiates the formation of defects and dislocations as shown in Figure (2-3) A.

Any type of mechanical deformation subjected to high shear and strain condition leads to the formation of nano grained material. A ball mill consists of a hollow cylindrical shell rotating about its axis. The axis of the shell may be either horizontal or at a small angle to the horizontal. It is partially filled with balls as shown in Figure (2-3) B usually under controlled atmospheric conditions to prevent unwanted reactions such as oxidation **[22]**.
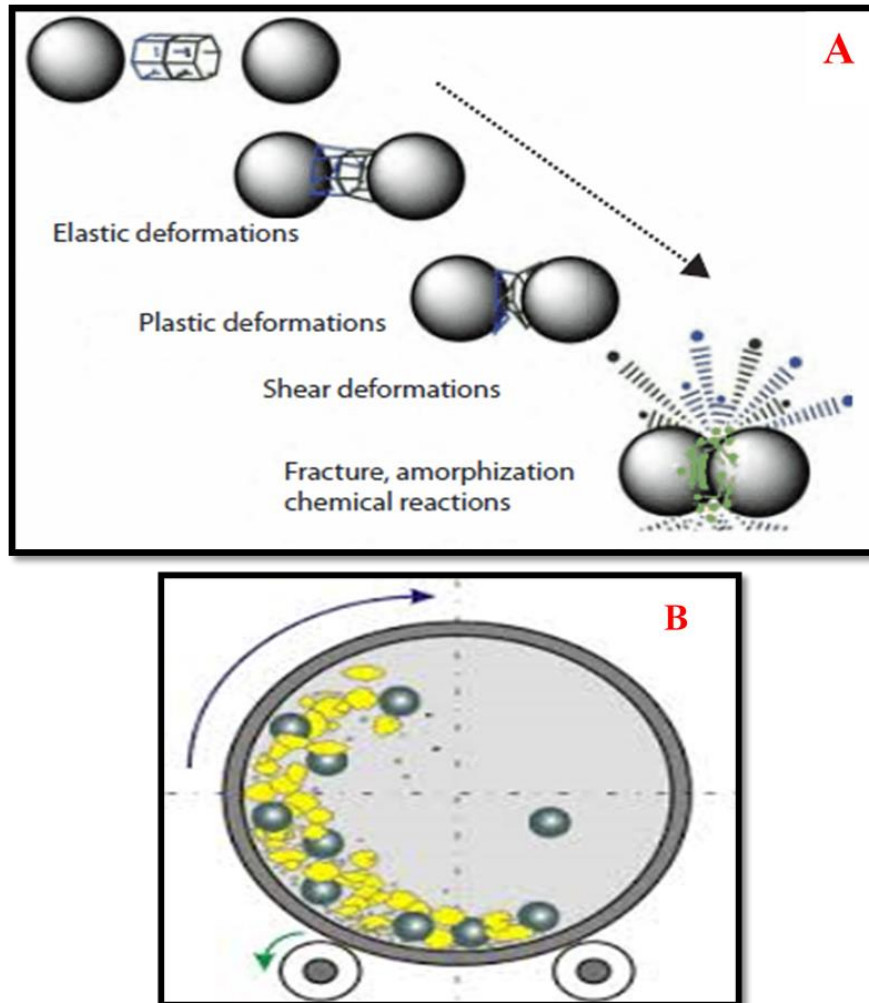
Figure (2-3) A: Deformations in the material trapped between two colliding balls during ball milling. B: Schematic representation of the Ball milling process [22].

2.3. Self-Compacting Concrete (SCC)

2.3.1. Definition and Development of Self-Compacting Concrete

Self-compacting concrete is a special type of concrete that can fill the reinforcement gaps and the mould corners without any vibration and compaction desideratum **[24]**. SCC's development was a reaction to poor workmanship in the Japanese construction industry and low-quality end products **[25]**. It was developed at the University of Tokyo by Professor Okamura in 1988 **[26]**. It spread through Japan-Asia to Sweden in mid-1990s via transportation civil work and shifted completely to Europe in 1993 **[27, 28]**. Whereas, for North America, it expanded to over 1 million m³ in 2002, and it used first time in the same year in South Africa. Further, SCC was used started in construction activities in 2002 and expanded up to 400 000 m³ in 2008 in the UK **[29]**.

SCC utilizes for in-situ casting as well as precast concrete, and practical applications were investigated to improve its physical and mechanical characteristics and its development for utilizing in construction activities **[28]**. Figure (2-4) shows the major developments and global spread of SCC.

Figure (2-4): Basic timeline of SCC development [29]

As SCC has high fluidity and resistance to segregation, the shape and amount of reinforcement steel bars or structures' arrangement have no affect; it can even be pumped to a longer distance. Vibration removal leads to increased concrete efficiency,

reduced skilled labor, and shortened building time. On the other hand, vibrating the concrete creates noise that has a noxious physical effect on workers and affects the surrounding neighborhood **[30]**.

Self-compacting concrete is widely used in sections of post or pretension concrete. It can mold into any shape and it is used in congested areas where it is not possible to use compaction equipment.

2.3.2. Advantages and Disadvantages of Using SCC

As with any material, when used for the right application, SCC can provide an-advantage. The following advantages and disadvantages have been reported in the previous studies for SCC.

2.3.2.1. Advantages

- The main difference between conventional concrete and SCC is the addition of mineral admixtures. Additionally, the viscosity modifies admixture (VMA) or filler materials are used to sidestep the parting and separation of bulk particles in SCC. Many mineral admixtures such as natural pozzolans, limestone powder, fly ash, silica fume, glass filler, ground granulated blast-furnace slag (GGBFS), and quartzite fillers are used to make SCC as cement less and structural material. As cement production is not an environmentally friendly, and most of these materials are industrial by- products, SCC could reduce the carbon footprint **[31]**.

- Increase construction speed, cost savings due to reduced labor requirements, overall energy savings during concrete placement, and increase site productivity **[31]**.

- It is easier to obtain aesthetically pleasing finishes **[32]**.

- Due to better compaction, it improves structural durability **[28]**.

- Overall, better design buildability and low on-site dust levels due to the absence of concrete vibration activities **[33]**.

12

- Better strength and workability, lower noise level and high quality of the concrete are possible **[34]**.

- Reduce the damage of molds due to the absence of vibration, freedom to shape design sections, and ease of casting through high density of steel reinforcement **[27]**.

2.3.2.2. Disadvantages

- The moisture content should be supervised more diligently as SCC is more sensitive to moisture deviations than traditional concrete **[31]**.
- SCC is sensitive to changes in the volume aggregate particles **[28].**
- Due to hydrostatic pressures, additional formwork is required. This means higher costs for formwork **[35]**.
- Increased raw material costs due to the addition of super plasticizer addition and higher binder content **[31]**.
- Due to the higher content of fines, SCC has more sensitivity to shrink the cracks in structural parts than traditional concrete (more brittleness) **[27]**.

2.3.3. Fresh Properties of Self-Compacting Concrete (SCC)

Any concrete mixture could be classified as SCC if it fulfills the following workability criteria:

 1**- Flowing Ability:**

   The concrete mixture (SCC) flows due to its own weight and can fill all the edges of the framework. The flowing ability of fresh concrete is determined by tests such as slump flow, V-funnel, etc.

2- Passing Ability:

   SCC is an able to flow under its weight through tight openings, such as spaces between steel reinforcement bars. The ability to pass can be measured by L-Box, U-box, J-Ring and Fill-box testing methods.

3- Resistance to Segregation:

The SCC must complete the filling capacity and the ability to pass with constant and fixed composition in the transport and placement route without segregation [36].

2.4. Types of Nano clays

Nano clay is nanoparticles, composed of layered mineral silicates, and according to their chemical compositions and morphologies, they are categorized into numerous categories such as bentonite, montmorillonite, kaolinite, halloysite, and hectorite. Table (2-3) and Figure (2-5) show the classification types of Nano clays and a schematic diagram of the structures. In this study, Nano clay is a kaolinite type. Kaolin or china clay is the name given to kaolinite-rich rocks [37].
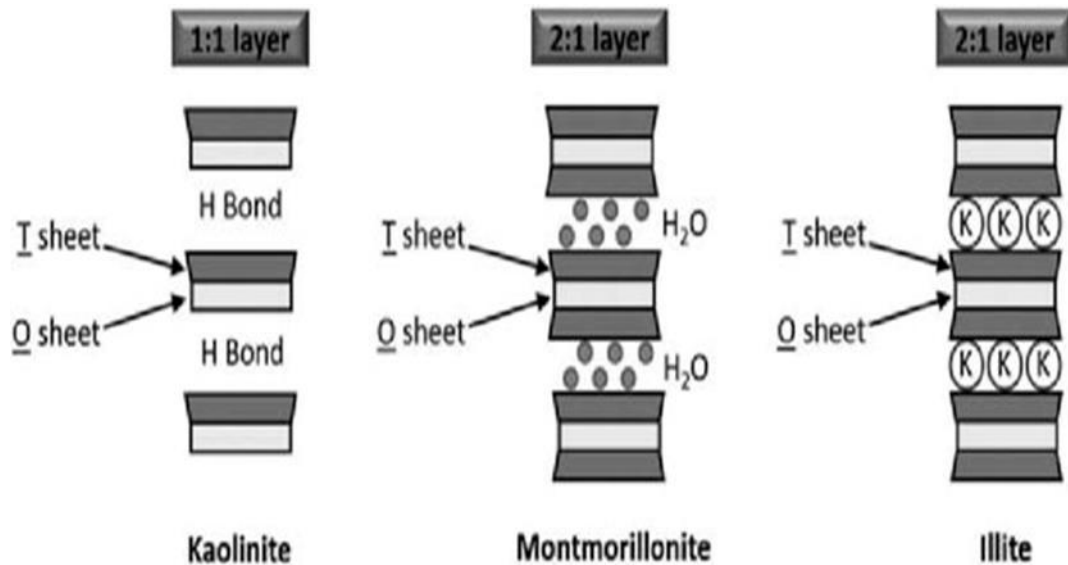
Figure (2-5): A schematic diagram of the Nano clays structure's [38].

It is a clay mineral that belongs to the industrial minerals group in which a layered silicate mineral along with one tetrahedral sheet is connected to octahedral sheet through oxygen atoms [39, 40].

Table (2-3) : Classification types of Nano clays [41].

Family	Group		Formula
Phyllosilicates	TO (1:1)	Kaolinite	The reference plate is formed from a tetrahedral plate T and an octahedral plate O., The thickness of the layer, is about 0.7 nm. Kaolinite $Al_4 Si_4 O_{10}.(OH)_8$
	TOT (2:1)	Smectite, Talc, Mica, Montmorillonite, Sepiolite	Two tetrahedral plates T on both sides of an octahedral plate O form the reference plate. The thickness of the layer is about 1 nm. The group includes many minerals that are major constituents of clays.
	TOT : O (2:1:1)	Chlorite, Bentonite, Saponite	The reference plate is formed of three plates TOT and another isolated O plate. The thickness of the layer is about 1,4 nm. Chlorite di-tri $Al_2Mg_3Si_4O_{10}(OH)_8$
Polysilicate	Natural	Kenyaite, Magadiite, Kanemite, Ilerite, Silhydrite, Zeolite	Magadiite $(Na_2Si14O_{29}.H_2O)$
	Synthetic	FluoroHectorite, Zeolite	
Double lamellar hydroxide	Synthetic	Hydrotalcite	Hydrotalcites: $(Mg_6Al_2 (OH)_{16})(CO_3{}^{2-})_4H_2O$

Where T: tetrahedral silicate sheet and O: octahedral aluminate sheet.

The basic structure of kaolinite, as shown in Figure (2-6), is formed of a sheet of top sharing SiO_4 tetrahedral forming six-membered silicate rings that are linked by common oxygen atoms parallel to the c-axis to a sheet of edge sharing AlO_6 octahedral forming four-membered aluminate rings. The silicate and aluminate layers are bound together by strong ion-covalent bonds via apical oxygen's, and these layers are bonded by much weaker hydrogen bonds [42].
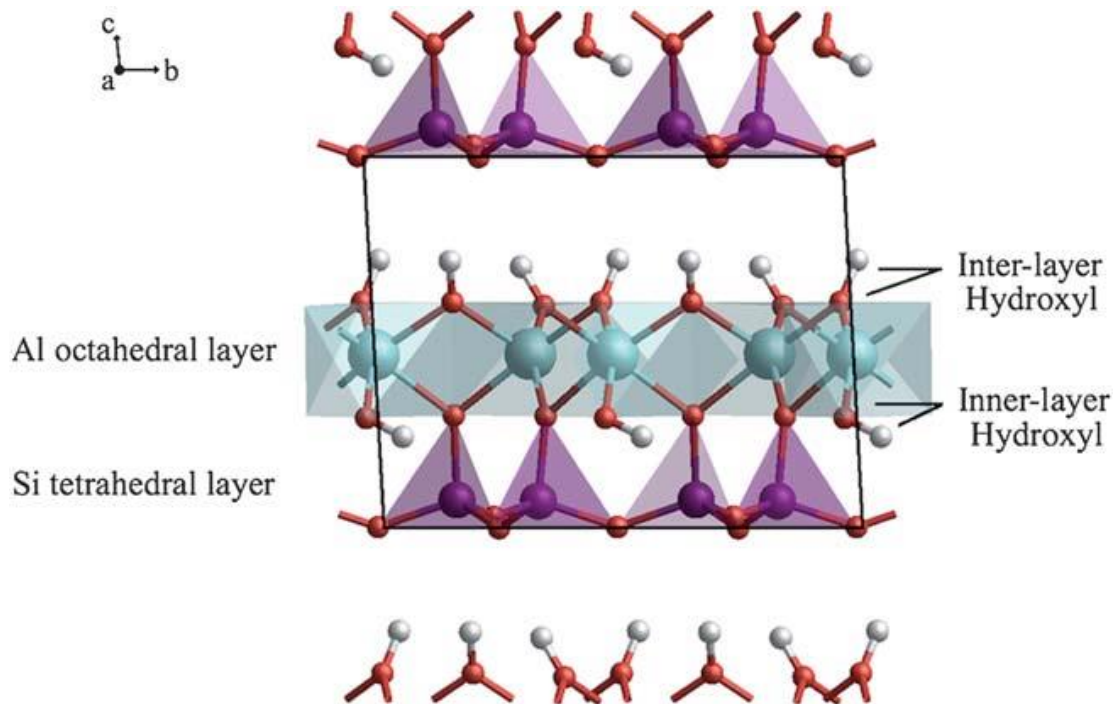
Figure (2-6): Ideal layered structure of kaolinite showing the constructed kaolinite unit cell. The location of the inter-and inner-layer hydroxyls is shown for clarity [42] .

The white mineral kaolinite, also known as dioctahedral phyllosilicate clay, contains dioctahedral phyllosilicate clay. It's made of clay formed by the chemical weathering of aluminum silicate minerals like feldspar [39, 43]. In mineralogy, the chemical formula for kaolinite is $Al_2Si_2O_5(OH)_4$.

2.5. Properties of Nano clay

2.5.1. Physical Properties

Nano clay (NC) is derivative of kaolin ($Al_2Si_2O_5(OH)_4$), which changes from crystal to amorphous after treatment or endothermic dehydration **[44]**. Subsequent to dihydroxylation at temperatures between 600°C and 800°C, the large portion of octahedral alumina is converted into penta and more active tetra coordinated units **[45]**. Additionally, the high amorphous metakaolin (MK) and disordered phase variation are formed when the bonds between kaolinite layers are damaged, or the crystal structure is fully and/or partially damaged **[46, 47, 48, 49]**. Finally, mechanical grinding is used to obtain NC. The equation (2.1) can be used to represent the exothermic dihydroxylation reaction at 500 °C~925 °C **[50]**:

$Al_2O_3 \cdot 2SiO_2 \cdot 2H_2O$(Kaolin) → $Al_2O_3 \cdot 2SiO_2$(Metakaolin)+$2H_2O$……Eq. (2.1)
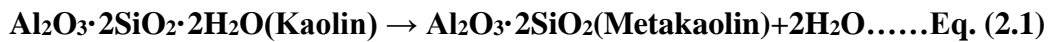
Metakaolin is a highly reactive pozzolan that has a similar reaction to silica fume. Compared to that silica fume, metakaolin has a refined microstructure which caused a better substantial strength and durability, permitting better water penetration resistance, and being cost-effective **[51, 52, 53, 54]**.

Table (2-4) illustrates that the surface area increases from 2 to 8 times when there is a change in clay size from micron to nanometer.

Table (2-4): Physical properties of Nano clay [55, 56, 57, 58, 59, 60].

Specimen	Particle Size (nm)			Mean Size (nm)	Surface Area (m^2/g)	Percentage of Nano Particles (<500 nm)
	D10, Effective Size	D30	D60			
Clay	1612	5585	13325	1202	18.231	-
Nano clay	176	395	767	1114	48~170	40%

2.5.2. Chemical Properties

The chemical compositions of NC are shown in Table (2-5). NC has the highest content of SiO_2 (45.5 % to 89.6%), followed by Al_2O_3 (18.9 % to 42.3 %), both of which are important in improving cement hydration rate and setting time, while NC has a low content of CaO.

Table(2-5): Chemical compositions of Nano clay [55, 56, 60, 61, 62, 63, 64].

SiO$_2$	Al$_2$O$_3$	CaO	TiO$_2$	Fe$_2$O$_3$	K$_2$O	LOI
45.5~89.6	18.9~42.3	0.17~3.59	0.82~1.82	0.1~10.9	0.03~4.55	13~13.47

2.5.3. Hydration

According to some studies, NC enhanced the cement hydration reaction **[65]**. In the cement hydration process, Shoukry et al. **[66]** observed that as the NC replacement rate increased, CH content and X-ray diffraction peak intensity decreased marginally, while the C-S-H peak value increased. Moreover, about 6.7% reduction in CH content of NC cement paste has been observed as compared to CH content of ordinary cement paste **[67]**. However, beyond 10% replacement, there was no considerable variation in CH content of NC cement paste **[68]**. The reduction of 30.23J/g to 14.17J/g for CH enthalpy was observed when the NC replacement increased from 0% to 8%, and led the phase transition from good crystal to non-crystal. Moreover, the enthalpies of C-S-H, C$_3$ASH$_6$ and C$_2$ASH$_8$ were raised from 45.81 J/g, 0.85 J/g and 0.289 J/g to 46.91 J/g, 0.881 J/g, and 1.68 J/g respectively **[57]**, as shown in Figure (2-7). It was also noted a considerable enhancement in the crystalline structural forms **[69]**.
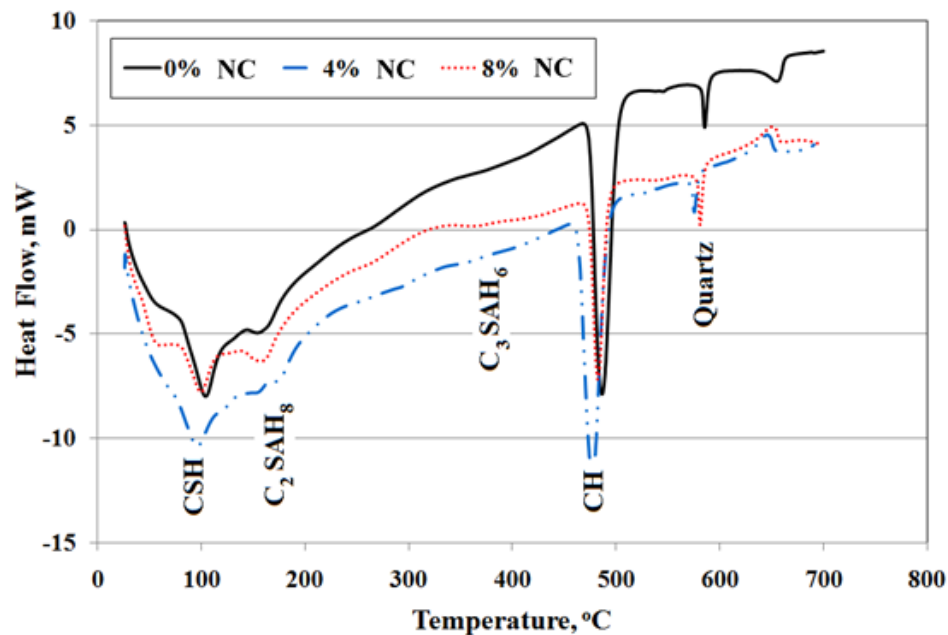
Figure(2-7): Differential scanning calorimetry (DSC) thermograms of NC mortar at 28 days [57].

The following points are the main aspects of the NC mechanism combination for accelerated cement hydration [70]:

1- The fine particles of NC promote the formation of nucleation, and consume free CH, and form needle-like secondary hydration products, which greatly shorten the hydration during the induction period.

2- When NC is added to cement particles, H_2SiO_4 is formed and reacts with the available Ca^{2+} which generates an additional more C-S-H, spreading in the water between the cement particles and are served as seeds for forming denser C-S-H phase.

3- The formation of C-S-H phase is not limited on the particle surface alone, as in the pure C_3S, but also takes place in the pore space.

2.5.4. Workability

Aiswarya et al. [71], found that the percentage of water required for producing a cement paste of standard consistency was increased with the increase in the amount of NC. When the content of NC was increased from 2% to 20%, the initial setting time and the final setting time of the cement paste were first increased and then decreased, and the maximum value was reached when the content of NC was 6% and 4%, respectively. A similar result was also obtained in the Ultra-High Performance Concrete (UHPC) test [14]. As far as the liquidity was concerned, with the nonlinear increase of NC content, cementitious materials showed a decreasing trend. When NC content was 9%, concrete slump was reduced by about 15.7%, and the workability of UHPC was reduced from 178mm to 150mm [56], which was consistent with the results of Senff et al [72].

This is largely due to the fact that NC has a large specific surface area, easy to form a flocculent network structure, show poor dispensability [73] and absorb more free water during wetting [74]. This phenomenon is more significant with the increase of the NC contents. However, the dispersion of NC in cement mortar was improved by ultrasonic dispersion and the prolongation of dispersion time (no more than 15 min) [63]. Hence, in order to obtain proper workability, the range of NC content should be controlled.
.

2.5.5. Mechanical Properties

2.5.5.1. Compressive Strength

It has been observed through numerous studies that the inclusion of NC caused an improvement in the compressive strength of the cementitious materials **[75, 76, 77]**. Table (2-6) displays the effects of the addition of NC on compressive strengths of cementitious materials at 28 days.

Table (2-6): Compressive strengths of cementitious materials with NC at 28 days.

Cementitious Material	w/b Ratio	Cont. of NC %	Compressive Strength Increment	Best Content %	Ref.
Cement paste	0.27	4 - 5	8%→20%→-15%	10	**[46]**
	0.3	2 - 16	16%→54%→-10%		**[78]**
		2 - 14	16%→48%→-10%		**[69]**
	0.33~0.5	2 - 14	8.6%→59.4%→46.6%		**[60]**
	0.44	3 - 10	16%→24.6%→22%	6	**[79]**
	0.5~0.59	2 - 10	10%→63%→20%		**[80]**
Cement mortar	0.3	2 - 10	9.3%→22.6%→-1.3%	4	**[81]**
	0.4	5 - 10	28%→20%	5	**[82]**
		5	9.64%	-	**[59]**
	0.485	3	54%	-	**[83]**
	0.5	2.5 - 10	15%→34%→19%	7.5	**[84]**
		6	18%	-	**[85]**
		2 - 8	1.2%→7%	8	**[57]**
		3	7.76%	-	**[63]**
	0.54	2 - 14	8.8%→42%→20%	10	**[62]**
		2 - 10	20%→57%		**[66]**
	0.6	5 - 15	23%→8%	5	**[86]**
Normal concrete	0.48	2 - 5	5.27%→15.45%	5	**[87]**
	0.5	10	26.32%	-	**[88]**
	0.53	3 - 10	42.2%→ 63.1%	10	**[13]**
Ultra high performance concrete (UHPC)	0.2	1 - 9	12%→ -16.5	1	**[14]**
		1 - 10	8.5%→-8.5%		**[56]**
SCC	0.34	1 - 3	2.3% →10.8%	3	**[89]**
	0.44	2 - 8	3.2% →15.8%	8	**[90]**

It could be seen from the Table that the inclusion of NC in cementitious materials has a significant effect on compressive strengths, and resulted in substantial increase in it a certain percentage of NC addition **[60]**.

However, a possible reduction in compressive strength can occur when the quantity of NC exceeds the best value. This is primarily due to the excess quantity of NC has a tendency to agglomeration and adsorbs around cement particles to cause the delay in the hydration reaction of cement and the decrease in the C_3S and C_2S phases in the matrix **[82, 12]**.

Additionally, the excess quantity of NC causes a weak interfacial transition zone (ITZ) in the matrix **[91]**, and its dispersion defect causes to produce fewer points of contact with the matrix and produce a negative effect on bonding with cement particles **[92, 93]**.

Although the other mixing information such as chemical and mineral admixtures, curing conditions, and w/b ratio are almost similar, but the best contents of NC has a significant effect on compressive strengths. As a result, more studies should be conducted and discussed better to apprehend the various effects of NC on compressive strengths **[94]**.

2.5.5.2. Flexural Strength and Splitting Tensile Strength

Table (2-7) shows that the addition of NC can significantly increase the flexural and splitting tensile strengths of cementitious materials.

Table (2-7): Flexural strengths and splitting tensile strength of cementitious materials with NC at 28 days

Cementitious Material	w/b Ratio	Cont. of NC %	Flexural Strength Increment %	Splitting Tensile Strength Increment %	Best Content %	Ref.
Cement paste	0.3	2 -14	14→36→-25	-	10	[69]
	0.33-0.5	2 -14	3.9→58→38	-		[60]
Cement mortar	0.5	2.5-10	6.4→29→19	-	7.5	[84]
		2- 8	-	10→49	8	[57]
	0.54	2 - 4	12.6→52→21	-	10	[62]
		2 - 10	20→59	-		[66]
	0.6	5 - 15	8→4	-	5	[86]
Normal concrete	0.5	10	-	25.87	-	[88]
	0.53	3 - 10	-	0→46.8	10	[13]
SCC	0.34	1 - 3	-	4.6 →18.5	3	[89]
	0.44	2 - 8	7 →10.5	5 →10	8	[90]

2.5.5.3 Mechanism of NC to Increase Strength

1-The influence of filling.

The smaller size (nanometers) of NC has a significant effect on the filling ability of cement materials. Although the NC particles are 1000 times smaller than the size of cement particles (micrometer), but still NC could fill the microstructure gaps, voids and could diminish the ITZ defects **[95, 96]**.

The SEM image as shown in Figure (2-8) shows that the incorporation of NC fills the voids and pores and resulting a more compact structure, also opposed to the weak microstructure of control mortar **[66]**, which corresponds with the other studies **[58, 63, 85]**.
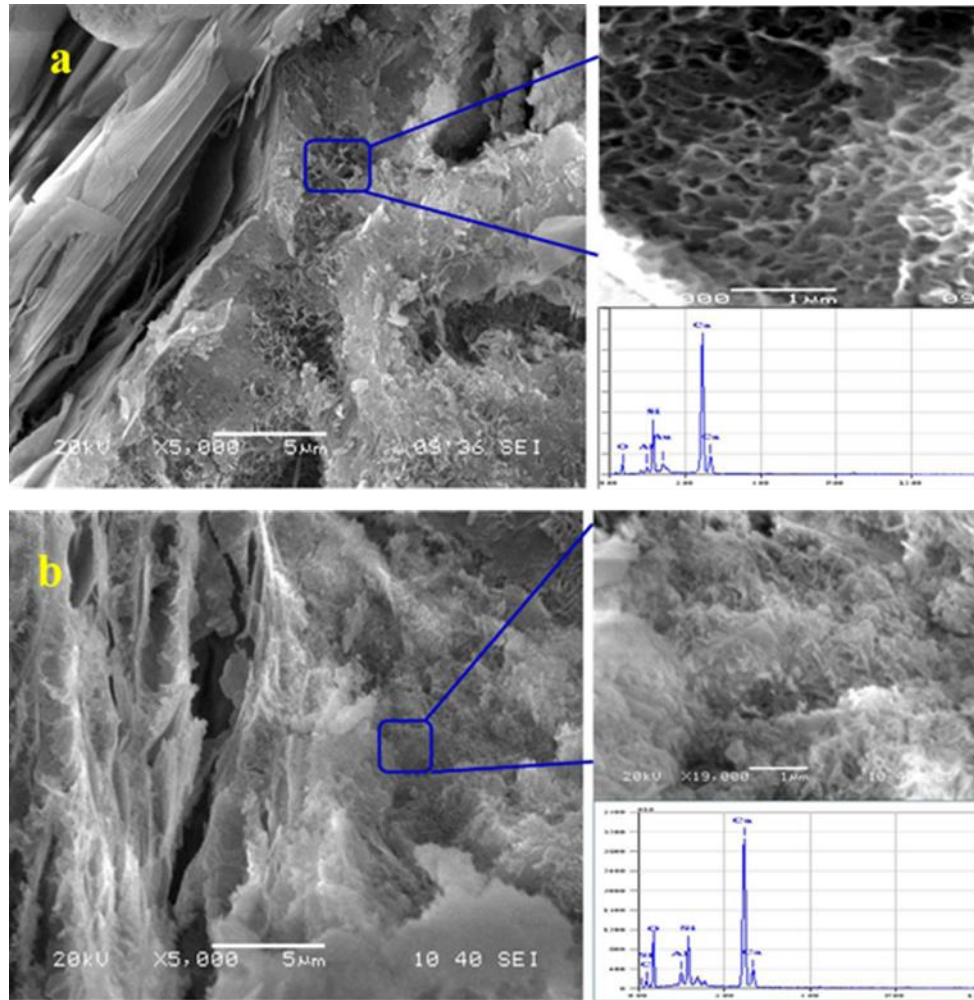
Figure (2-8): SEM images and EDX patterns of cement mortar
(a) 0% NC and (b) 10% NC [66].

2-The effect of nucleation.

Figure (2-9) depicts that the NC helps clinker hydration by the available surface area to sedimentation hydrates from the interstitial solution **[97]**.

The high surface energy of NC provides the thermodynamic drive for this process. Rather than critical nucleation, NC behaves as a source to initiate precipitation **[57]**, and the hydrate phases start as the ionic concentration reaches saturation. Meanwhile, NC enables continuous growth of the C-S-H phase, prefabricate nucleus for the hydration process, aggregation of C-S-H in the network structure. It could also promote hydration reaction of cement **[92]**, and develop uniform and dense microstructure **[98]**.

The nucleus of a crystal is beneficial for increasing the early strength of cement, but the nucleation effect is lost when the cement reaction completes **[65]**.
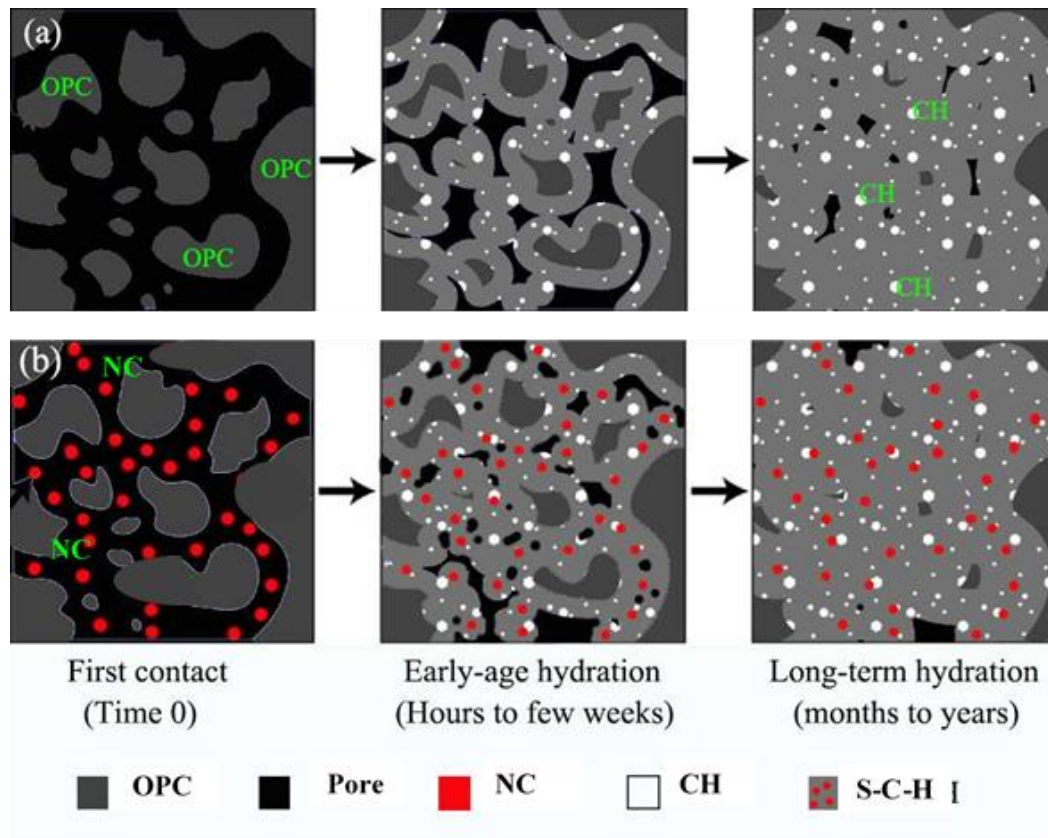
Figure(2-9): Conceptual model for hydration of (a) Ordinary Portland cement and (b) Concrete with NC [97].

3- The influence of bridging.

The inclusion of NC particles works as a fiber between cement products, creates bridge between matrix and reinforcement, and provides resistance to cracks and crack propagation as shown in SEM images Figure (2-10) **[57, 69, 85, 86]**.
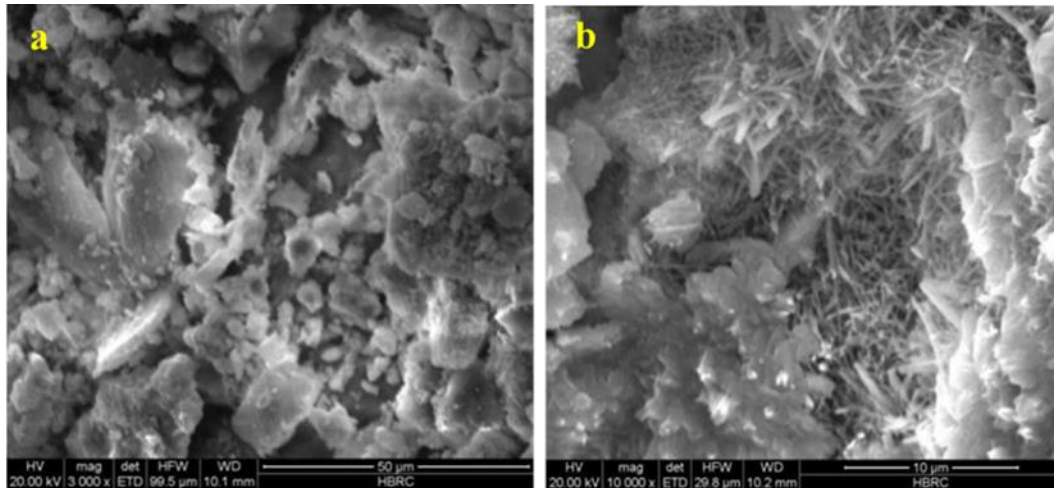
Figure(2-10): SEM images of mortar at 28 days (a) 0% NC; (b) 8% NC [57].

2.5.6 Durability

2.5.6.1 Water Absorption

Table (2-8) summarises the effect of NC on the coefficient of capillary water absorption of the cementitious materials. In general, as the NC content increases, the water absorption coefficient decreases **[99]**. Also, the geometry and size of the pore system should be directly linked to the mechanism of capillary water absorption **[100]**. The improvement of pore structure is mainly attributed to the additional C-S-H gel produced by the pozzolanic reaction of NC and its own micro aggregate effect, filling the micro pores between cement particle **[66, 67, 101]**, and reduced the water absorption of cement paste **[62]**.

Table (2-8): Capillary absorption coefficients of cementitious materials with NC at 28 days.

Cementitious Material	Cont. of NC %	Capillary Absorption Coefficient		Reduced by (%)	Ref.
		Control Sample	Sample with NC		
Cement paste	2 - 14	0.55 (kg/m^2) / $min^{-1/2}$	0.22, 0.41 (kg/m^2) / $min^{-1/2}$	25.4 - 60	**[60]**
	6	0.266 (kg/m^2) / $s^{-1/2}$	0.154 (kg/m^2)/ $s^{-1/2}$	42	**[80]**
Cement mortar	2 - 14	0.33 (kg/m^2) / $min^{-1/2}$	0.12,0.22 (kg/m^2) / $min^{-1/2}$	33 - 63.6	**[62]**
	5 - 10	-	-	38.02 - 51.34	**[82]**
	2 - 10	0.056 (kg/m^2) / $min^{-1/2}$	0.014, 0.04 (kg/m^2) / $min^{-1/2}$	28.5 - 75	**[66]**
Normal concrete	3 - 10	-	-	16.6 - 25.6	**[13]**

2.5.6.2. Resistance to High Temperature

Morsy et al. **[86]** studied the effect of adding different NC by weight percentages (5%–15%) on the compressive and flexural strength of cement mortar at various high temperatures. The compressive and flexural strengths were gradually increased with increasing temperature up to 250°C, and beyond this temperature, both strengths decreased until the temperature reached 800°C. At 250°C, compressive and flexural strength increased by 5.2%~36.6% and 3.4%~27%, respectively, while compressive strength decreased by46.5%~61.5% at 800°C for mixes of (5,10 and 15) % NC.

Based on similar experiments, Wang et al. **[102]** investigated the compressive strength and thermal conductivity coefficients of SCC at (25–1000) °C for one hour with NC contents varying from 0.1 % to 0.5 %. The results showed that when the temperature was below 300 °C, NC concrete increased strength; when the temperature was between 440 and 580 °C, strength was significantly reduced; and when the temperature exceeded1000 °C, the strength was less than 10% of its original strength.

The excess hydration of unhydrated cement particles results steam effect due to internal autoclaving, and the pozzolanic reaction of NC resulted extra C-S-H gel with smaller Ca/Si ratio. The additional hydration products help to bridge the pore system, reduce the thermal stresses around the pores. Moreover, the calcium aluminates hydrate (C-A-H) phases can increase the compressive strength of blended cement mortars up to 200°C~250°C **[103, 104]**.

Furthermore, the incorporation of NC in cementitious products would be made the cement matrix had higher contents of gel-like hydration products which could make it more fire resistant. However, the excess hydration can cause a loss in strength of the cementitious products. It is mainly due to that CH decomposes into CaO and H_2O at 500°C, and $CaCO_3$ decomposes with the effusion above 600°C,, and caused a reduction in free water, and decreased strength and elasticity modulus **[105]**. Furthermore, the temperature gradient causes high thermal tension, which leads to an increase in micro cracks and a weakening of structure's compactness **[106]**.

2.5.6.3. Resistance to Sulfate Attack

The porosity and pore size distribution of concrete significantly impacts its durability. Moreover, such factors influenced the transport properties of the main harmful agents such as gases, water, and ions. These transport properties can be deteriorated concrete by physical and/or chemical attack **[107, 108]**. The presence of sulfate ions in seawater, groundwater, and soil can decline reinforced concrete structures by means of spalling, swelling, cracking, expansion, softening and surface scaling of concrete elements. These characteristics can be caused by a variety of factors such as the type of cement, type of sulfate cation, sulfate concentration, and exposure period. Many sulfate-damaged structures need rehabilitation or, in the most violent cases, reconstruction **[109]**.

Sulfate ions can react with sources of alumina (hydration products such as mono sulfa aluminate (AFm) and unhydrated tricalcium aluminate (C_3A)) to produce ettringite. Also, the produces gypsum with the help of calcium (calcium hydroxide (CH)) or C-S-H gel). However, such production resulting in loss of substantial strength and crack initiation and propagation. It is mainly because of the driving force of crystallisation

pressure impacts on the pore walls, and such driving force results crystal growth of gypsum and ettringite [110, 111, 112]. Tian et al. [113], obtained (3–4) MPa tensile strength for cement-based materials, and concluded that the tensile stress caused by gypsum formation had a significant part for the crack initiation and expansion. Müllauer. [114] concluded that the formation of ettringite in tiny pores (10–50 nm) resulted tensile stress of 8 MPa, and caused crack expansion which led to failure of the cementitious structure.

If the attack solution is magnesium sulfate (MgSO4), all cement minerals, including C-S-H, are targeted. The stability of the C-S-H gel is reduced by the formation of the relatively insoluble and poorly alkaline brucite $(Mg(OH)_2)$ due to reaction with dissolved CH. Furthermore, MgSO4 targets calcium silicate hydrate directly, converting it to gypsum and a weak magnesium silicate hydrate (M-S-H). Because of a thick brucite layer on the surface, surface damage is imperceptible until late in the attack, while strength reduction starts early [115, 116]. Equations (2.2) and (2.3) can illustrate the mechanics of the magnesium sulfate attack

$$Ca(OH)2 + MgSO4 + 10H2O \rightarrow CaSO4. 2H2O + 2Mg(OH) + 8H2O .. Eq. (2.2)$$

$$C - S - H + MgSO4 + 10H2O \rightarrow 3CaO. Al2O3. CaSO4. 13H2O + Al(OH)3 + Mg(OH)2 + H2O .... Eq. (2.3).$$
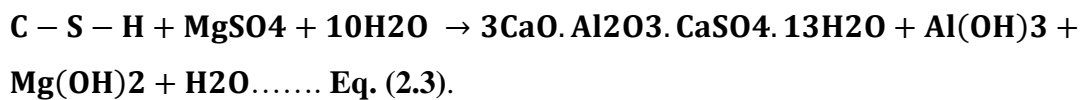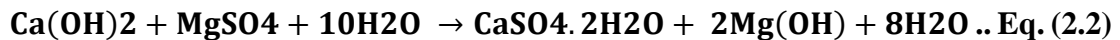
Many researchers have shown in recent years that using nanomaterials can significantly improve the properties of cement-based materials' resistance to sulfate attack, with this effect becoming more pronounced at earlier ages [117, 118].

The high pozzolanic reactivity that caused the reduction of CH, as well as its effects on the microstructure of hardened cement-based materials, were investigated [119]. Only a few researchers have examined the effect of Nano clay on the properties of cement mortar and concrete for sulfate attack. In cement mortar, Nano clay acts as a filler and strengthens the microstructure. It also serves as a mortar activator, encouraging the pozzolanic reaction.

 Hakamy et al. [12] investigated the effects of Nano clay on cement composite properties. They reported a decrease in porosity and water absorption in cement

nanocomposites containing 1 w.t% Nano clay. They also discovered that cement nanocomposites had higher in density, strength, fracture toughness, and hardness than the control mix.

Hosseini et al. **[120]** studied the effects of adding 0.25, 0.50, 0.75, and 1% Nano clay to SCC mix. It was founded that water penetration depth was reduced by 17, 27, 39, and 43 percent, respectively. The overall durability of the SCC mix is improved by reducing the depth of water penetration which can increase resistance to sulfate attack.

CHAPTER THREE

RESERCH

METHODOLOGY

and

MATERIALS

CHARACTERIZATION

Chapter Three

Reserch Methodology and Materials Characterization

3.1. Introduction

This chapter contains details of used materials in addition to the mixes design. Also, tests conducted to assess the effect of incorporating prepared Nano clay (NC) and quicklime (QLP) on the rheological, mechanical, and durability of self-compacting concrete are presented.

3.2. Experimental Work

Experimental work consists of two parts:

1. The first part is preparing the Nano clay from kaolin clay by ultrafine grinding (Ball milling) procedures.

2. The second part was divided into three stages. The first involved preparing the reference SCC mixture (SCC0), by producing SCC mixtures with (2%,4%, and 6%) of NC cement replacement by weight. At the same time, the second stage involved the preparation of mixtures with (50, 75, 100) kg of quicklime(QLP), which was conducted by using (16, 23.4, and 29%) QLP by weight of cement as partial replacement. Based on the fresh properties tests performed at the first stage of the work, the influence of 4% of NC was evaluated with (50,75, and 100) kg of QLP as partial replacement of cement in the third stage.

   Figure (3-1) shows methodology and experimental work of this study. It is worth mentioning that most tests of this research were implemented at the materials laboratory of the Civil Engineering Department / College of the Engineering / University of Anbar except SEM, EDX, XRD, PSA, SSA and XRF tests.
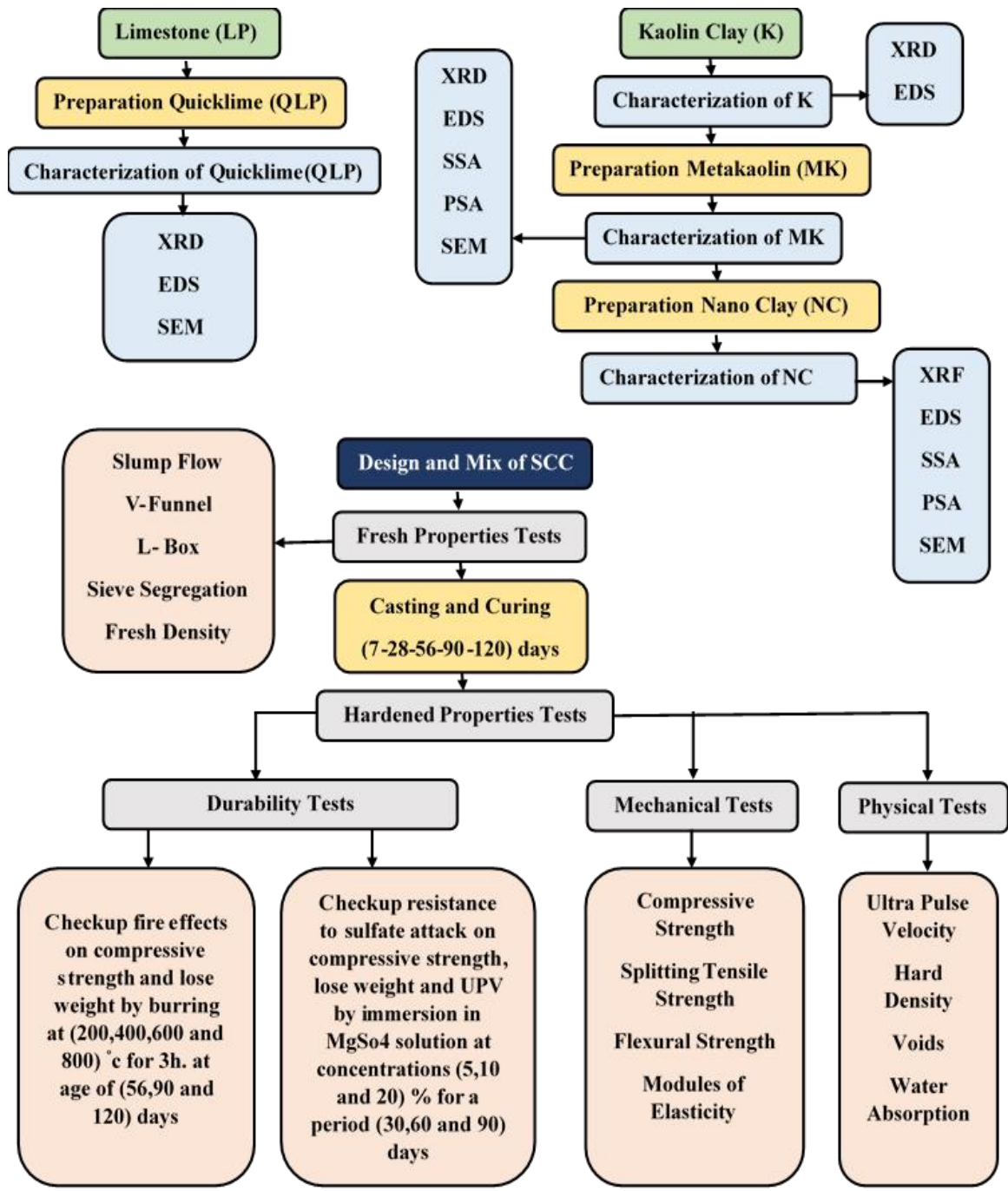
Figure (3-1) Schematic diagram representation of the methodology and experimental program.

3.3 Equipment and Chemicals

Table (3-1) shows the equipment and chemicals that used in this study.

Table (3-1): Types of equipment and chemicals.

No.	The Equipment	Specification
Preparation of Nanoclay (NC)		
1	Ball mill	250 rpm
2	Mechanical Shaker, Heidolph,	UNIMAX 1010/ PROMAX 1020, Germany
3	Ultrasonic	750 Watt Ultrasonic Processors – VCX Series
4	PH meter	Hanna 211, Romania
5	Electrical Furnace	(20-500)°C
6	Mixer for leaching process	(20-100) rpm
7	Magnetic Stirrer	Heidolph - Models, MR. Hei-Tec.40rpm

Chemicals			
No.	Name	Purity	Supplier
1	H_2SO_4	99%	India- Thomas Baker

No.	The Equipment	Specification
Samples Preparation and Testing		
1	Mixer for preparation SCC samples capacity	$0.07m^3$
2	Mixer for making the suspended Nano clay solution	Home mixer
3	Electrical Furnace	Local made
4	Compression and splitting testing machine	BESMAK materials testing machines
5	Flexural testing machine	
6	Electric balance for weighing materials	Incco electronic scale

Chemicals			
No.	Name	Purity	Supplier
1	$MgSO_4.7H_2O$	99.5-100.5%	**Belgium Zedelgem**

3.4. Steps Preparation of Nano clay (NC)

The preparation process of NC included ten steps:

1- The Iraqi natural kaolin rocks were broken into medium pieces and then it grinded to the powder by crushing machine and balls milling.

2- The kaolin clay was burned at 700 °C for two hours to obtain metakaolin.

3- Metakaolin(MK) was washed and cleaned with water to remove mud particles.

4- MK was upgraded by acid (leaching process) at room temperature to get a high-purity metakaolin.

5- Then raw material was washed by the water until the PH becomes natural (7.6).

6- Filtrating the extracted solution.

7- Drying solid particles at 120 °C for 1 hour.

8- Characterisation of metakaolin. The clay was sieved using Sieve Shaker to a size of 300 μm.

9- Ultra milling by ball mill. The clean clay was then inserted into the grinding jar together with the different diameters of grinding balls ranged (10-20) mm and milled for 2 hours

10- Characterisation of Nano clay (NC). the ball-milled NC was analysed using Malvern Instruments (Mastersizer2000) analyser for particle size and size distribution.

These steps are described in the flow diagram in Figure (3-2).
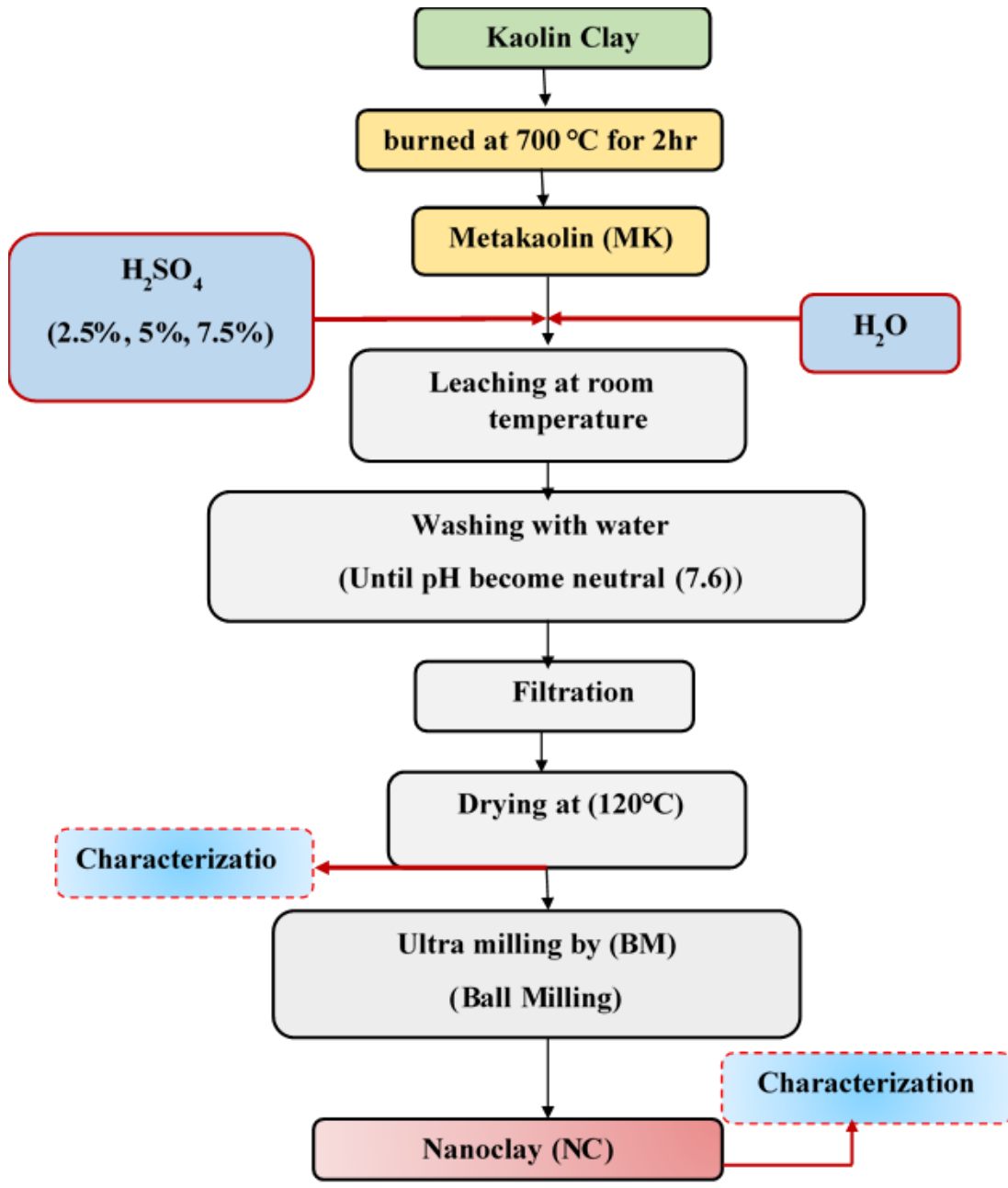
Figure (3-2): Schematic process of preparation of NC

3.4.1. Upgrading of Kaolin clay

The Iraqi natural kaolin clay used in this research was obtained from the Geological Survey Company. Kaolin was taken away from the region and brought (Wadi Houran quarries in Western Sahara / Anbar Province) as rock form. By crushing machine and balls milling as shown in Figure (3-3), the rocks were broken into medium pieces and then it grinded to the powder. The size of the powder has to pass sieve number equal to or less than 63 microns.
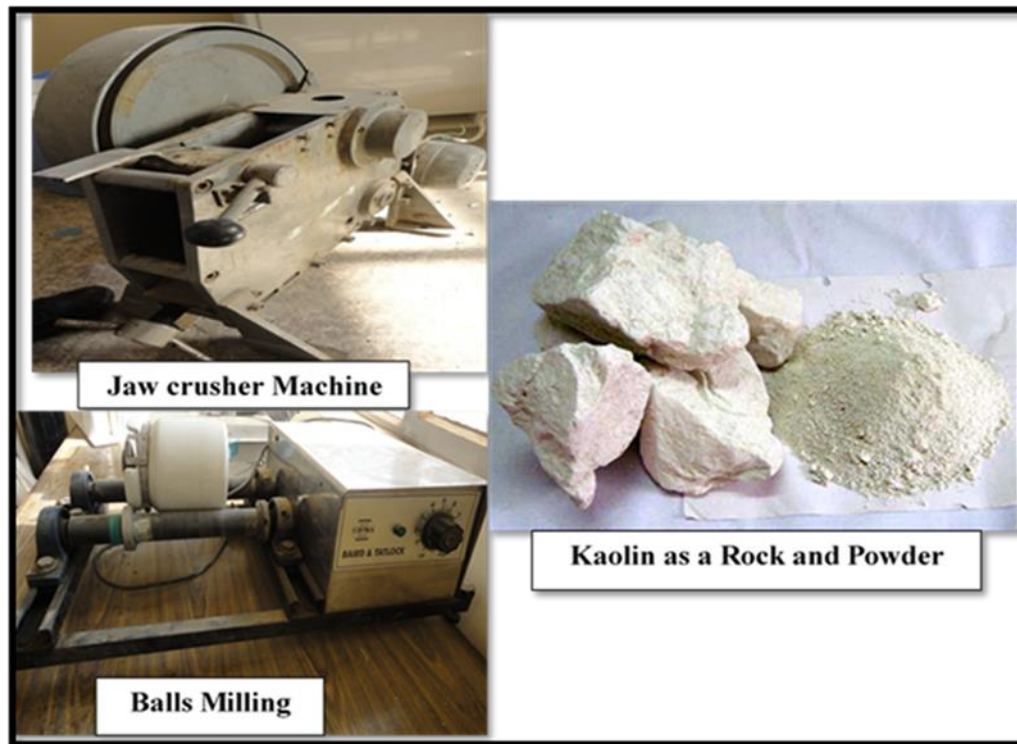
Figure (3-3): Crushing machine and balls milling

Kaolin or china clay (K) ($Al_2Si_2O_5(OH)_4$)) was transformed into an amorphous phase which known metakaolin (MK). It was obtained from the calcination of kaolinite at $700°c$ for 2 hours at the University of Technology, Department of Materials Engineering as shown in Figure (3-4). It was noted that there was a certain change in kaolin colour to light orange during burring. This change might attribute to the shifts that get to metaphase during the burning kaolin.
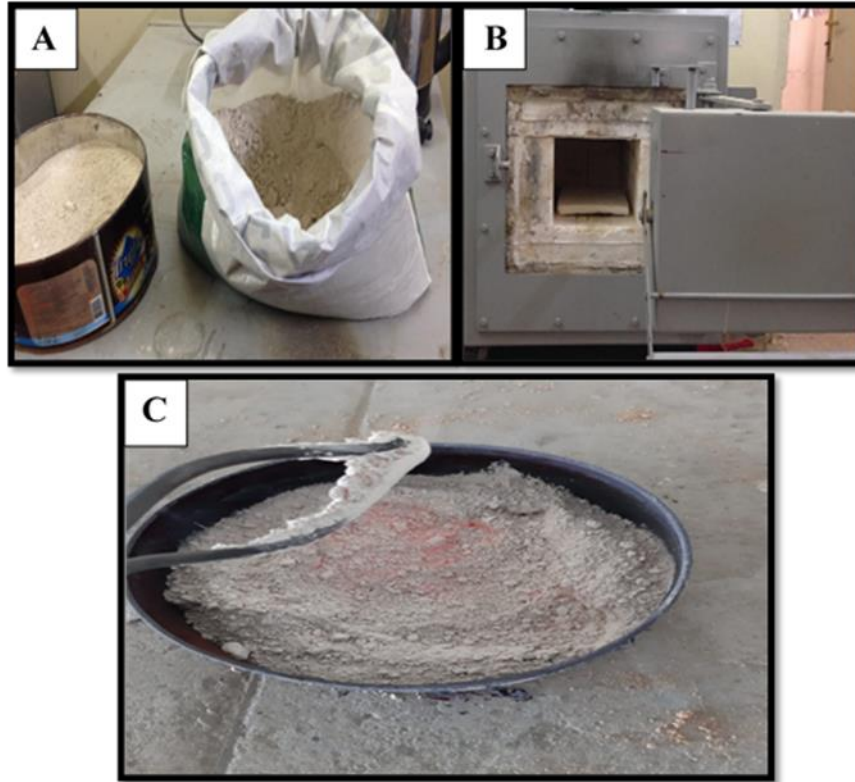
Figure (3-4): Photographs of calcination of kaolinite process. (A) Kaolin clay. (B) Burring oven. (C) Metakaolin(MK).

The clay was firstly washed with water to remove impurities. The upgrading of the clay process was carried out by using an acid leaching process with H_2SO_4 to reduce metal impurities of K_2O, Al_2O_3, Fe_2O_3, CaO, and MgO contents, as shown in Figure (3-5), especially the iron oxides and aluminium oxides content in the final product and followed by water washing.

The leaching process was carried out with a reliable content of (20%) by a variety of acid concentration (2.5%, 5%, and 7.5%). Leaching was performed at room temperature for 4 hours. To remove residual iron content from the ore surface, the leaching process was followed by water washing (Neutralization). Thus (H_2SO_4) has dual functions:

- The first one is to extract impurities from the material; this context (H_2SO_4) is well known its efficiency.

- The second one is to reduce the grain size by erosion, and this process was enhanced the filtration process **[121]**.
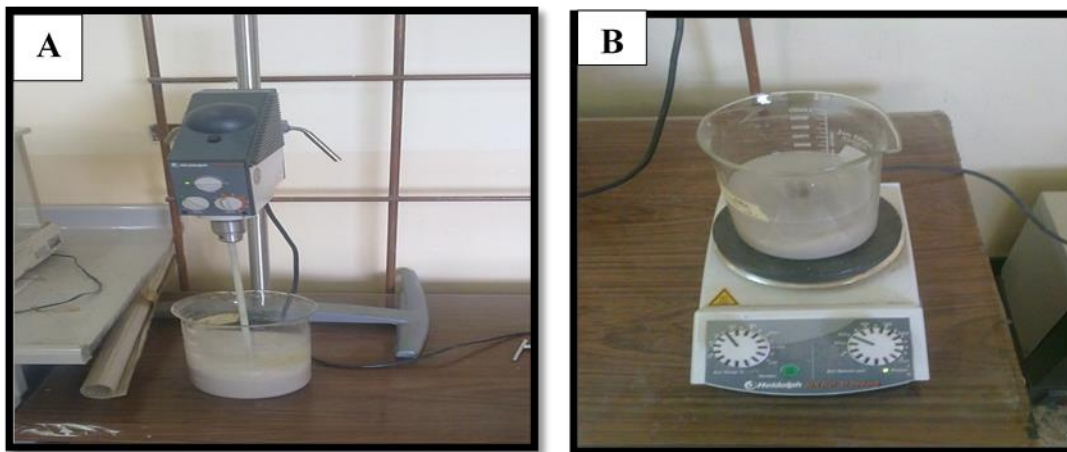
Figure (3-5): Photograph of the leaching process. (A) washing water. (B) added acid process.

3.4.2. Washing (Neutralisation) and Filtration

Metakaolin was washed with distilled water after the leaching process until the PH of water became neutral (PH 7.6), as shown in Figure (3-6).
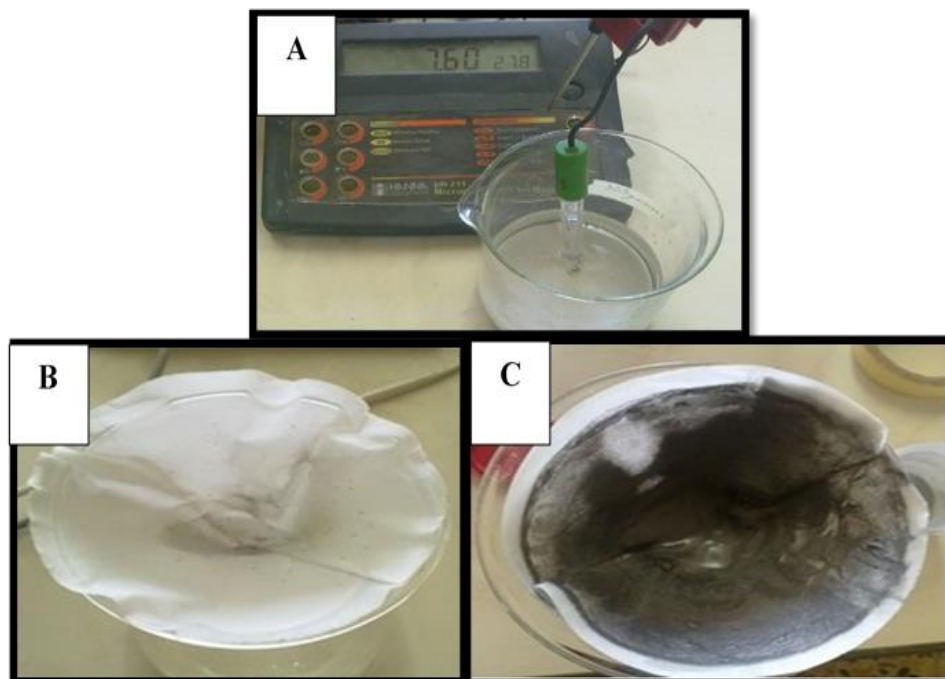
Figure (3-6): Photograph of the neutralisation and filtration. (A) PH measurement. (B), (C) Filtration process.

3.4.3. Drying

After filtration, the samples were dried in the oven at 120℃ for 1 hour, as shown in Figure (3-7). The prepared MK was ready for milling, as shown in Figure (3-8).

Figure (3-7): Drying of metakaolin (MK).
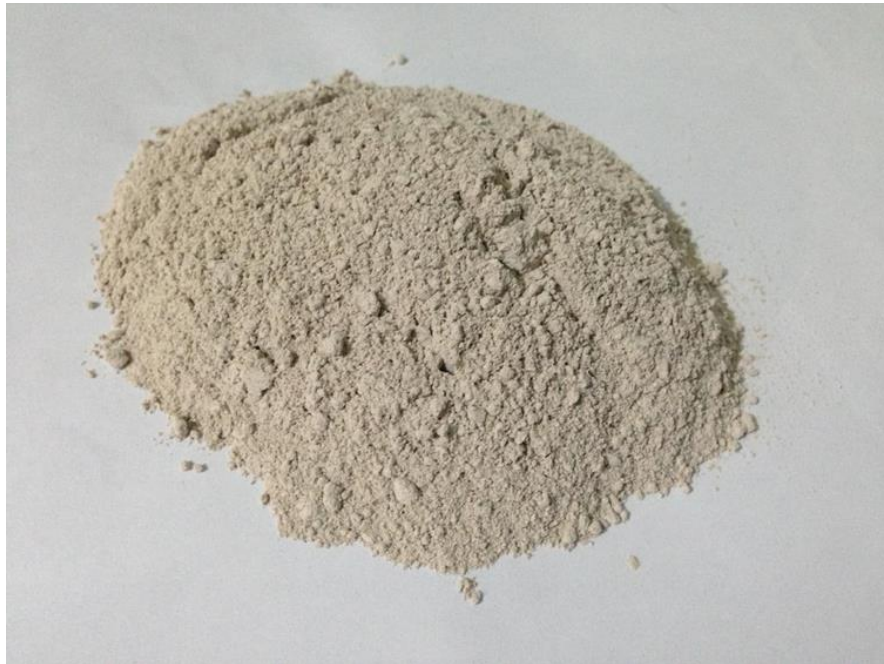
Figure (3-8): Prepared metakaolin (MK).

3.4.4. Ultra Milling by Ball Mill

The high purity MK was grinded to achieved nanoparticles using a dry ball mill with porcelain balls grinding media. This high energy milling is known as one of the "Top-down" nanoparticle type approaches, which generally relies on physical methods for their production. This work was used to reduce the macro and micro-scale of MK to a nanoscale particle size. The high-energy milling processes involve the comminution of bulk materials. The comminution principle is applying physical forces to bulk material to affect breakage into smaller size particles **[122]**.

The clean MK was then inserted into the grinding jar together with the different diameters of grinding balls ranged (10-20) mm and milled for 2 hours. After 2 hours of milling, the clay has sieved for the size below $300\mu m$. The purpose of the sieving step is to remove hard agglomerates that may build up during milling. After the clay has screened, it was again dried in the oven at 120°C for 1 hour, as shown in Figure (3-9) A and B.

The sieving and drying process was reiterated 2 hours of milling until the total milling time reached 40 hours. The screened sizes used were $600\mu m$, $300\mu m$, $140\mu m$, and $100\mu m$. After 10 hours of milling, the ball-milled NC was analysed using Malvern Instruments (Mastersizer2000) analyser for particle size and size distribution **[23]**. Figure (3-9) C and D show ball-milled Metakaolin for 10 hours of milling.
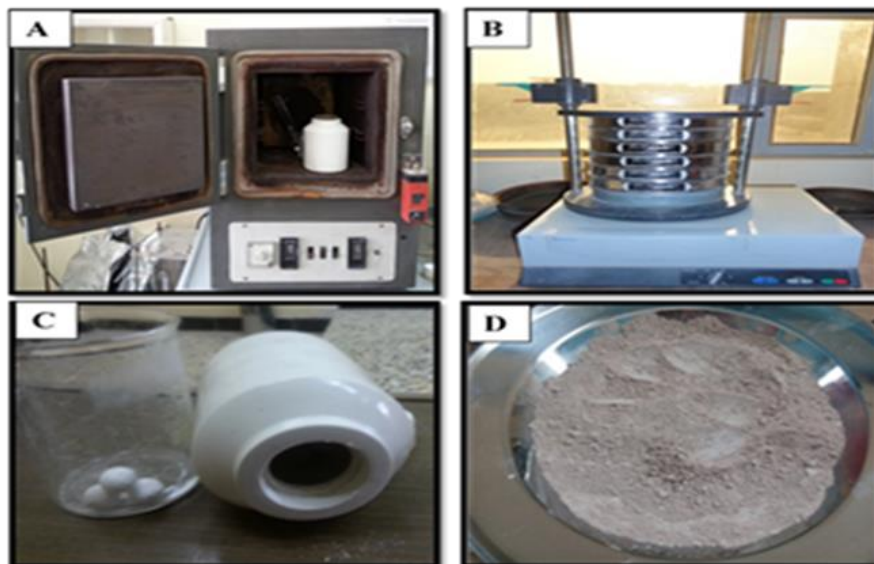
Figure (3-9): (A) drying (B) meshing process of ball-milled NC.
(C) Jar mills (D) prepared ball-milled NC.

3.4.5. Parts of Equipment for Milling

A. Jar Mills

These Jar mills are cylinders in shape with a capacity of about (0.5 to 2.0) liters. The jars carry on the batch and the milling media, so the milling media does the grinding. Jar mills are usually rotated on mill racks rather than with a single drive **[123]**.Figure (3-10) A shows jar mills and porcelain ball mills.

B. Ball Mills (Milling Media)

In general, high-density and different diameters balls give better results because of the high impact forces on the powders. The balls should be denser than the material to be milled. The best media shape is spheres to obtain best grinding efficiency. It has been predicted that the highest collision energy can be obtained if balls with different diameters are used **[124]**. Figure (3-10) B shows porcelain ball mills.
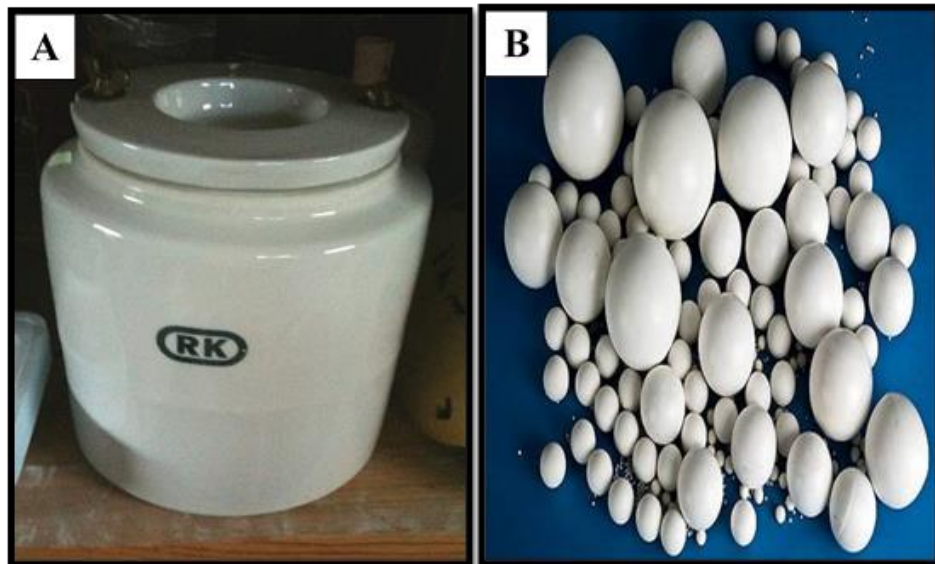
Figure (3-10): (A)jar mills and (B) porcelain media

C. Mill Racks

Laboratory jar mills are usually rotated on a mill rack. The rack is a steel frame with two rollers per tier with usually one to rotated three tiers. On each tier, there are two rollers: a drive roller and an idler. the drive roller is usually driven with a chain and sprocket connected to a gear reduction motor. Since mills come in different diameters, there is

advantageous to have a variable speed drive and a tachometer for each tier. The drive roller must have a force vector pulling down on the mill body, as shown in Figure (3-11).
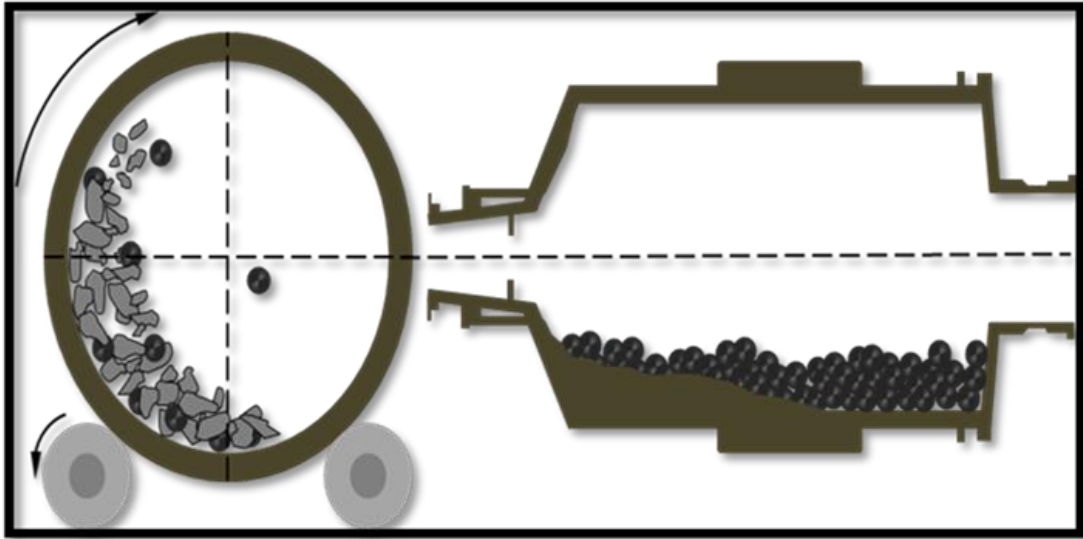
Figure (3-11): Schematic of Jar mills and the rack.

The proper speed is 60-70% of the critical speed. As the mill rotates, the grinding media is subjected into to two accelerations, gravitational force and centrifugal force. When these are equal or centrifugal acceleration is the greater, the media will just ride around and does not do any grinding. Jar mills are filled about half of full with grinding media. While the jar is over filled, there is not enough space for the media to tumble. As well as, if the jar is under filled, there is excessive media wear.

Media that cascades with too much energy can chip or break. These mills use (10-20) mm diameter spheres of porcelain. When the media is too dense, the weight of the media can prevent churning (the action that does the milling). To obtain the desired particle size, the milling time is specified.

Any change in that time will produce a different particle size distribution with a coarser size when the time is shorter and a finer size while the time is longer **[123]**. Figure (3-12) shows the ball milling Equipment (GW, Korea).
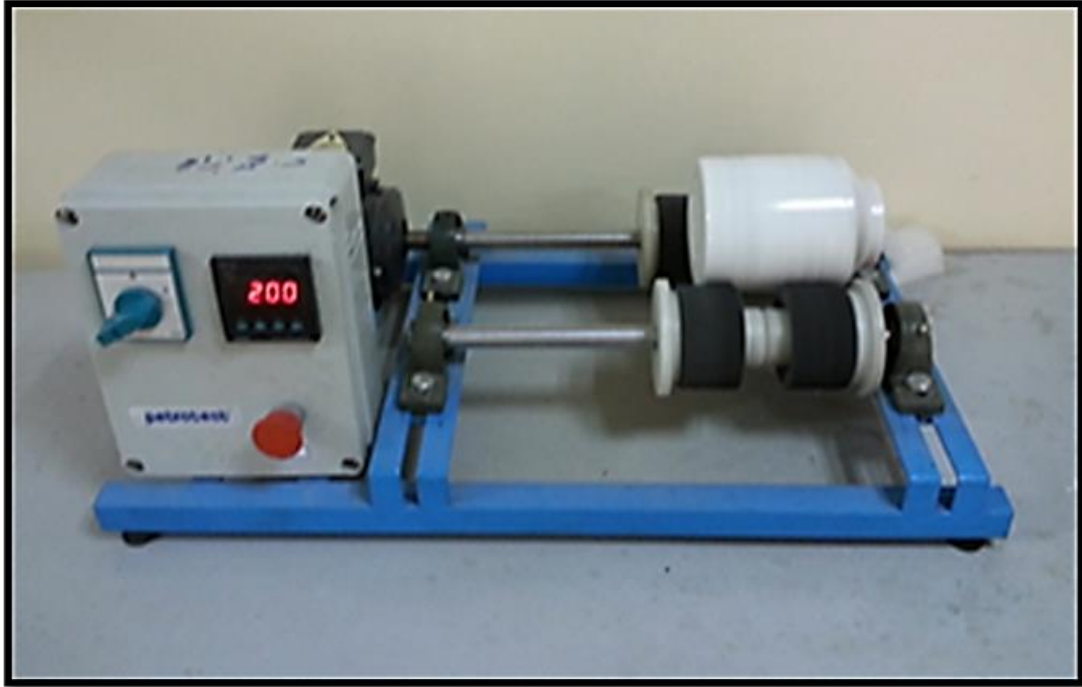
Figure (3-12): Ball milling equipment

3.5. Tests of Materials

3.5.1. X-Ray Diffraction(XRD)

X-ray diffraction (XRD) is a rapid analytical technique primarily used for phase identification of a crystalline material and can provide information on unit cell dimensions. The analyzed material is finely ground, homogenized, and average bulk composition is determined.

Fundamental Principle of X-ray Diffraction (XRD) is depended on Bragg's Law **[125]** that describes how an X-ray beam is reflected or diffracted in a crystal lattice at shown in equation (3.1).

$$n\lambda = 2d \sin \theta. \dots\dots\dots \text{Eq. (3.1).}$$

where **n**: is any integer, **λ**: is the wavelength of the incident-beam X-ray, **d**: is the spacing between crystal planes (d spacing), and **θ**: is the angle between the crystal plane and the diffracted beam (the Bragg angle).

This law relates the wavelength of electromagnetic radiation to the diffraction angle and the lattice spacing in a crystalline powder sample.

XRD patterns are produced by a goniometer, which is rotated at specific angles while bombarding the sample material with X-rays. The diffraction pattern peak intensities are determined by the distribution of atoms within the lattice. The XRD pattern is specific to the periodic atomic arrangements in a given material, which is compared to the ICDD standard database of XRD patterns for phase identification **[126]**. Figure (3-13) shows principle of the X-Ray diffraction test.
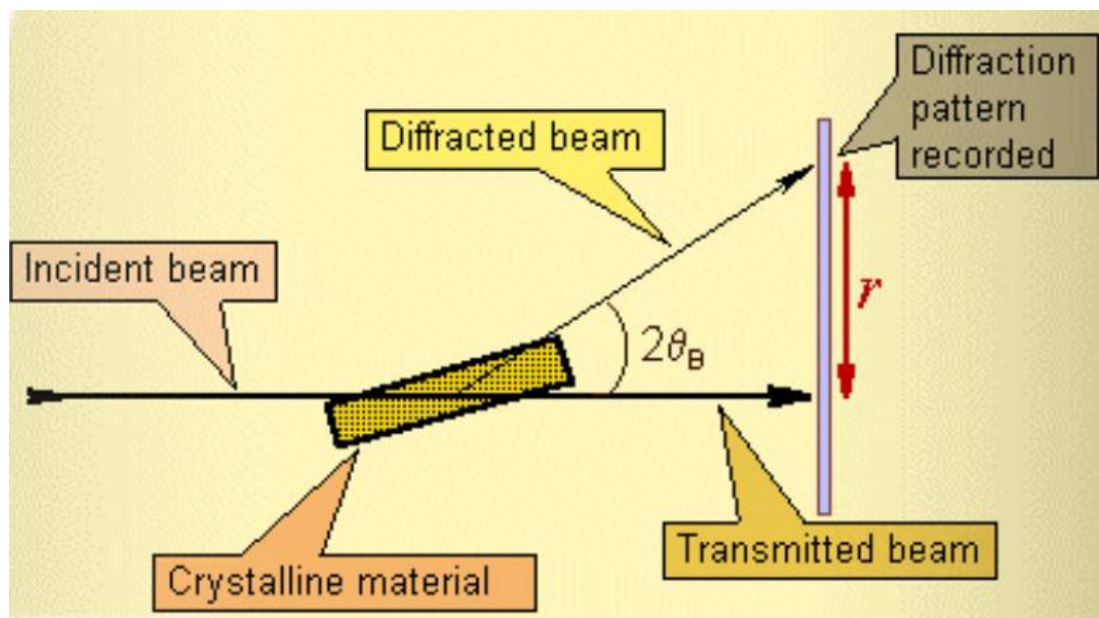
Figure (3-13): Principle of the X-Ray diffraction test [126].

In the current study, X-ray diffraction (type XRD-6000, Shimadzu), scan range is (10.0 – 60.0) deg, scan mode (continuous scan), scan speed (5 deg. / min) was done in the Ministry of Science and Technology/Advanced Materials /, Baghdad / Iraq. The photograph of the XRD machine is shown in Figure (3-14).

Figure (3-14): XRD machine

3.5.2 Energy-Dispersive X-Ray Spectroscopy (EDS or EDX)

EDS is a technique in which characteristic X-rays generated from the electron beam-sample interaction is resolving to supplied the elemental composition of the sample in the form of spectra (histograms). Individual elements can be identified.   Coinciding with any images obtained by SEM, EDS can be used to obtain elemental information about the area of interest. So it uses the same SEM device to get the results of this scan (shown in Figure (3-16)).

3.5.3. Scanning Electron Microscope (SEM) Observations

The scanning electron microscope (SEM) analysis allows us to examine and characterize particles and nanoparticles, fracture surfaces, surface morphologies, composites and their constituents, and microstructures of prepared cross-sections. SEMs use electrons rather than light waves to examine surfaces, permitting much greater magnification, resolving power and depth of field. SEM analysis provides us with high resolution imaging at magnifications up to 300,000X. With the addition of

energy dispersive x-ray spectrometry (EDS), we can simultaneously determine the elemental composition and morphology of different materials **[127]**.

When the electron beam strikes the sample, a large number of signals (shown in Figure (3-15)) are generated. We can divide the signals into two broad categories: electron signals, and photon signals **[128]**.
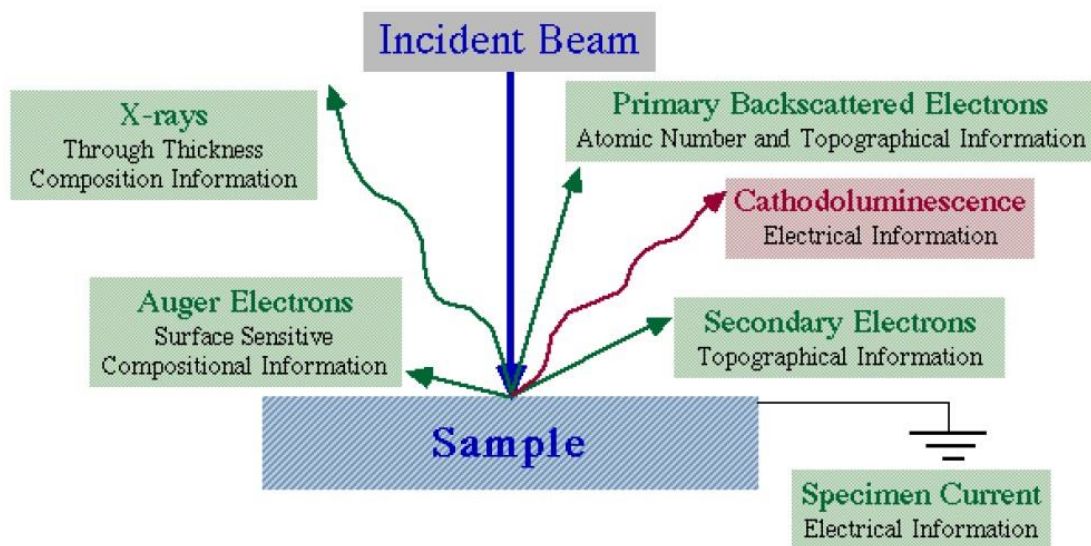
Figure (3-15): The signals generated when electron beam

strikes the sample [128].

Scanning electron microscope (SEM) (Type TESCAN, Vega III/Czech Republic) which is available at the Ministry of Science and Technology/Advanced Materials /Iraq was used in this study. The photograph of the SEM apparatus is shown in Figure (3-16).
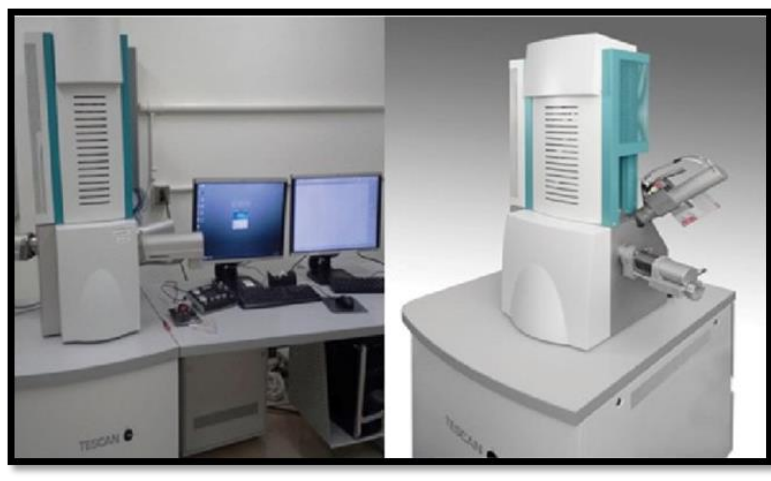
Figure (3-16): SEM (Model number: TESCAN, Vega III/Czech Republic)

3.5.4. Laser Particle Size Analysers (LPSA)

Malvern Mastersizer 2000 is a versatile laser diffraction-based analyser capable of measuring particle size distribution, emulsions, suspensions, and dry powders ranging from 0.02 to 2000 microns. The measurements were conducted at the Ministry of Science and Technology/Advanced Materials /Iraq. The photograph of the (PSA) apparatus is shown in Figure (3-17).

Figure (3-17): Malvern master size 2000

3.5.5. Measurement of The Specific Surface Area(SSA)

The special surface area (SSA) technique for natural particles is an important parameter for the quantification of surface processes such as dissolution and adsorption. The SSA of the prepared NC was determined by surface area analyser (Q Surf 1600, USA) using Brunauer, Emmett, and Teller (BET) method. Figure (3-18) displays a picture of the surface area measurement instrument. The measurements were conducted at the Ministry of Science and Technology/Advanced Materials /Iraq.

Figure (3-18): Surface area measurement instrument

3.5.6. X-Ray Fluorescence (XRF)

The X-Ray Fluorescence (XRF) technique is used for qualitative and quantitative analysis of the elemental composition. The chemical composition of NC is determined using the X-ray fluorescence spectrometry model (LAB CENTER XRF – 1800, Shimadzu). The measurements were conducted at the Ministry of Science and Technology/Advanced Materials /Iraq. The photograph of the XRF apparatus is shown in Figure (3-19).

Figure (3-19): X-ray fluorescence (XRF)

3.6. Materials to Prepare SSC Specimens

3.6.1. Portland Cement

Iraqi Sulfate Resisting Cement (SRC) Type V with the marketable name (Al-Mass) manufactured by Bazyan cement factory was used throughout this investigation. The used cement conforms to the Iraqi Specification No.5/2019 **[129]**. Tables (3-2) and (3-3) show the physical and chemical properties respectively, and Figures (3-20), (3-21) and (3-22) show the cement and its EDS and XRD, that used in this research.
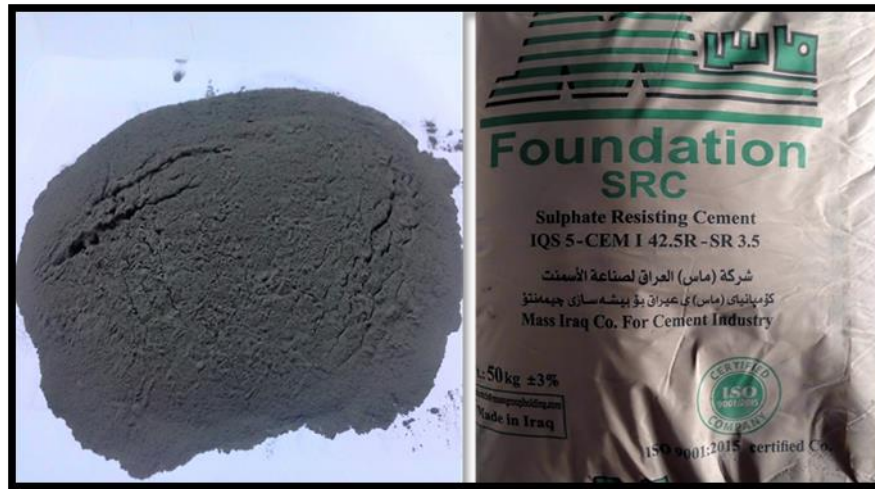
Figure (3-20): Iraqi Sulfate Resisting Cement

Table (3-2): Physical properties of the Sulfate Resisting Cement (SRC)

Physical Property	Test Results	Limits of Iraqi Specification No.5/2019 [129]
Specific gravity (g/cm^3)	3.16	**-**
Specific surface area (m^2/kg)	314	≥ 230
Setting Time (Vicat's Method)		
Initial setting time (minutes)	153	≥ 45
Final setting time (hours)	3.3	≤ 10
Compressive Strength of Mortar (N/mm^2)		
2 days	20	≥ 10
28 days	43	≥ 32.5

Table (3-3): Chemical composition based on (EDS) teste and main compounds of the Sulfate Resisting Cement (SRC)

Element	Oxide	Oxide % by Weight	Oxide % Sigma	Number of Ions	Limits of Iraqi Specification No.5/2019 [129]
O				3.00	
Ca	CaO	67.08	0.54	1.68	-
Si	SiO$_2$	16.25	0.41	0.38	-
Al	Al$_2$O$_3$	3.42	0.25	0.09	≤ 3.5
Fe	FeO	5.84	0.34	0.11	-
Na	Na$_2$O	0.19	0.20	0.01	-
Mg	MgO	2.38	0.22	0.08	≤ 5.0
S	SO$_3$	3.75	0.29	0.07	-
K	K$_2$O	1.09	0.12	0.03	-
Total:		**100.00**		**2.46 (Cation sum)**	
Main Compounds (Bogue's Equation)					
Element	**Oxide % by Weight**				
C$_3$S	51.90				
C$_2$S	31.01				
C$_3$A	8.96				
C$_4$AF	7.98				
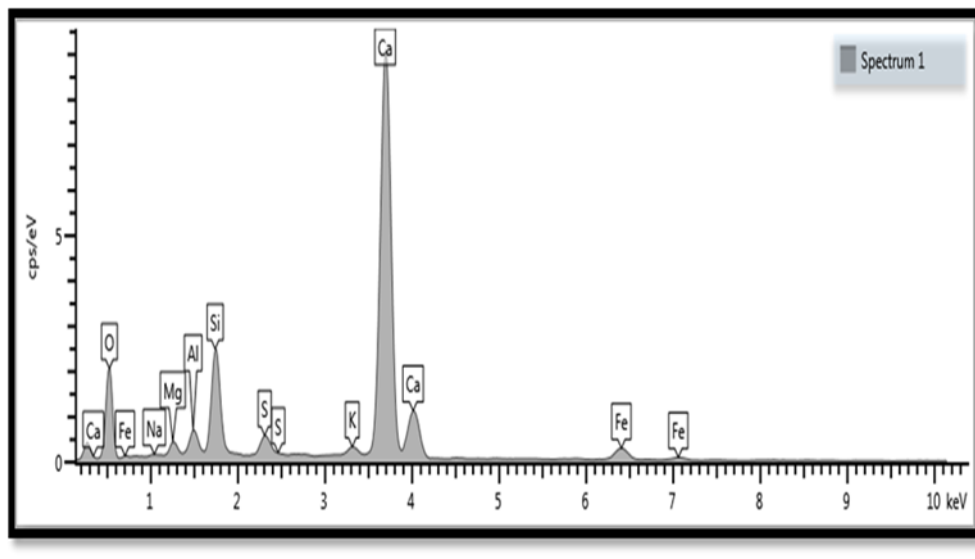
Figure (3-21): Energy-Dispersive X-Ray Spectroscopy (EDS) of Cement Powder (SRC)
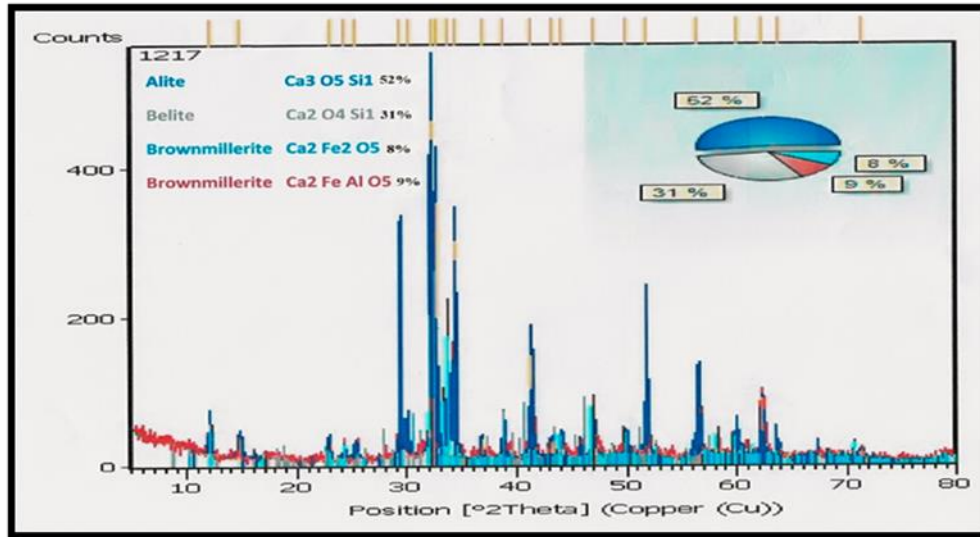
Figure (3-22): X-Ray Diffraction (XRD) of Cement Powder (SRC)

3.6.2 Fine Aggregate

Fine aggregate was used for the AL-Usaila sand factory in Anbar. The grading of sand was compiled the ASTM C33/C33M − 13 **[130],** as shown in Table (3-4) and Figure (3-23)]. The chemical and physical properties of natural sand are explained in Table (3-5) according to ASTM C 128 – 01 **[131]** and ASTM C33/C33M – 13 **[130]**.

Table (3-4): Grading of fine aggregate and specification.

Sieve Size (mm)	% Accumulative Passing	% Accum. Passing According to Limits of ASTM C33/C33M – 13 [130]
4.75	100	95 to 100
2.36	85.1	80 to 100
1.18	70.5	50 to 85
0.60	58.66	25 to 60
0.30	28.41	5 to 30
0.15	7.2	0 to 10
0.075	1.9	0 to 3
Fineness Modulus	**2.5**	2.3 to 3.1

Table (3-5): Chemical and physical properties of natural sand.

Property	Specification	Result	Limits
Specific Gravity (gm/cm^3)	ASTM C 128 – 01	2.54	-
Absorption, %	ASTM C 128 – 01	0.82	-
Material finer than 75µm sieves, %	ASTM C33/C33M − 13	1.15	≤ 3
Sulfate content as SO$_3$,%	-	0.18	-
Maximum particle size mm	-	2.36	-
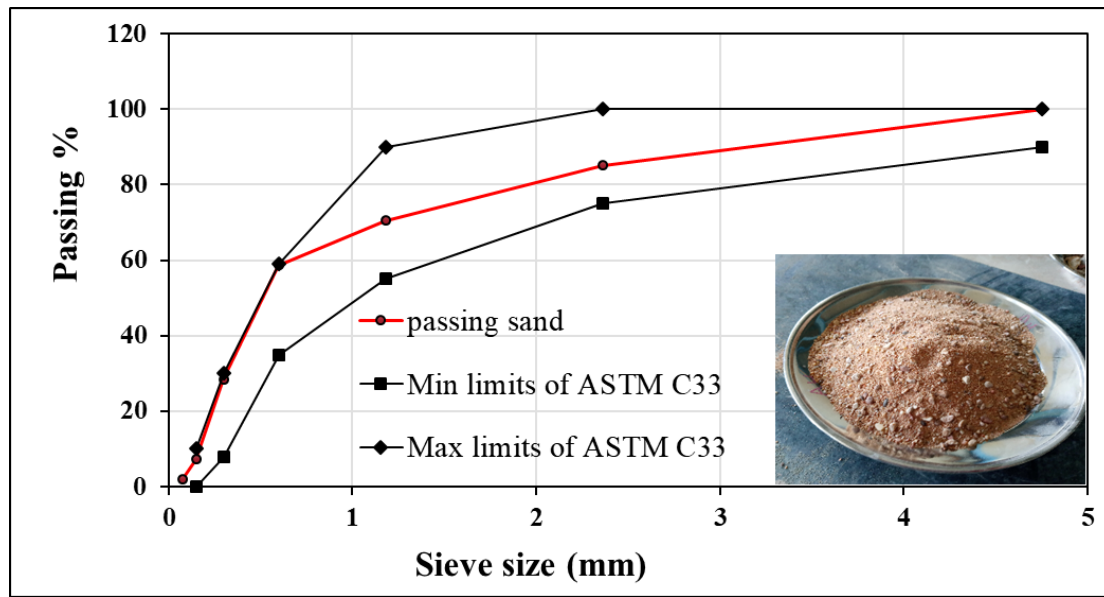
Figure (3-23): Grading curve for fine aggregate

3.6.3 Coarse Aggregate

The coarse aggregate used was with crushed to 12 mm maximum size. It was obtained from the Nebai source. Table (3- 6) and Figure (3-24) show the grading of coarse aggregate, which conforms to the ASTM C33/C33M – 13 **[130]**. Table (3-7) describes chemical and physical properties of natural coarse aggregate according to ASTM C33/C33M – 13 **[130]**, ASTM C128 – 01 **[131],** ASTM C131/C131M−4 **[132]** and ASTM C88-76 **[133] .**

Table (3-6): Grading of coarse aggregate

Sieve Size (mm)	Selected % passing	% passing ASTM C33/C33M – 13 [130]
12.5	100	100
9.5	86.76	85 to 100
4.75	14.12	10 to 30
2.36	0.16	0 to 10

Table (3-7): Chemical and physical properties of coarse aggregate.

Property	Specification	Result	Limits
Specific gravity (gm/cm^3)	ASTM C 128 – 01	2.62	-
Absorption %	ASTM C 128 – 01	0.4	-
Sulfate content as SO_3%	-	0.08	-
Hardness by Los Angeles abrasion test (%)	ASTM C131/C131M – 14	20.56	10-45
Soundness of aggregates by magnesium sulfate (%)	ASTM C 88 - 76	3	≤ 18
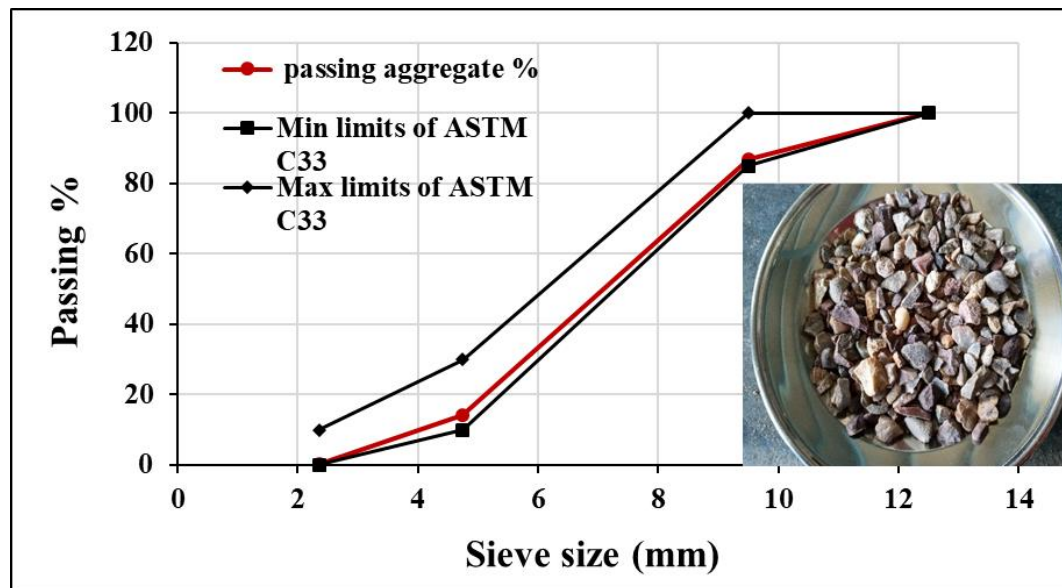
Figure (3-24): Grading curve for coarse aggregate

3.6.4 Water

In this research, drinking tap water was used to mixing and curing all concrete specimens.

3.6.5 Superplasticizer (SP)

High range water-decreasing mixture HRWRA (polycarboxylate) commercially known as (Sika Visco Crete-5930) **[134]** was used. It was satisfied to the ASTM- C494 Types F **[135]**. The properties of this SP was shown in Table (3-8).

Table 3-8: Properties of Superplasticizer (SP).

Properties of Superplasticizer	Effectiveness
Appearance	Turbid liquid
Density	1.095 kg/lt
Chloride content	There is no
PH	7 to 9

3.6.6 Addition of Raw Materials

A. Nano clay (NC)

NC was used at three percentages (2, 4, and 6) % as a partial replacement of cement by weight. The kaolin and metakaolin were examined by XRD and EDS tests, as shown in Figures (3-25), (3-26), (3-27) and (3-28), respectively.
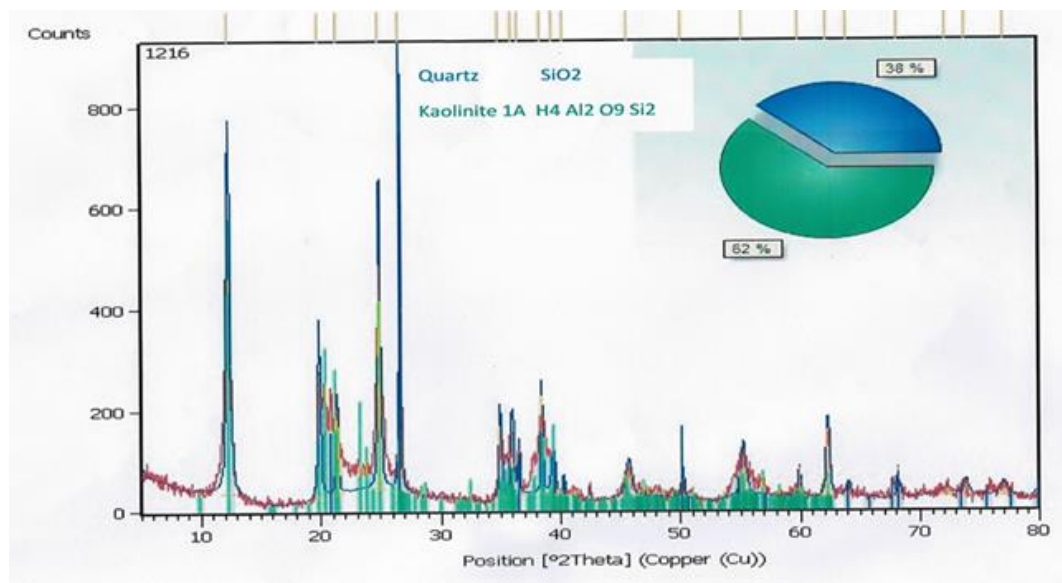
Figure (3-25): X-Ray Diffraction (XRD) of kaolin before burning
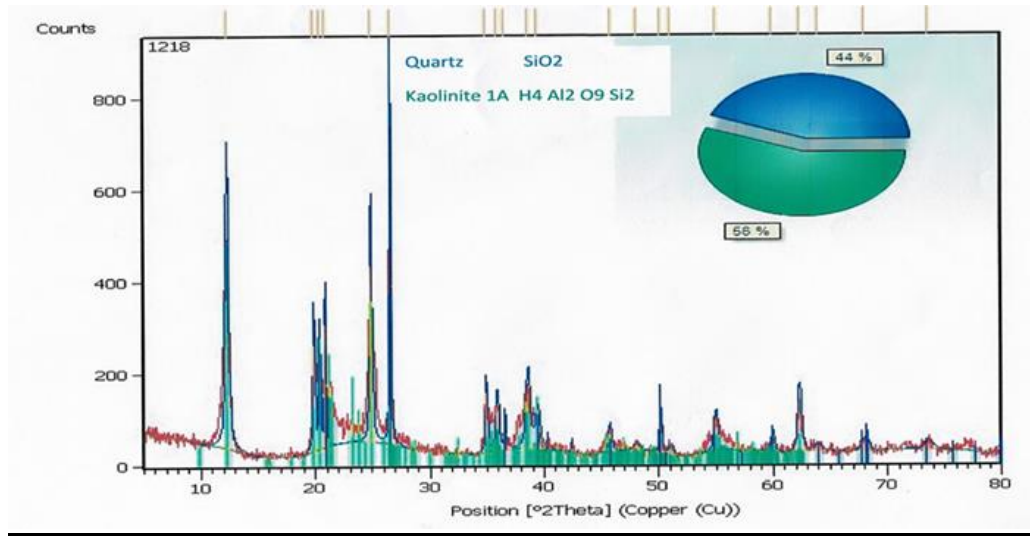
Figure (3-26): X-Ray Diffraction (XRD) of metakaolin (kaolin after burning)
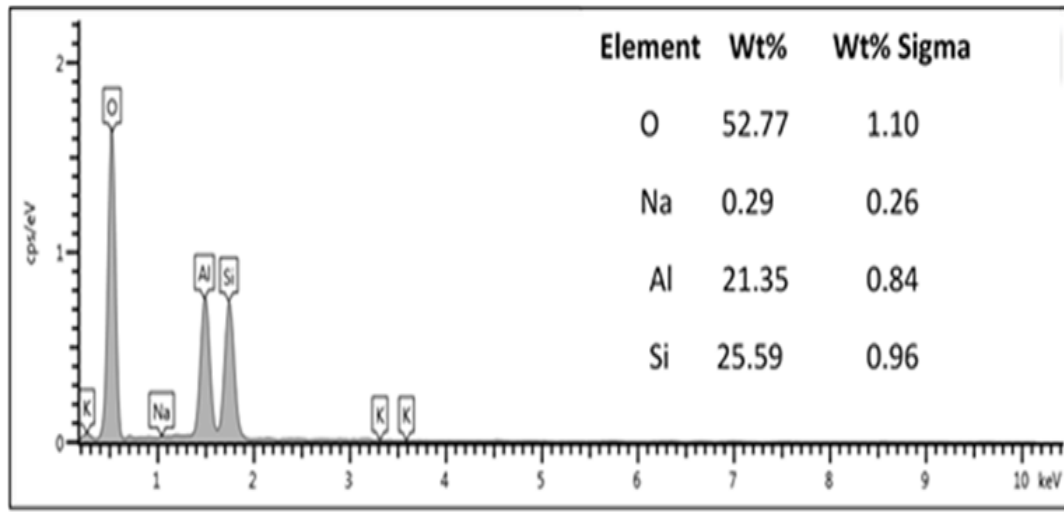
Figure (3-27): Energy-Dispersive X-Ray Spectroscopy (EDS) of Kaolin

Oxide	Oxide %	Oxide % Sigma	Number of Ions
Na2O	0.12	0.17	0.00
Al2O3	41.06	0.59	0.78
SiO2	54.26	0.76	0.87
SO3	0.10	0.25	0.00
K2O	0.62	0.13	0.01
CaO	0.54	0.16	0.01
TiO2	1.72	0.27	0.02
FeO	1.58	0.29	0.02
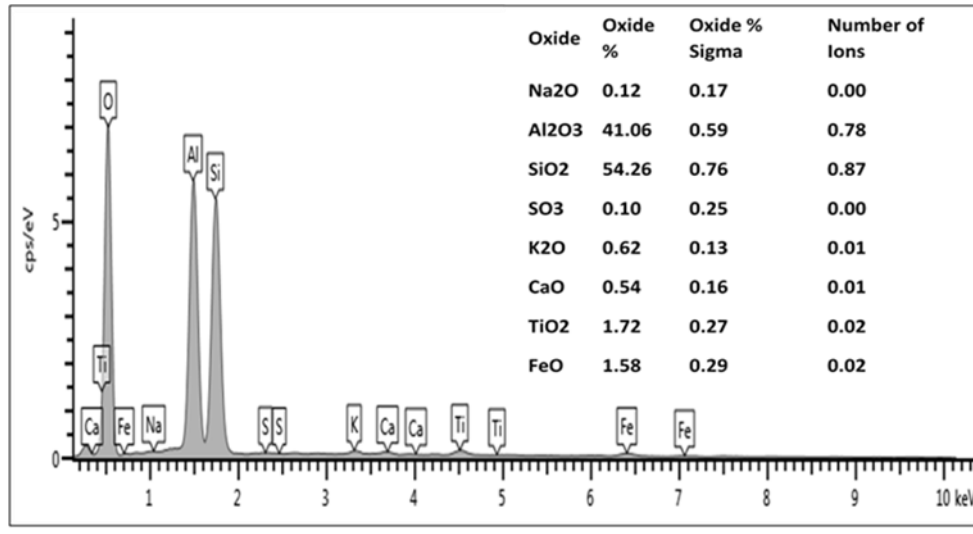
Figure (3-28): Energy-Dispersive X-Ray Spectroscopy (EDS) of metakaolin

B. Limestone (LP)

The limestone particles used in this study were prepared from Al-Qusair located south-west Karbala City, middle of Iraq by product of stone crushing operations. The specific gravity of LP was 2.68 (gm/cm^3), and the particle size was less than 75 microns; thus, it was used in SCC formulation as a partial substitute for cement and micro fillers. Lime, also is known as calcium oxide, is one of the oldest and most vital chemicals in humans. Since then, it has been discovered that heat has turned calcium into a new and different material **[136]**. Therefore, limestone was burned at atemperature700 °C for 2 hours to be transformed to quicklime, as shown in Figure (3-29). The limestone was verified by XRD, EDS and SEM tests, as shown in Figures (3-30), (3-31), (3-32), (3-33), (3-34) and (3-35), respectively.

In this study, various LP ratios are used with Sulfate Resisting Cement (SRC) containing 450 kg/m^3. The limestone contents by weight are 0%,16%, 23.4% and 29% for production of SCC samples.
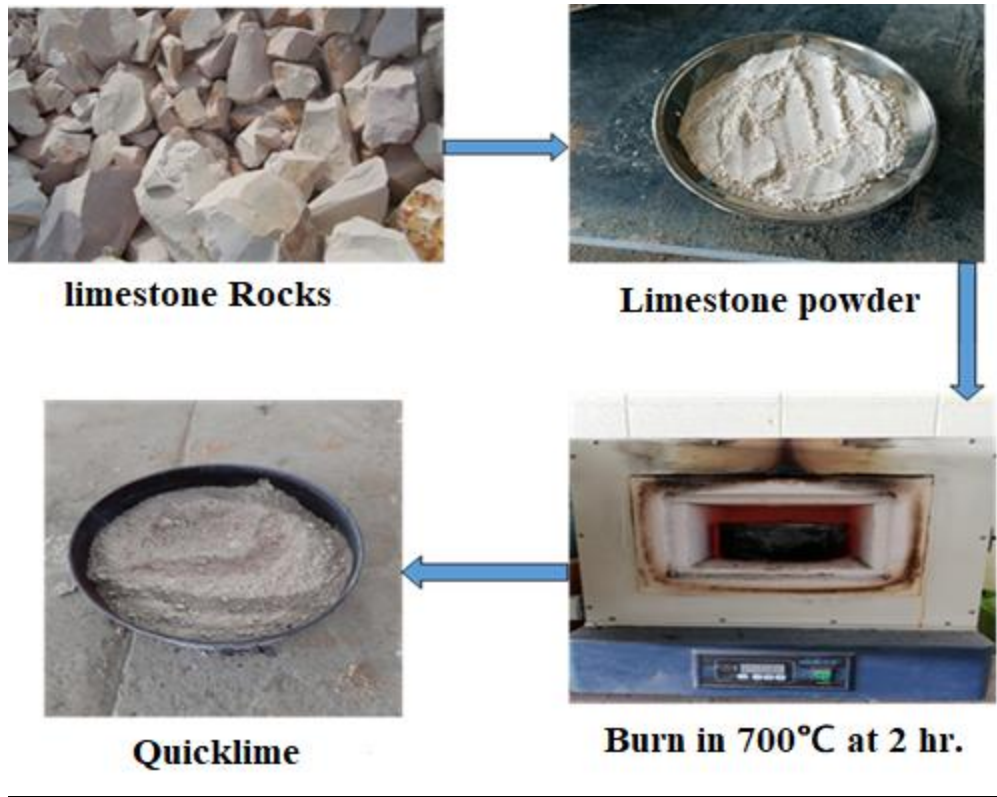
Figure (3-29): Limestone burning process
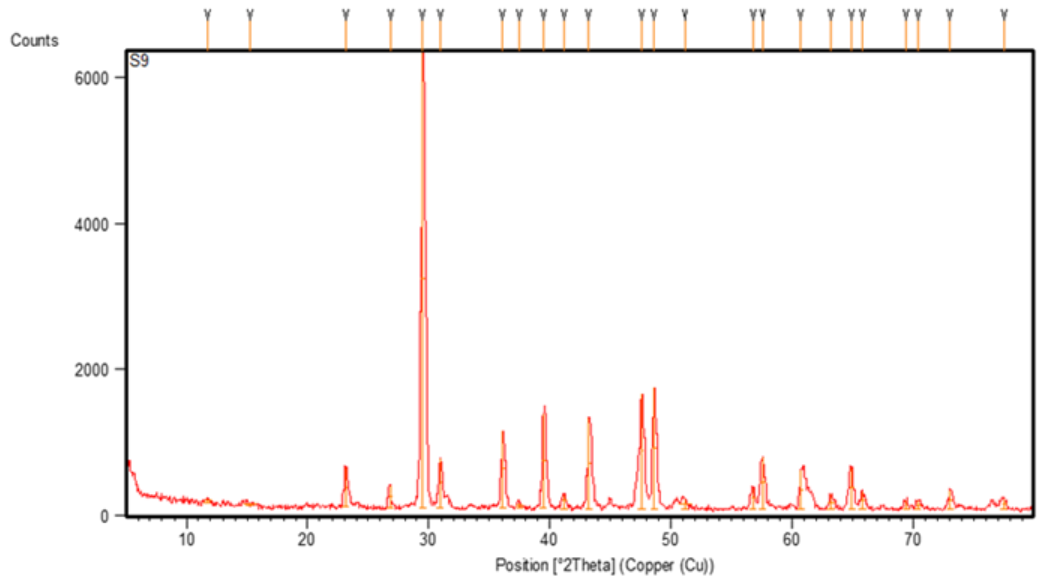
Figure (3-30): X-Ray Diffraction (XRD) of limestone before burning
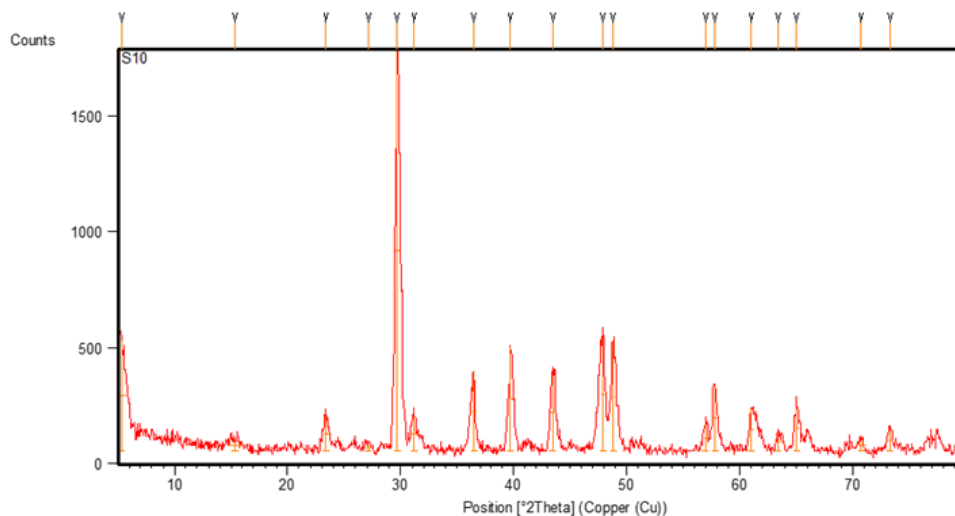
Figure (3-31): X-Ray Diffraction (XRD) of limestone after burning

Element	Wt%	Wt% Sigma
Co	57.1	1.0
O	30.4	0.9
C	11.3	0.7
Si	1.1	0.3
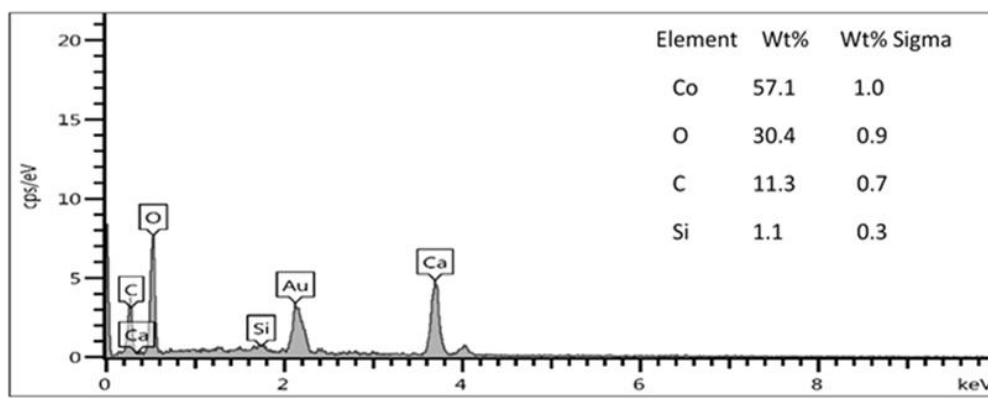
Figure (3-32): Energy-Dispersive X-Ray Spectroscopy (EDS) of limestone before burning

Element	Wt%	Wt% Sigma
Co	43.2	1.5
O	29.1	1.2
C	13.0	0.9
Si	1.5	0.3
Mo	7.7	2.0
Mg	4.6	0.4
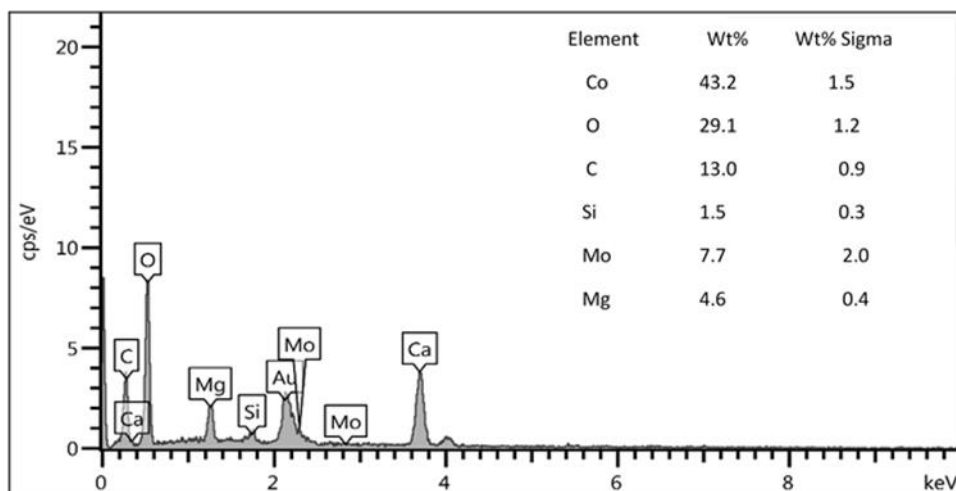
Figure (3-33): Energy-Dispersive X-Ray Spectroscopy (EDS) of limestone after burning
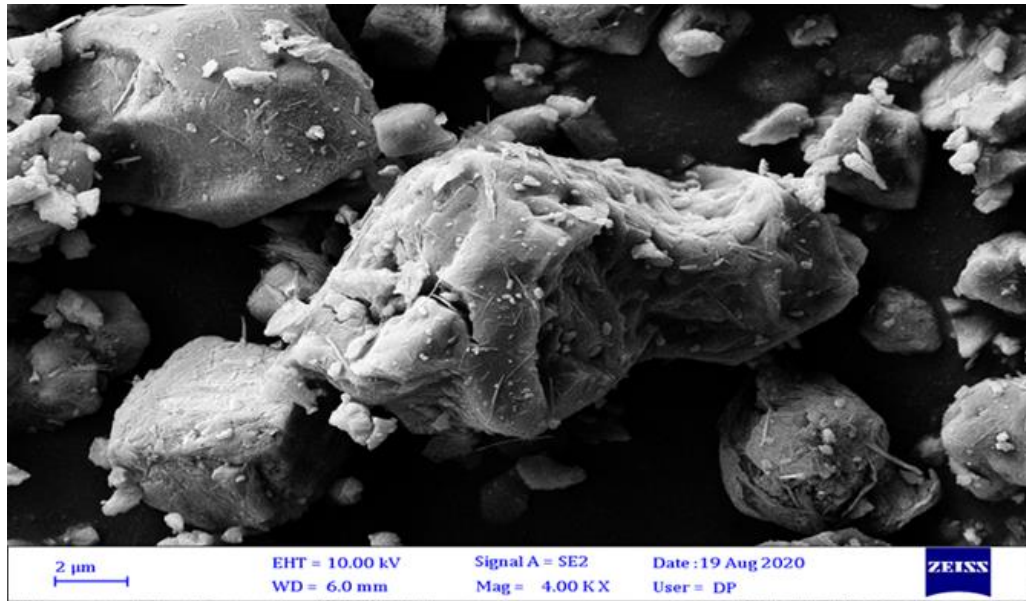
Figure (3-34): Scanning Electron Microscope (SEM) of limestone before burning
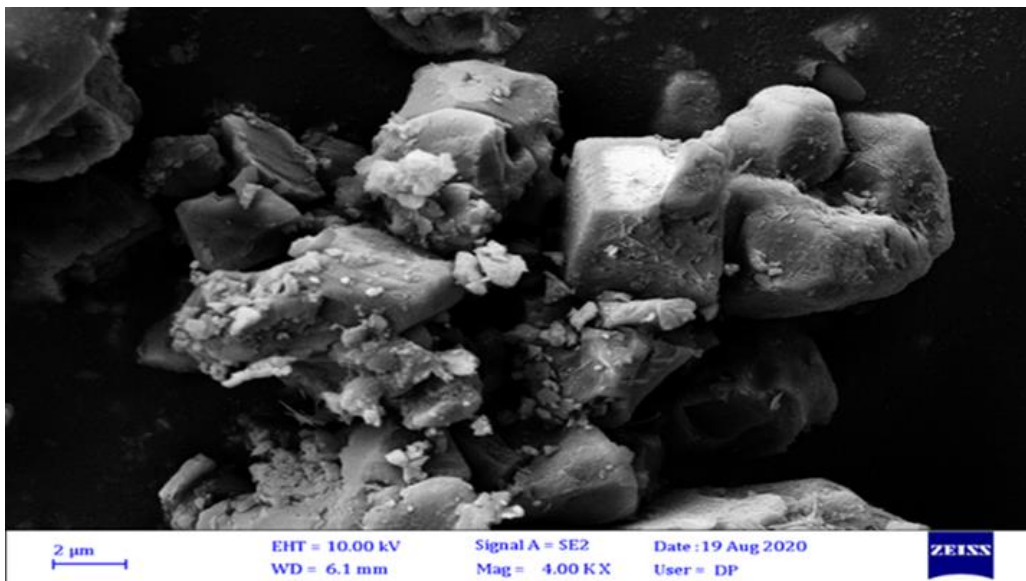
Figure (3-35): Scanning Electron Microscope (SEM) of limestone after burning

3.7. Experimental Program to Prepare SCC Mixtures

3.7.1. Mix Design

Design methods of SCC can be divided into six groups based on different principles and parameters, including empirical design method, statistical factorial design method, strength-based design method, rheology of paste method, particle packing method, and

SCC mixture design method. The development of SCC mixtures is not an easy process, and none of these methods provides all the objectives or parameters for ensuring the requirements. Any of the above models achieve robustness and durability while others are better with regard to the technical characteristics of SCC. The SCC development model or method should therefore be chosen in terms of requirements and application. There are no standard codes for the mix design of self-compacting concrete except for a few methods developed by researchers and many institutions **[137].**

The mix design should be satisfied the requirement of a standard containing workability and strength SCCs.The strength of the SCC is given by the aggregate binding of the SCC paste in hardened conditions. In contrast, the binding paste gives the SCC's workability at a fresh state **[138]**.

In this research, the European Self-Compacting Concrete Guidelines (EFNARC-2005) **[28]** which represented a state-of-the-art document addressed to those specifications, designers, manufacturers, and users who wish to develop their knowledge and usage of conventional concrete to design control SSC mixture and all following mixes could flow it. Two mixtures were tested with different values of sand, aggregate contents, w/c, and SP to achieve the desired workability using the standard slump test and strength by comparison results obtained in compressive strength tests from these mixtures at 7 days. The trials to produce a control mixture are presented in Table (3-9).

The control mix would use which had a higher slump flow diameter (SFD) (800mm) and a higher compressive strength (58.46 MPa), that would suit the requirement for SCCs, with different types of pozzolan materials includ Nanoclay and limestone.

Table (3-9): Trials mixture of the control mix of SCC

No. Trail	S.R.C kg	F.A kg	C.A kg	W kg	SP kg	SFD mm	T_{500} sec	Comp. Strength.at 7 days(MPa)
T-1	450	930	870	165	8	700	3.4	56.65
T-2	450	915	885	170	10	800	2.19	58.46

Where **: C**: Iraqi Sulfate Resisting Cement, **F.A**: Fine Aggregate, **C.A**: coarse aggregate. **W**: drinking water, **SP**: Superplasticizer, **SFD**: slump flow diameter, T_{500}: slump flow time,

3.7.2. Accelerated Pozzolanic Strength Activity Index of Nano clay (NC)with Portland Cement

The strength activity index with portland cement test is used to determine if natural pozzolan results in an acceptable level of strength development when used in concrete with hydraulic cement[139]. The accelerated pozzolanic index of NC has been determined as per ASTM C 311 – 04 **[139]**.

To determine the compressive strength, four mixes mortar were perpetrated,control mix and three mixes morter at three percentages of NC (2 , 4, and 6) % as a partial replacement by weight of Sulfate Resisting Cement (SRC) at ages of 7days as specified in test method ASTM C109 **[140]**.

They were cast in steel moulds cubes (50x50x50) mm and covered to prevent the loss of water during the first 24 hours, then stored in water at room temperature. After 7days of demolding control and test mixtures, the mortar cubes' compressive strength was determined, and the average of the three control mixture samples and the three specimens of each of the test mixtures is reported.

The Equation (3-1) was used to calculate the strength activity index with portland cement **[139]** as follows:

Strength activity index with portland cement = (A / B) x 100 …….Eq (3-1)

where: **A** : average compressive strength of test mixture cubes (MPa) , and

B : average compressive strength of control mix cubes (MPa).

 The activity index was 7% and 3% higher than the control at 4% and 6% NC, respectively. Table (3-10) gives the pozzolanic activity of the control and test mixtures.Figure(3-36) shows the compressive strength test.

Table (3-10) : Accelerated pozzolanic index (AP I) for Nano clay .

Mix ID	Standard Sand (gm)	Water (gm)	S. R.C. (gm)	NC (gm)	Comp. Strength at 7 days (MPa)	(%) of Cont.	Limit ASTM C 311 – 04 [139]
Control Mix	660	88	220	0	42.71	100	-
Mix 2% NC	660	88	215	4.4	42.17	99	> 75
Mix 4% NC	660	88	211.2	8.8	45.54	107	> 75
Mix 6% NC	660	88	206	13.2	44.17	103	> 75

Figure (3-36): Casting and Compressive strength test for NC.

3.7.3. Specimen Preparation and Curing

To achieve this research's goals, three groups were prepared and investigated with a total number of 10 concrete mixes. Table (3-11) illustrates the mixes design of all mixes. The mixes were divided into three groups representing the key variables in the experimental study. The first group was designed using different prepared Iraqi Nano clay ratios as a cement replacement with percentages of 2, 4, and 6%, respectively.

The second group with different quantities from quicklime that would add to SCC mixtures include (50, 75, 100) kg by weight of cement. The third group with a hybrid mix between 4% Nanoclay (NC) and quicklime (QLP) quantities. The experimental mold consists of 74 specimens for each mix distributed to cubs (100 x 100 x 100) mm, prisms (100 x 100 x 400) mm and cylinders {(100 x 200), (150 x 300)} mm. After preparing all ingredients needed, they were weighed using digital balance according to the proportions designed for each mixture, while standard moulds were prepared and oiled simultaneously. To prevent the adhesion of dry materials, the sides of the used mixer were cleaned and moistened with a horizontal basin and its capacity 0.07 m^3.

Table (3-11): Self compacting concrete mixes design.

Mix ID	Sand (kg)	Gravel (kg)	Water (kg)	S P (kg)	S.R. Cement (kg)	NC (kg)	QLP (kg)
Control Mix	915	885	170	10	450	0	0
SCC 2%NC	915	885	170	10	441	9	0
SCC 4% NC	915	885	170	10	432	18	0
SCC 6% NC	915	885	170	10	423	27	0
SCC 50 QLP	915	885	170	10	391	0	50
SCC 75 QLP	915	885	170	10	361	0	75
SCC 100 QLP	915	885	170	10	331	0	100
SCC 4% NC+50 QLP	915	885	170	10	375.36	15.64	50
SCC 4% NC+75 QLP	915	885	170	10	345	14.44	75
SCC 4% NC+100 QLP	915	885	170	10	318	13.24	100

The mixing process was carried out in several stages:

1- Nano clay Group:

One of the most critical points is putting the nanomaterials in concrete mixes, keeping their original composition and physical characteristics from any change. Nanoparticles are very active and that they will be gathered, producing a larger particle size after putting it in water, thus using a dispersion technique to keep the particles in nano size.

In this research, a wet mixing technique was applied using a mixer motor where nanoparticles were mixed for two minutes with part of the mixing water until the mixture became homogeneous, then slowly added to the concrete mix. The coarse and fine aggregate was put in the mixer firstly, then cement was added, and mixed for 30sec. The part of the mixing water would then be added to the mixture. Simultaneously, the Nano clay water was added to the mix in the automatic mixer for 2 min. The superplasticizer was dissolved with the rest of the water quantity according to the prescribed dosages. It then gradually adds to the mixture, and the mixture continues for another three minutes to ensure the superplasticiser's complete dissolution.

2- Quicklime(BPL) Group:

Mixing cement with quicklime at the required quantity and dry state using a trowel for a suitable time, was done to obtain the best dispersion for QLP in the dry mix. The coarse and fine aggregate were placed in the mixer, and added cementation materials (cement + QLP), after that mixed for 1 minute, then applied 50 % of the mixing water to the mixture gradually. The remaining water was used with superplasticizer to ensure its dissolution, then applied to the mixture and mixed for another 3 minutes to ensure that the superplasticizer was completely dissolved. Figure (3- 37) shows mixing materials and concrete mixer.

Figure (3-37): Mixing materials and concrete mixer.

After finishing the mixing process, the casting process was done. The moulds were covered with polyethylene sheets to avoid cracking of plastic shrinkage, and they were kept in the laboratory for 48 hours. Then the samples were demolded carefully and immersed in water for curing until the time of the test. Figure (3-38) shows samples inside and outside of the water basin for the curing process.

Figure (3-38): [A] Casting of samples, [B] Covered of samples with polyethylene sheets, [C] Curing of samples.

3. 8. Test Methods

3.8.1. Fresh Properties Tests

Characteristics of fresh Mixes tests have been classified according to the EFNARC procedure **[28].**

3.8.1.1. Slump Flow Diameter Test

In the absence of obstructions, the slump-flow diameter and T_{500} time is a test for determining the flow ability and flow rate of self-compacting concrete. It is based on the slump flow diameter test defined in BS EN 12350-8-2010 **[141]**. The result is an indicator of the self-compacting concrete ability to fill. The T_{500} time also represents a measure of velocity of flow and hence the viscosity of the self-compacting concrete **[28]**. It is the most commonly used test, and it doesn't indicate the ability of the concrete to pass between reinforcement only, but may give some indication of resistance to segregation by noticing the extent of the aggregate particles spread in the center and edges of the spread concrete.

A flow table was used with a smooth surface at dimensions (1m x1m) that had circles of 200 and 500 mm diameters coinciding with the center of the plate, slump test cone, funnel, metric tape measure, stopwatch, spirit level tool and sample container. The flow table was wetted, after installed, and insured the surface tropical. Then the cone was placed in the flow table center, and filled without rodding. Allowed the filled cone to stand for no more than 30 secs; then any spilt concrete was removed from the flow table during this time. After that, in one movement, the cone was vertically lifted without interfering with the concrete flow.

The time from lifting the slump cone to the moment the concrete reaches 500 mm in diameter represents T_{500}. While this, the diameter of the slump flow can be determined by using Equation (3-2) to measure the mean of two horizontal perpendicular diameters d1 and d2. Figure (3-39) the shows steps of the slump flow test for SCC.

The upper and lower limits of slump flow classes (SF) shall be classified as 550 mm to 650 mm (SF1), 660 to 750 mm (SF2), and 760 to 850 mm (SF3) based on the EFNARC provisions.

$$SFD = \frac{d1+d2}{2} \qquad \text{…………Eq (3-2)}$$

Where; d_1: largest diameter of flow spread (mm), d_2: flow spread at 90° to d_1, **SFD**: slump flow diameter (mm).

Figure (3-39): Slump flow test for SCC

3.8.1.2. V-Funnel Test

The V-funnel test is used to evaluate the plastic viscosity, risk of blocking and filling ability of self-compacting concrete with a maximum coarse aggregate size of 25 mm or less by determining the V-funnel flow time for it. It is based on the V-funnel test defined in BS EN 12350-9-2010 **[142]**.

In this test, the funnel and the bottom gate were cleaned and oiled the entire inside surface, including the gate. The gate then was closed and poured about 12 liters of the concrete sample into the funnel, without any rodding after that the container was put under the funnel to retain the concrete to pass. After 10sec from filling the funnel, the gate was opened and measured the t_v time, from opening the gate to first seeing through the funnel vertically into the container below. The time of the V-funnel flow is t_v. Figure (3-40) shows the V-funnel test for SCC.

Figure (3-40): V-funnel test for SCC.

3.8.1.3. L- Box Test

The L-Box test asserts SCC 's ability to fill and pass through which subjected to reinforcement blocking, and serious lack of stability (segregation) can be observed visually. Subsequently, sawing and inspecting sections of concrete in the horizontal section may also detect segregation. The test is generally used which is suitable for laboratory and perhaps site use. It is based on the L-Box test defined in BS EN 12350-10-2010 **[143]**.

The apparatus level was set to firm ground and ensure that the sliding gate would open easily and then close it after inside surface was oiled of the apparatus. the vertical section of the apparatus was filled with the concrete mix, then was left it to stand for 1 minute, about 14 liters of concrete needed to perform the test.

The sliding gate was then raised, and the concrete was allowed to flow into the horizontal section. As the concrete starts moving, the distances "**H1**" and "**H2**" are determined. The blocking ratio of **H2 / H1** was calculated. If the concrete flows as freely as the water, it will be horizontal at rest, so **H2 / H1=1**. Whenever, the blocking ratio test value   was nearly to one, the flow of concrete was better. Figure (3-41) shows the steps of the L-Box test for SCC.

Figure (3-41): L-Box test for SCC.

3.8.1.4. Sieve Segregation Resistance Test

Resistance to segregation refers to the ability to retain the coarse components of the mix and maintain homogeneous material. Stability depends primarily on the cohesiveness and viscosity of the concrete mixture, which can be improved by decreasing the amount of free water and increasing the fines **[144]**. It is based on Sieve Segregation Resistance test defined in BS EN 12350-11-2010 **[145]** .

This test records the mass of the materials, passing through a sieve 5mm size after a standard period. Sieve with 5mm square opening, flat balance platform (0.01 kg accuracy), timer, and container for the sample are used as tools for this test. 10 L (+/-0.5) of fresh concrete is poured into a sample container for 15 minutes. Then, about 5 kg of concrete is poured in the sieve from a height of 500 mm. After 120 secs later, the sieve is lifted vertically without agitation, the weight of the concrete mortar that passed through the sieve is recorded, and is divided by the poured quantity weight. Figure (3-42) shows the sieve stability test. Therefore, in some situations, the mixtures that suffer from segregation may be passed through the sieve by a high amount of mortar. It indicates the high risk of separation into a poured concrete. The segregation index (SI) was calculated by using Equation (3-3):

$$SI = \frac{M_{pass}}{M_{total}} \times 100 \qquad\qquad …………Eq\ (3\text{-}3)$$

Where **SI**: segregated index, **M$_{pass}$**: mass of passed materials (gm), and **M$_{total}$** :initial mass of placed on the sieve (gm).

Figure (3-42): Sieve segregation resistance test for SCC.

3.8.1.5. Fresh Density Test

The engineer is interested in the density of both fresh and hardened concrete for many reasons, including its effect on durability, strength, and permeability resistance. This test method includes the determination of density of freshly mixed concrete. According to ASTM-C138 / C138 M − 14[146], Figure (3-43) shows the fresh density test for SCC. The fresh density can be determined by using Equations (3-4).

$$D_{fresh} = \frac{W_C}{V_m} \qquad\qquad …………Eq\ (3\text{-}4)$$

Where:

W$_C$: mass of fresh concrete (kg), **V$_m$**: volume of the casting mold (m^3) and **D$_{fresh}$**: fresh density (kg / m^3).

Figure (3-43): Fresh density test for SCC

3.8.2. Physical Tests of Hardened Concrete

3.8.2.1. Ultra Pulse Velocity (UPV) Test

This test is non-destructive test and it is done by an ultrasonic pulse velocity method to evaluate the quality of concrete **[147]**. The technique consists of measuring the travel time of an ultrasonic pulse that passes through the tested concrete. Comparatively higher velocity is achieved when the quality of the concrete is good in terms of density, uniformity, homogeneity, etc. This test was performed using a device (CONTROLS) based on the procedure described in ASTM C597-09 **[148]**, as shown in Figure (3-44). The test's principle depended on calculating the time of passage of pulse in concrete at a distance L to evaluate the velocity of the pulse (UPV) value. The contact surface should be dried, cleaned and grease-lubricated to ensure wave transmission from the transmitter to the concrete at high accuracy. Average of two specimens measured at ages of (7, 28, 56, 90 and120) days for each mixture. The Equation. (3-5) for calculating the velocity of the pules:

V= L/T 　　　　　　　　**…………Eq (3-5)**

Where; **V:** ultrasonic pulse velocity UPV value (km/sec), **T:** transit time (μs), and **L:** path length of the sample (mm). This test gives the possibility of determining the

concrete quality based on the longitudinal pulse velocity **[149]**, as shown in Table (3-12).

Figure (3-44): UPV test for SCCs

Table (3-12): Quality limits of concrete according to UPV test [149]

Quality of Concrete	Longitudinal Pulse Velocity (km.sec⁻¹)
Excellent	≥ 4.5
Good	3.6 - 4.5
Questionable	3 – 3.6
Poor	2.1 - 3
Very Poor	≤ 2.1

3.8.2.2. Dry Density

The test was conducted following the ASTM C138 **[146]**, based on equation (3-6) determines the density of solid concrete cubes (100 x 100 x 100) mm. The dry density test for SCC is shown in Figure (3-45).

$\rho = M_c / V_c$ **…………Eq. (3-6)**

Where:

ρ: dry density (kg/m^3), M_c: mass of concrete (kg) V_c: volume of concrete (m^3).

Figure (3-45): Dry density test for SCCs

3.8.2.3. Volume of Permeable Pores (Voids)

In this work, ASTM C642 **[150]** was adopted to recognize the voids in a hardened SCC. The specimen was a cube with (100 x 100 x 100) mm. Form each SCC mixture, a total of 8 cubs have been prepared. The testing of samples was carried out at the age of 28, 56, 90, and 120 days. The voids of each SCC mixture on two specimens was calculated as an average of measurements. The test procedure for testing voids in hardened SCC is summarized as follows:

1- At 110 °C for 24 hr., the specimens were dried in an oven until stable weight. They were then weighted on oven-dry specimens to get their respective mass (**A**).

2- The samples were subsequently submerged in water for 48 hr. Then after, the specimens were wrapped with a dry towel when they were removed from the water to avoid any moisture on the samples' surface. The mass of samples saturated dry surface (SSD) after immersion was determined (**B**).

3- The specimens of the SSD were then put in a suitable receptacle, covered with tap water, and boiled for 5 hr. The boiled samples were allowed to cool down to a final temperature of 20-25°C by natural heat loss for a time of no less than

14 hr. Any moisture on the surface of specimens was then removed, and the
SSD mass of samples was then calculated after boiling (**C**).

4- The specimens were then immersed and weighted the definition of their
apparent mass in water (**D**). Figure (3-46) shows the voids test process.

The Equation. (3-7) for calculating the voids of the hardened SCC:

$V_o = ((C-A))/((C-D))$ ……………………… Eq. (3-7)

  Where:

V_o : is a volume of permeable pore space (voids). **A** : mass of oven-dried sample in the air

(kg), **C** : mass of surface-dry sample in the air after immersion and boiling (kg),

D: apparent mass of sample in water after immersion and boiling (kg).

From eq. (3-7), the porosity for SCC could be found by using eq. (3-8) :

$P_o = (V_o / V_{Cube}) \times 100$ ……….………..…..……Eq. (3-8)

  Where:

P_o: porosity %, **V_{Cube}**: volume of the cube (m^3), **V_o**: as similar as in Eq.(3-7).

| Dry mass | Saturated mass | Boiling mass | Apparent mass |
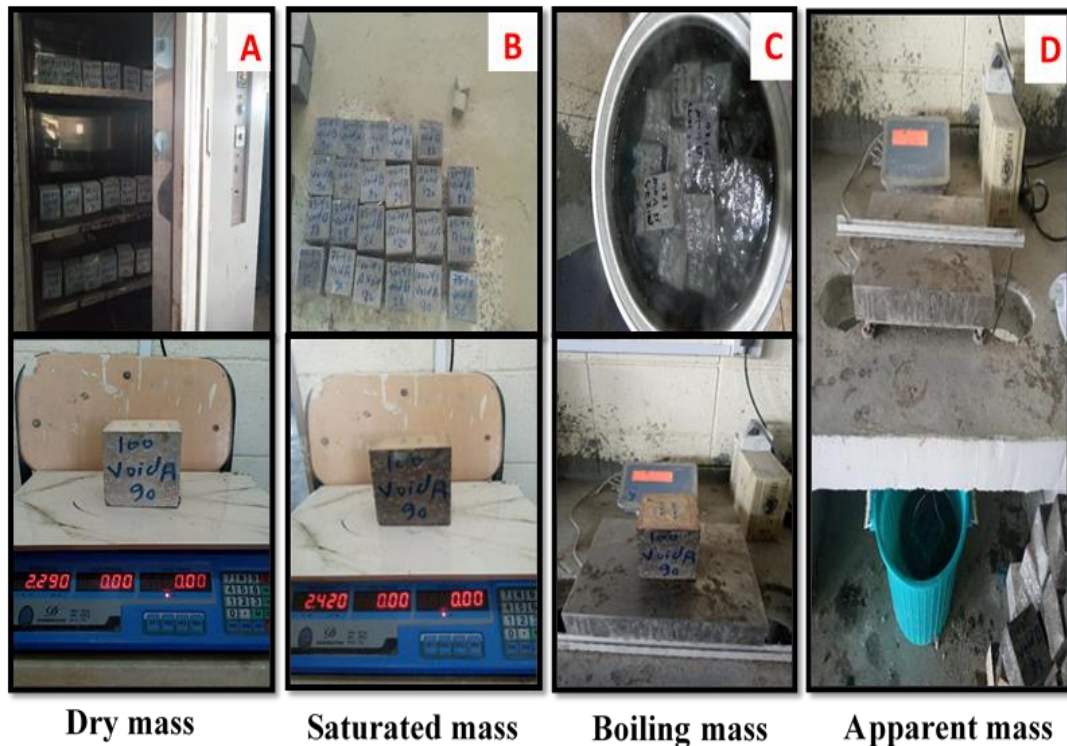
Figure (3-46): Voids test process

3.8.2.4. Water Absorption

The absorption was measured by evaluating the oven-dried and saturated weights. It is based on the absorption test defined in ASTM C642 **[150]**. The water absorption was determined by using Equation (3–9) for the same samples and results of the voids investigation.

W % = [(B-A)/A] ×100   …………Eq (3-9)

Where, **W**: Water absorption%, **A**: as similar as in Eq. (3-7) **B**: mass of surface-dry sample in the air after immersion (full saturated) (kg).

3.8.3. Mechanical Tests of Hardened Concrete

3.8.3.1. Compressive Strength Test

The compressive strength was tested using cube of (100 x 100 x 100) mm, following BS EN 12390-3 **[151]**. The cubes were tested under compression using a 3000 KN capacity measuring machine, and the load rate was 3 kN / sec. Figure (3-47) indicates the testing and the tested sample. The testing results are the mean values of two cubic samples at 7, 28, 56, 90, and 120 days for each mixture. Equation (3-10) has been used to determine the compressive strength.

f_{cu} = P / A_{cube}   …………Eq. (3-10)

Where: f_{cu}: compressive strength of concrete (MPa), **P**: maximum applied load (N), and **A_{cube}**: cross-sectional area of the cube (mm^2).

Figure (3-47): Compressive strength test for SCCs

3.8.3.2. Splitting Tensile Strength Test

Cylindrical samples (100 mm x 200 mm) were used to calculate the splitting tensile strength of mixtures, as shown in Figure (3-48). According to the test procedure defined by ASTM C496-C **[152]** and BS EN 12390-6 **[151]**, the test was done, and the testing machine for compression is also used. The load was performed uniformly with a load rate of 0.94 kN / sec. An average of two cylinders at ages of 28, 56, 90 and120 days was reported for every mixture. Equation (3-11) was used to calculate the tensile splitting strength:

$f_{SP} = 2P/\pi D_{cy} L_{cy}$ …………Eq (3-11)

Where: f_{SP}: splitting tensile strength (MPa), L_{cy}: length of the cylinder (mm), **P**: maximum applied load (N), D_{cy}: diameter of the cylinder (mm).

Figure (3-48): Splitting tensile strength for SCCs.

3.8.3.3. Flexural Strength Test (The Modulus of Rupture)

The strength value of bending failure to concrete prism was measured according to ASTM C78-15a **[153]**. The prism samples are 400 mm long with a cross-section of (100 x 100) mm tested under a two-point load using a 200 kN flexural machine. This machine and a tested sample are shown in Figure (3-49). The specimens were put on the machine's support blocks, and the load is applied continuously until failure.

The average of two prisms examined on 28, 56, 90 and 120 days for each mixture was formed. The Equation (3-12) used was as follows:

$$f_r = PL_{pr} / b_{pr}d_{pr}^2 \qquad \text{…………Eq. (3-12)}$$

Where: f_r: flexural strength (MPa), L_{pr}: net length of a prism (mm), P: maximum applied load (N), b_{pr}: width of a prism, mm, d_{pr}: depth of a prism (mm).

The formula above used when the failure occurs inside the middle third of the length of the span in the tension surface. In contrast, when the failure seemed outside the middle third of the sample span length but did not exceed 0.5 % of the sample span length, the Equation (3-13) should be used:

$$f_r = 3Pa / b_{pr}d_{pr}^2 \qquad \text{…………Eq (3-13)}$$

Where: **a**: measured distance from line failure to nearest support (mm).

Figure (3-49): Flexural strength for SCCs

3.8.3.4. Modules of Elasticity (Young's Modulus) Test

The elasticity module was measured according to ASTM C469-02 [154] and is based on the chord modulus method. This method involved drawing a relationship between stress and strain curve for concrete after 90 days of water curing by drawing the line slop between the point longitudinal strain of 50×10^{-6} strains to the point equivalent to 40% of the ultimate stress, based on previously tested specimens in accordance to ASTM C 39 [155]. The test is shown in Figure (3-50).

A cylinder sample of (150 x 300) mm dimensions was used. Two cylinders were tested for each mixture. To measure the strain, the gage length of 150 mm with dial gage has been used with an accuracy of 0.001 mm/div. The (3-14) Equation was used for calculating the elasticity modules:

E= (S₂ – S₁) / (ε₂-0.000050) x1000   …………Eq. (3-14)

Where**: E:** chord modulus of elasticity (GPa), **S₂:** stress corresponding to 40% of the ultimate stress (MPa), **S₁:** stress corresponding to a longitudinal strain of 50 x10^{-6} (MPa). **ε₂:** longitudinal strain corresponding to the **S₂** stress, **ε₁:** strain 0.000050, and, therefore, does not appear in the formula for E.

Figure (3-50): Modules of elasticity test for SCCs

3.8.4. Durability Tests of Hardened Concrete

3.8.4.1. Influence of High-Temperature Environment on SCC Properties

After various ages (56, 90 and 120 days) for samples, the compressive strengths were obtained and measured at room temperature (25ºC), other samples of the same age were also measured at elevated temperatures (200, 400, 600, 800) ºC for 3 hours.

At first, the samples were dried in the oven at 110 ℃ for 24 hours, and the mass was recorded. After exposure to the specified degree of burning, the specimens were naturally cooled in the room's air. The mass was also measured to calculate the mass loss by using the Equation (3-15). After that, the burned specimens' compressive strengths were measured and compared with the strength of reference by using cubic samples of (100 x 100 x 100) mm. Figure (3-51) shows the burning test process.

Mass Loss % $= \dfrac{m0-mb}{m0} X \ 100$ …………Eq (3-15)

Where: **m_0**: mass of the dry sample by degrees 110 ℃.

   m_b : mass of the burning sample at degrees (200, 400, 600, 800) ℃.
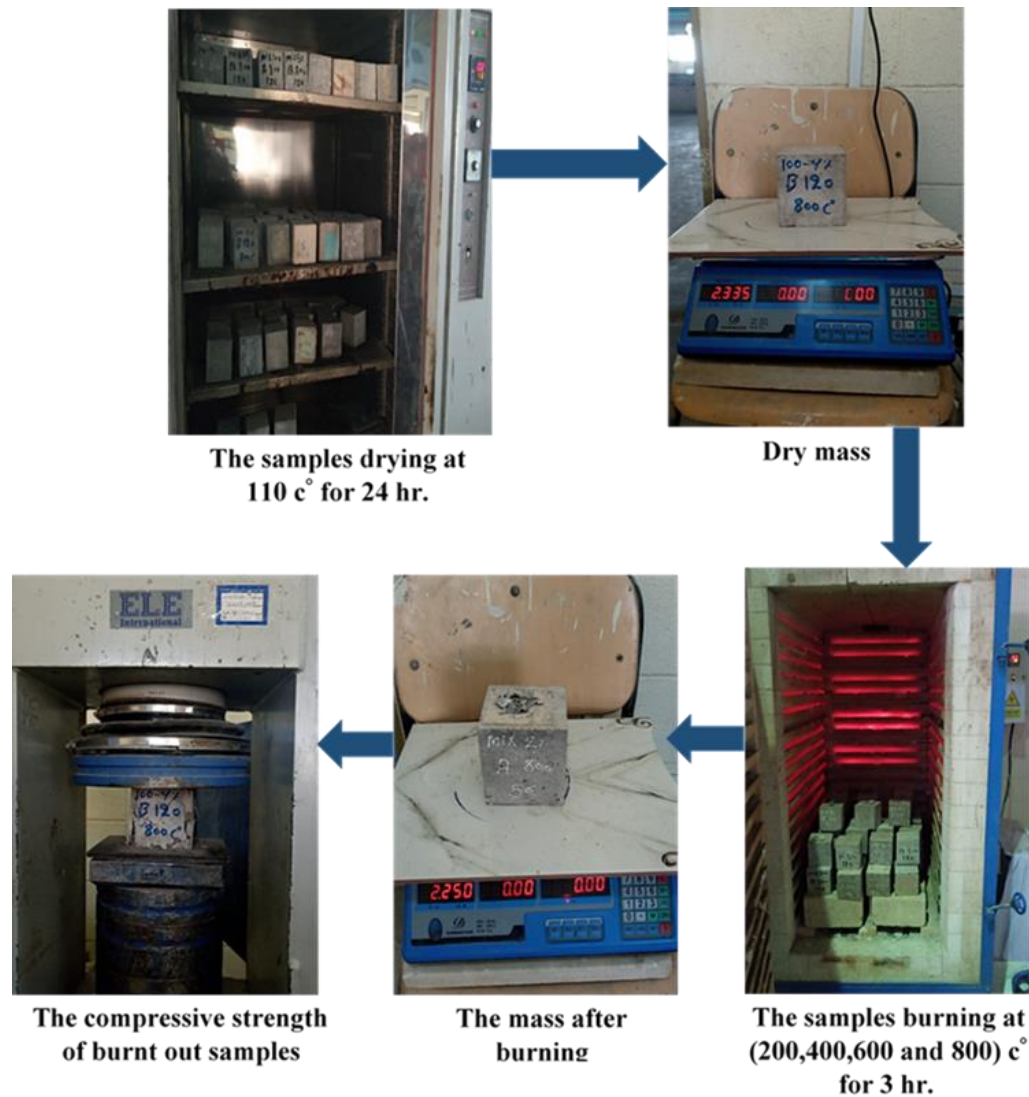
Figure (3-51): Burning test process

3.8.4.2 Influence of a Magnesium Sulfate Attack Environment on SCC Properties

In this study, the effect of external sulfate attack on SCC samples was investigated after curing at age 28 days in ordinary water then completely immersed in three different concentrations of magnesium sulfate ($MgSO_4$) at 5%, 10%, 20% of water weight. The ratio of loss mass, loss of ultrasonic pulse velocity and loss of compressive strength of specimens was determined after immersion in cycles wet and dry magnesium sulfate for 30, 60 and 90 days. The results were compared with those of specimens stored at the same ages in freshwater at ages 56, 90, and 120 days. There is no typical test method for measuring concrete durability under sulfate attack, but the most common method to investigate is accelerated testing through continuous wetting and drying cycles. This has been done to accelerate the ingress of sulfate ions into the concrete specimens, but not occur that for submerged continuously **[115]**. In this study, the cycle period for all samples was 72 hours dry in room air and 72 hours of immersion. Figure (3–52) shows samples' treatment and tests process immersed in a magnesium sulfate solution.

Figure (3-52): Treatment and test process for the samples immersed in magnesium sulfate solution

CHAPTER FOUR

RESULTS

and

DISCUSSION

Chapter Four

Results and Discussion

4-1 Introduction

The experimental results are presented and discussed in this chapter. It includes the results of characterizing the prepared Nano clay and its effect on the concrete mixture at different replacement ratios (0, 2, 4, 6) % of the cement weight at ages of 7, 28, 56, 90 and 120 days. Results for a series of self-compacting concrete mixtures in both the fresh and hardened states were presented. All SCC mixtures were extensively examined in the fresh state using the slump flow, L-box, V-funnel, fresh density, and sieve stability tests. The hardened state was tested in terms of compressive strength, dry density, ultra-pulse velocity, splitting tensile strength, flexural strength, modulus of elasticity, water absorption, and porosity tests at ages of 7, 28, 56, 90 and 120 days. While the durability properties of concrete mixes were tested by resistance to high temperatures of 200, 400, 600, and 800 degrees at ages of 56, 90 and 120 days, and Magnesium sulfate resistance at concentrations of (5, 10, and 20) % of water by weight of immersion period in 30, 60 and 90 days after curing with fresh water for 28 days and with the aid of wetting -drying cycles for each 72 hours.

4.2 Nano clay Characterization

4.2.1 Laser Particle Size Analysers (LPSA)

The Nano clay obtained from the ball milling process was verified by a particle size analyzer (PSA), as shown in Figure (4–1) (A, B). According to this technique, clay has successfully been reduced to a particle size of less than 100 nm sized millings within (40) hours.
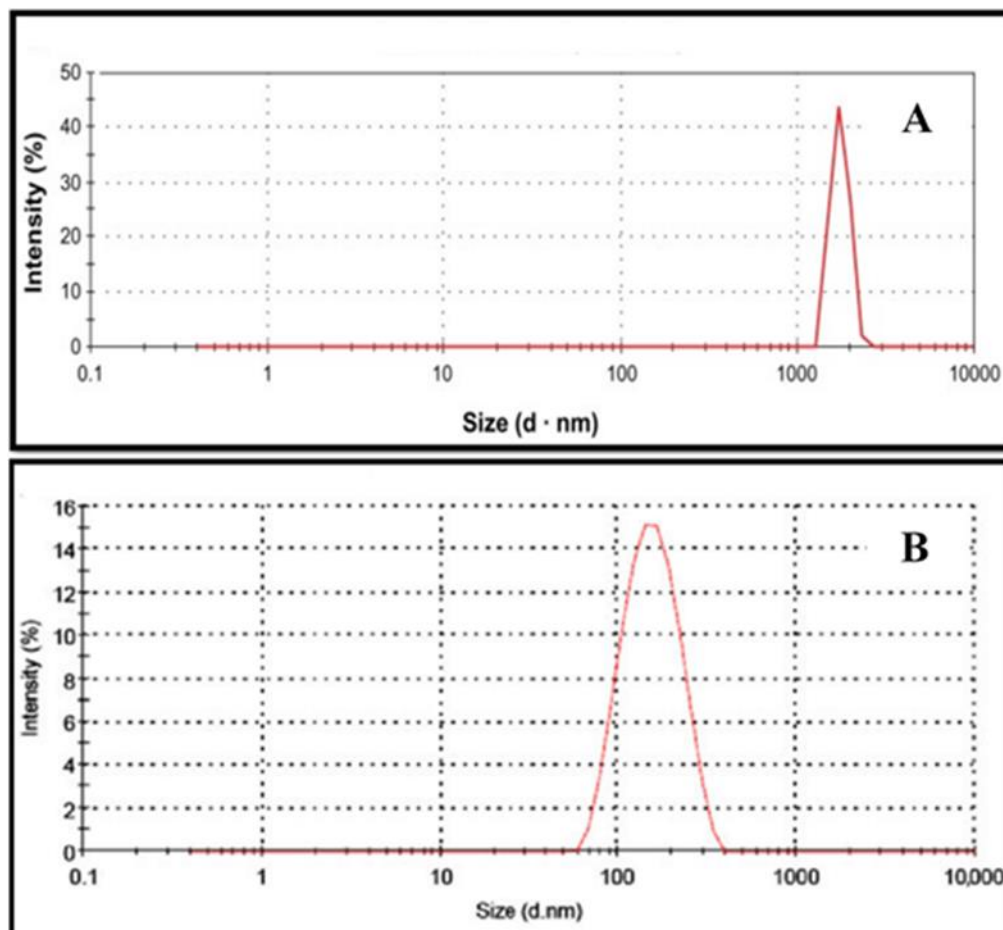
Figure (4–1): Laser Particle Size Analysers A (Clay). B (Nano clay)

4.2.2. Measurement of The Specific Surface Area m(SSA)

The total specific surface areas (SSA $_{total}$) and pore structure parameters calculated from the adsorption isotherms by using the BET and BJH plot methods, respectively for clay and Nano clay. The results were presented in Table (4-1), which determined that (SSA $_{total}$) increased from 24.875 to 27.248 m^2g^{-1} for Nano clay. From Figure (4–2), it could be noticed that (SSA $_{total}$) for Nano clay was type of IV. This means that pore had a diameter between 2 nm and 50 nm **[156]**. The pore volume distributions in the mesoporous of Nano clay using BJH analysis was shown in Figure (4–3).

Table (4-1): SSA and pore volume of clay and Nano clay

BET Plot	Clay	Nano clay	Units
V_m	5.7152	6.2604	$[cm^3\,(STP)g^{-1}]$
a_s, BET(total specific surface	24.875	27.248	$[m^2\,g^{-1}]$
Total pore volume	0.153	0.1423	$[cm^3\,g^{-1}]$
Mean pore diameter	24.601	20.896	(nm)
BJH Plot	**Clay**	**Nano clay**	**Units**
V_p (specific pore volume)	0.154	0.1361	$[cm^3\,g^{-1}]$
a_p (pore area)	30.971	32.031	$[m^2\,g^{-1}]$
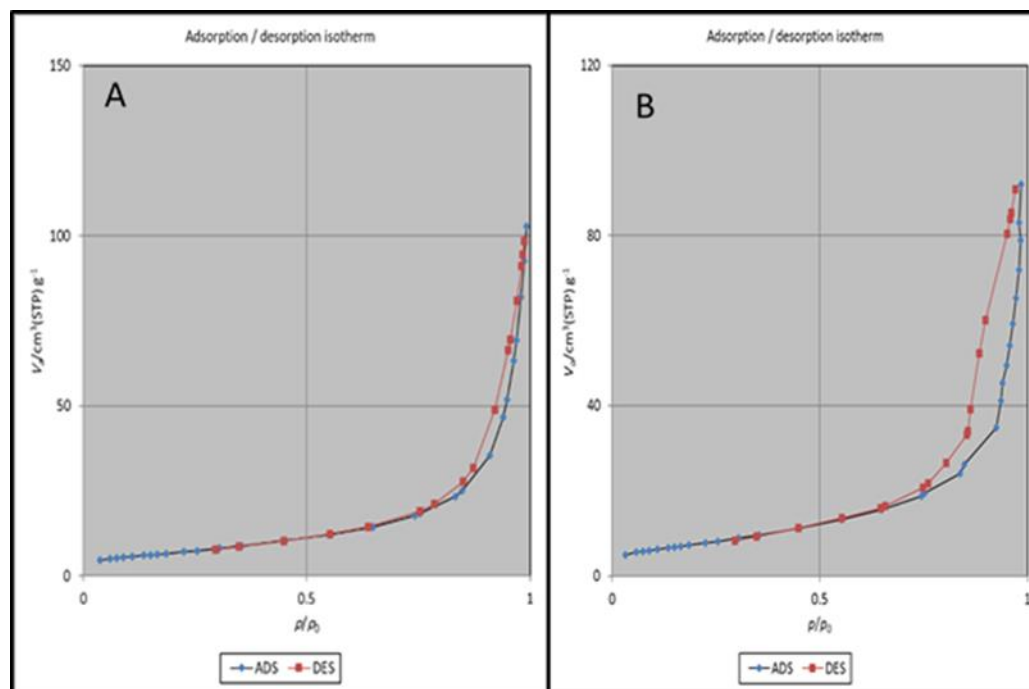
Figure (4–2): SSA total of A (clay). B (Nano clay) by BET
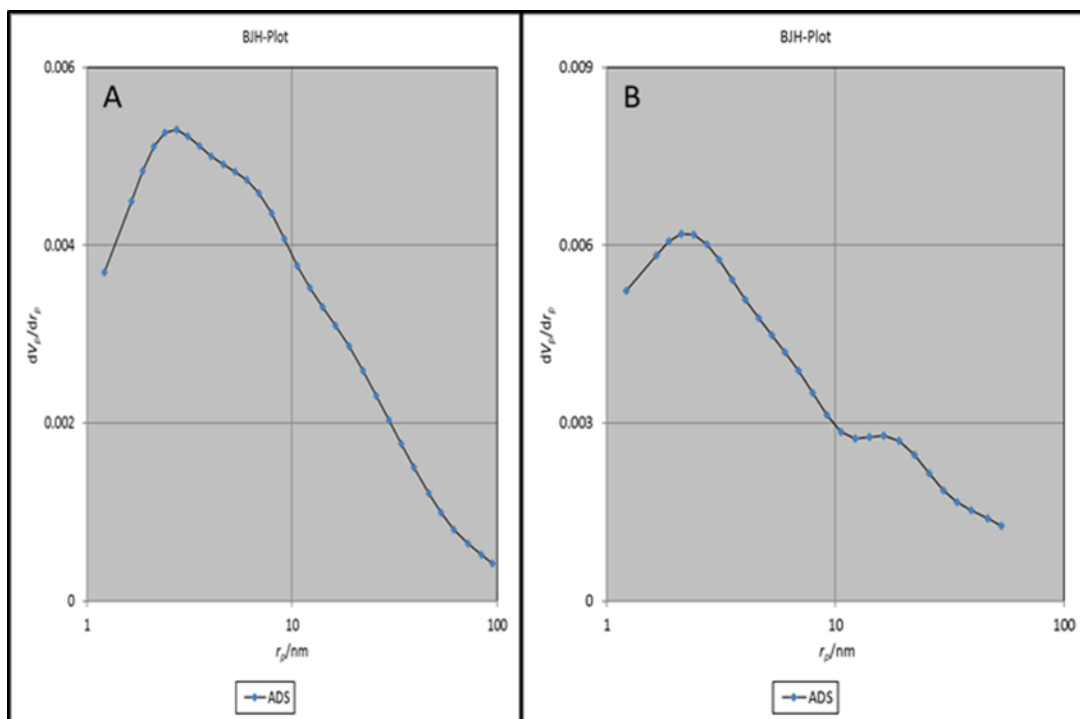
**Figure (4–3): Pore volume distributions in the mesoporous by BJH:
A (clay). B (Nano clay)**

4.2.3. X-Ray Fluorescence (XRF)

The results obtained from the XRF technique are represented in Table (4-2), which shows the chemical composition of Nano clay.

Table (4-2): The chemical composition of Nano clay (wt.%).

SiO_2	Al_2O_3	Fe_2O_3	CaO	Na_2O	K_2O	MgO	TiO_2	MnO	P_2O_5
53.994	11.098	5.193	7.846	0.696	0.581	3.384	0.879	0.031	0.478

4.2.4. Energy-Dispersive of The X-Ray Spectroscopy (EDS or EDX)

The individual chemical elements were determined through this technique in the form of spectra (histograms), as shown in Figure (4-4).

Element	Wt%
Na	1.07
Mg	1.07
Al	22.62
Si	23.73
Ca	1.05
Ti	0.58
Fe	0.43
C	2.75
O	45.35
S	1.36
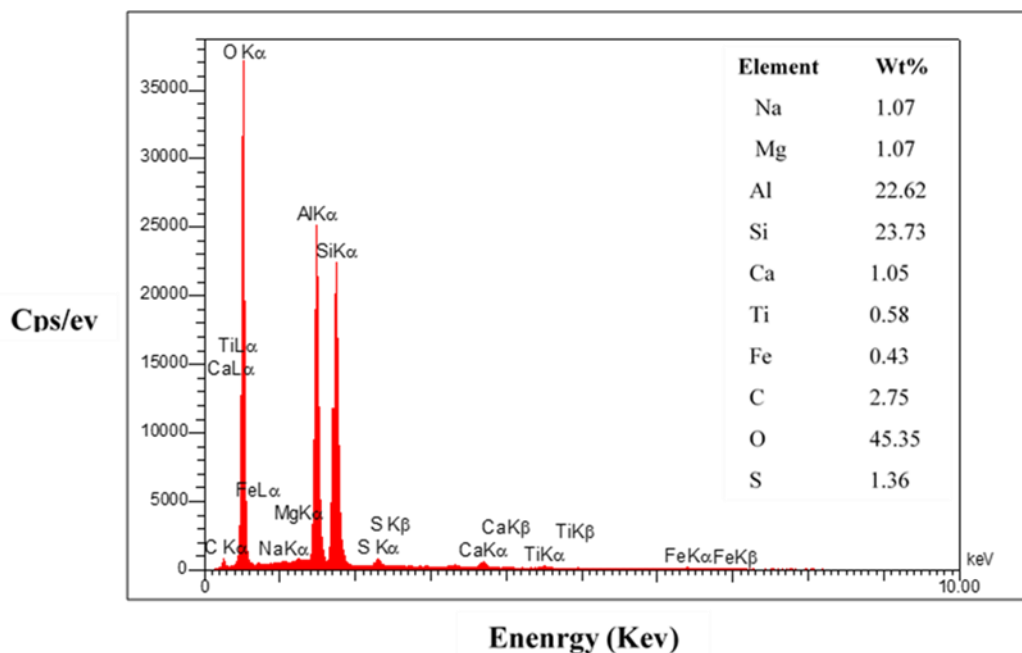
Figure (4–4): EDS analysis of Nano clay

4.2.5. Scanning Electron Microscope (SEM) Observations

4.2.5.1.SEM of Prepared Nano clay.

By scanning electron microscopy SEM, the structural, quality, and morphology analysis of the prepared NC can be identified. The SEM image is shown in Figure (4-5) which shows the calcined kaolin clay (metakaolin) before milling, while figures (4-6) A and B illustrate the morphology, size, and distribution after 40 hours of milling of ball-milled metakaolin (micro-clay). It can be seen that various structures of the (NC) particles including spherical particles and irregular shape particles as well as agglomerates were produced due to the squeezing action of the ball-milling process. The Van-der-Vaal forces acting between the individual particles induce this strong tendency for agglomeration that exists in the particles. Thereafter ball-milled clay nanoparticles formed wide range of shapes from irregular or spherical particles and agglomerates to rounded nanoparticles. As shown from the results, several primary particles seem to cluster or fuse at their faces and ranges (22.37, 35.66, 36.26) nm. The particle size of NC is not homogeneous.
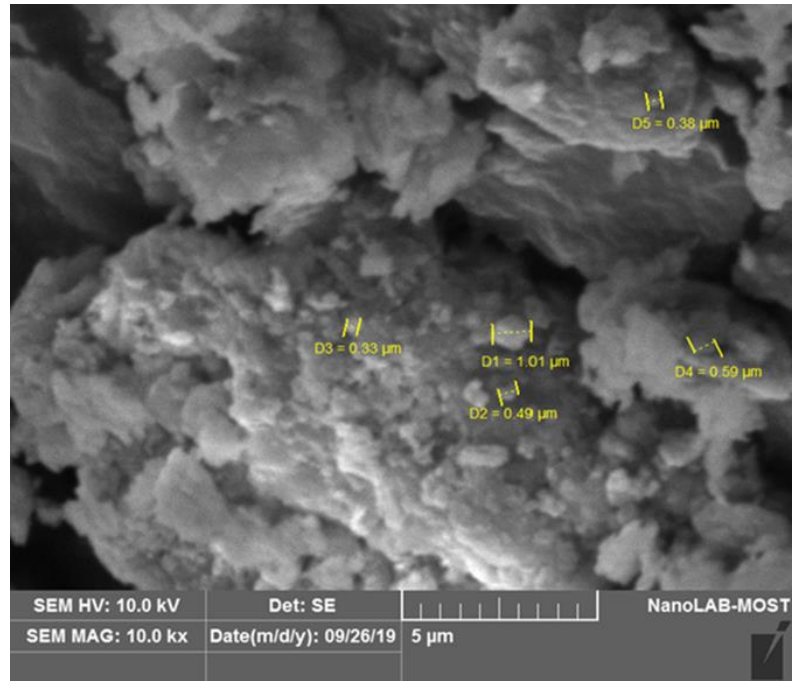
Figure (4-5): Scanning Electron Microscope (SEM) of calcined kaolin clay (metakaolin) before milling
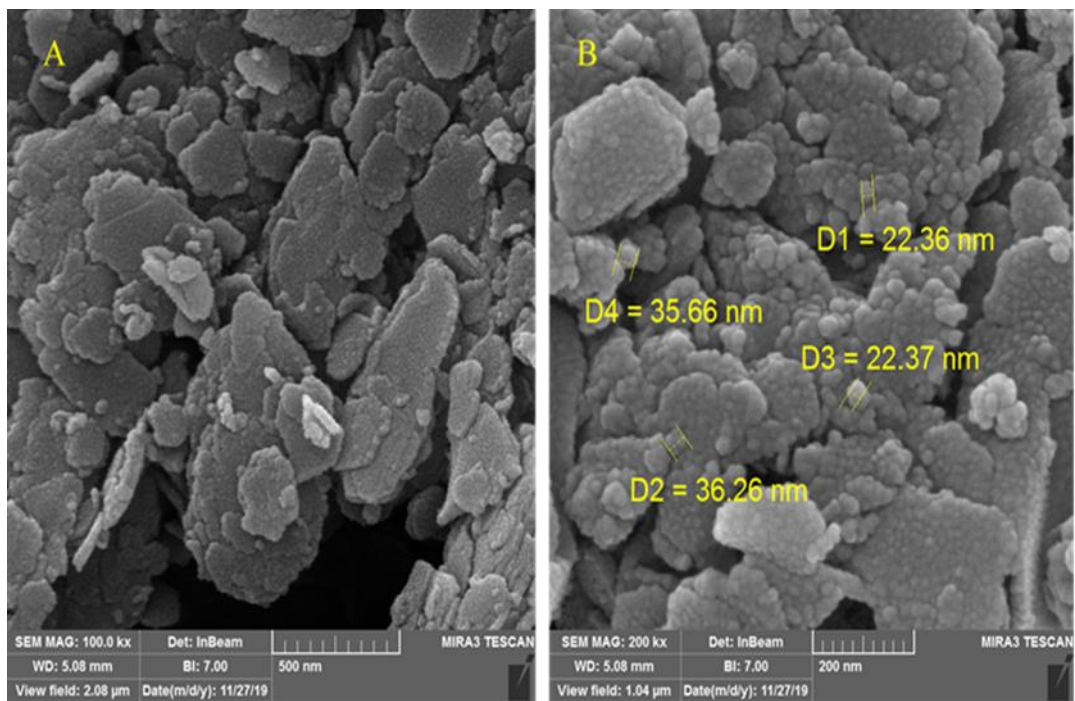
Figure (4-6): Scanning Electron Microscope (SEM) of Nano clay after milling

4.2.5.2. SEM Observations and Microstructure Analysis of the Self-Compacting Concrete Specimens with and without Nano clay.

The morphology observations through scanning electron microscopy (SEM) was carried to understand the microstructure of the reference SCC and SCC specimens mixed with NC. Figures (4-7), (4-8), (4-9), and (4-10) represent the morphological features of the SCC microstructure with and without Nano clay particles at the age of 56 and 120 days, respectively. SEM micrographs of control mix hydrated for 56 days are shown in Figure (4-7) (A). The morphology showed the proper distribution of cement paste and other elements in the SCC structure. Furthermore, the visible cracks can be seen in the SCC surface's morphology due to lower hydration and numerous complex physio-chemical reactions.

 In addition, the micrograph shows wet products such as C-S-H crystals and calcium hydroxide $Ca(OH)_2$ crystals attached to a large-pore C-S-H gel. By increasing the duration of curing, it could be observed that the disappearance of $Ca(OH)_2$ and a moderate increase in matrix density as shown in Figure (4-7) (B), which represents the SEM micrographs of the aqueous control mixture at 120 days. Moreover, at 120 days of curing age, thin cracks can be seen, which means the upper curing age improved the crack resistance. Furthermore, improving the crack resistance is evidenced for higher mechanical strengths at the upper curing age (120-days).

Figures (4-8), (4-9), and (4-10) A and B show an SEM micrograph of a 2%, 4%, and 6% SCCs replacement for 56 and 120 days, respectively. From the NC micrographs, it can be easily recognized that NC particles reduce the void ratio within the matrix and results in a denser matrix. This belongs to two reasons. The first is the NC particles' interaction with the residual CH from the cement hydration process, which results in a greater amount of C-S-H gels, and the second is the filling effect in which the clay nanoparticles fill all the nonporous. The mechanism by which nanoparticles can improve the strength of cement slurry as follows: When a small amount of nanoparticles is uniformly dispersed in the cement slurry, due to their large surface energy during hydration, the cement hydrate products precipitate on the nanoparticles and grow to form a mass containing the nanoparticles as nuclei.

The cement slurry nanoparticles as the core improve and accelerate the cement's hydration because of its high activity. A good microstructure with uniformly distributed agglomeration may be formed when considering the case of uniformly dispersed nanoparticles. By increasing the rate of nanoparticle replacement and increasing the curing time of the concrete mixtures, as shown in figures, it can be noticed that an increase in the microstructure's improvement is formed. At the age of 120 days, the best representation of the replacement percentage is 6 % NC.
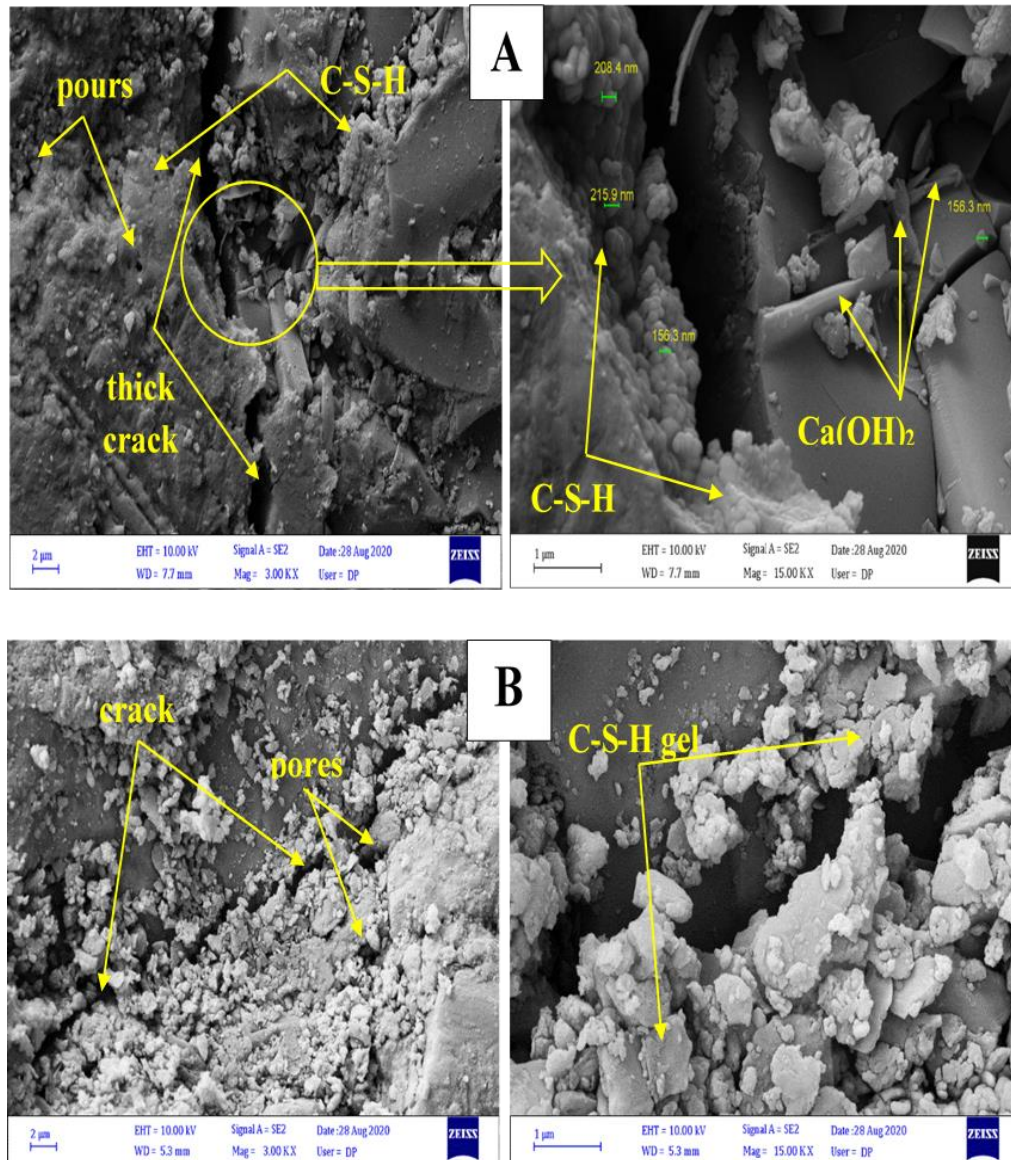
Figure (4-7): SEM images of the control mix: (A) at age of 56 days.

(B) at age of 120 days
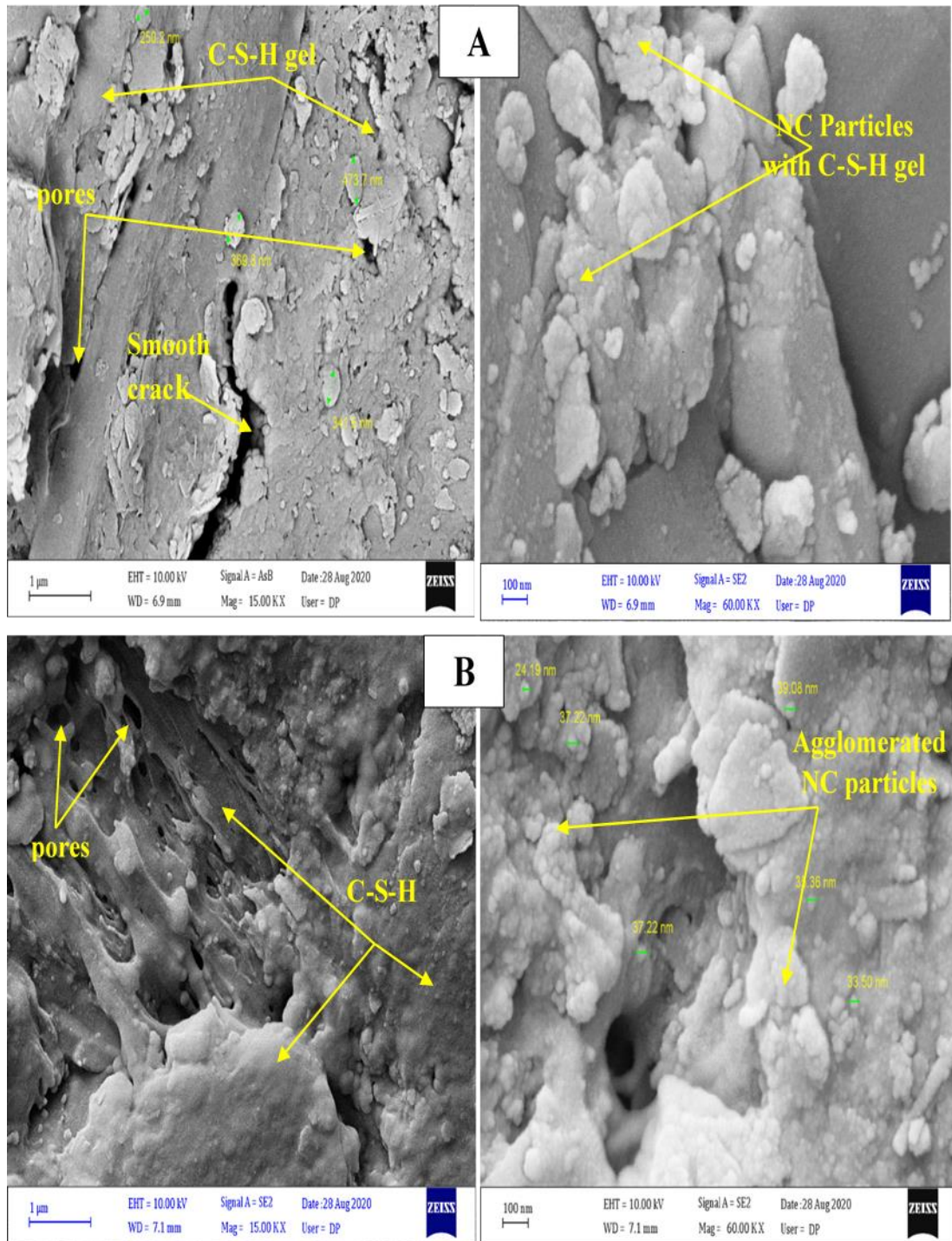
Figure (4-8): SEM images of the SCC 2% NC: (A) at age of 56 days.
(B) at age of 120 days
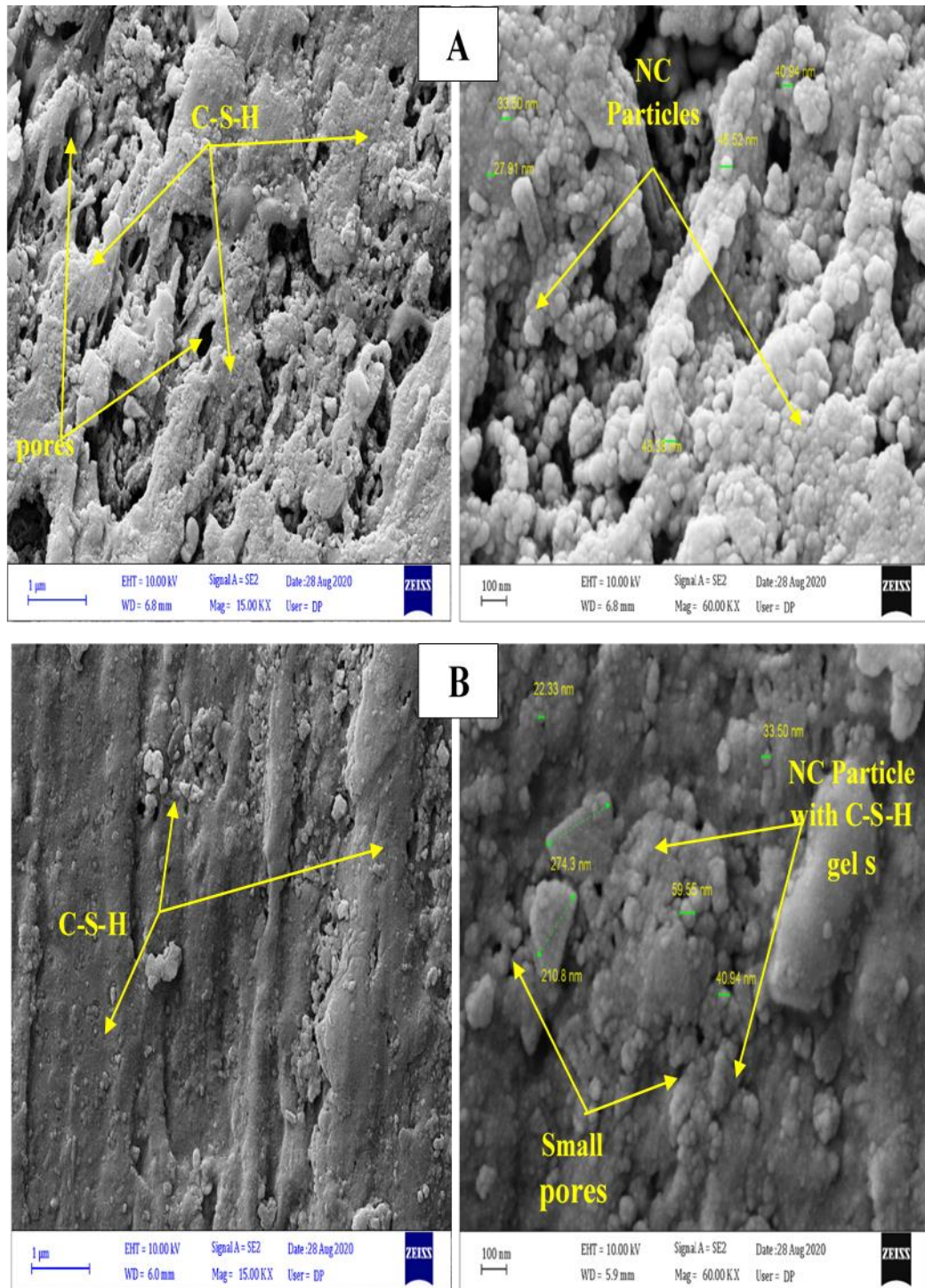
Figure (4-9): SEM images of the SCC 4% NC: ((A) at age of 56 days.
(B) at age of 120 days
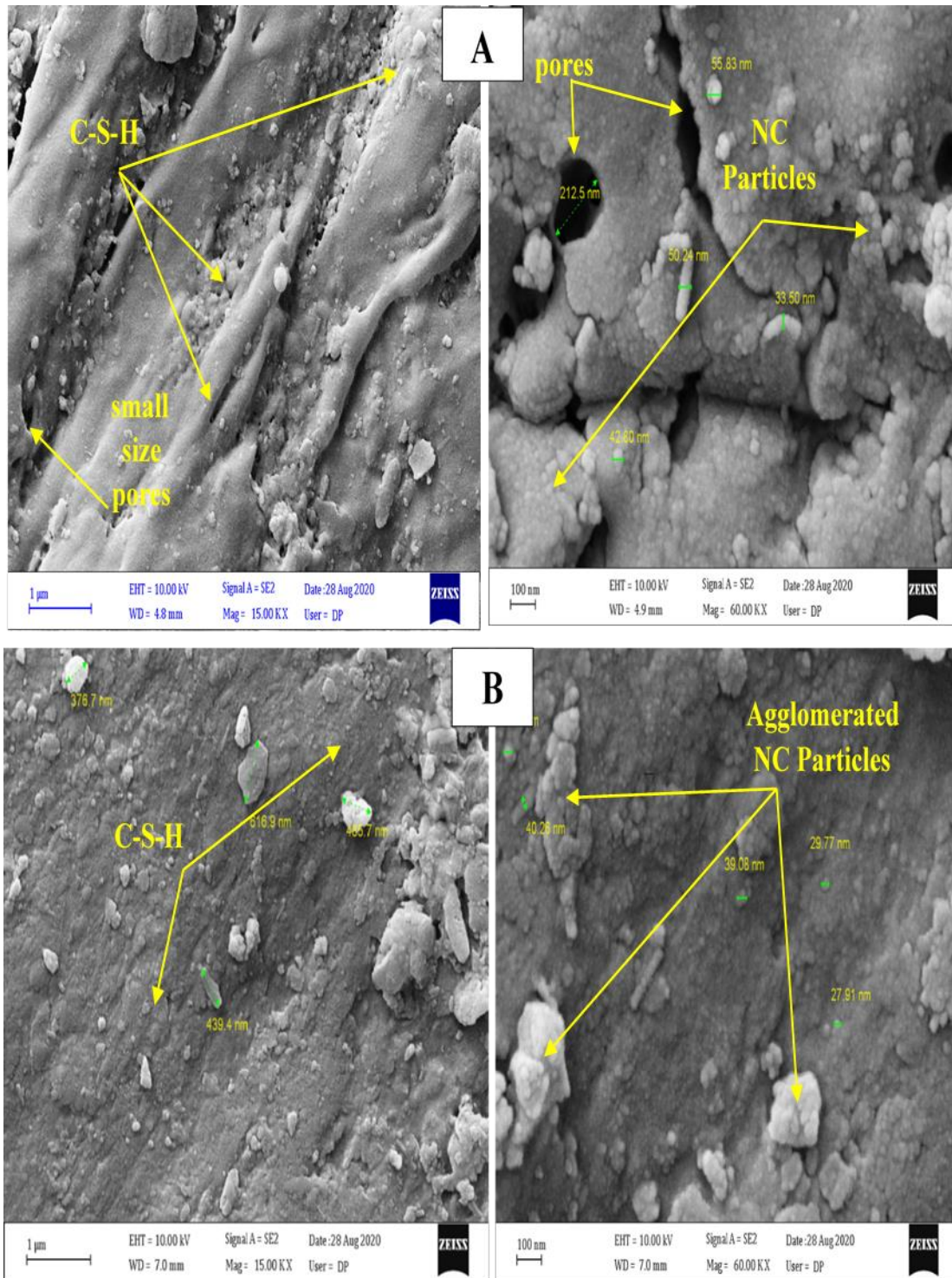
**Figure (4-10): SEM images of the SCC 6% NC: (A) at age of 56 days.
(B) at age of 120 days**

4.3. Fresh Properties Results

Fresh properties of SCC mixture containing NC and QLP were analyzed based on the EFNARC criteria. The latest characterizations of all mixtures have been evaluated, and the findings are outlined in Table (4-3) (see Appendix A) and Figures (4-11), (4-12), (4-13), (4-14), (4-15), (4-16), (4-17) and (4-18).

4.3.1. Slump Flow Diameter(SFD) Results

The slump flow diameter (SFD) of all the SCC specimens is illustrate in Figure (4-11).The SFD results for all SCC mixes were classified between the SF2 and SF3 groups as per EFNARC (2005) standards **[28]**. Furthermore, the SFD results revealed that the SCC0 mix has the highest value of 800 mm and lied in the SF3 classification only.
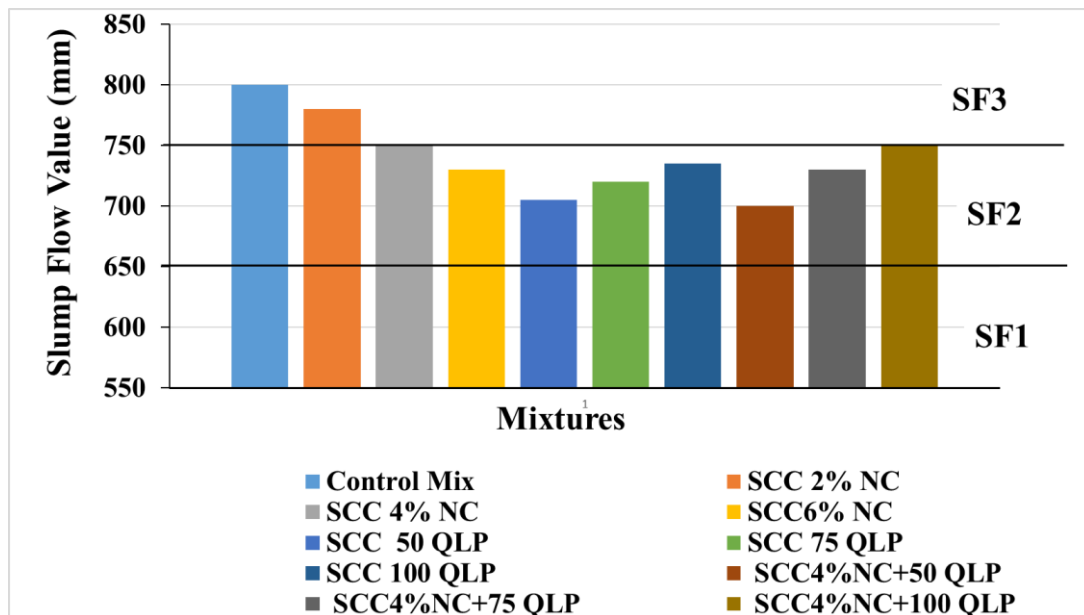
Figure (4-11): Slump flow values of all mixes

However, the addition of NC and QLP caused a reduction in the SFD of the SCC mixes, and the lowest value of 700 mm was obtained for SCC 4% NC- 50 QLP. Thus, the obtained results revealed that the slump flow for NC addition at 2, 4, and 6% in mixture reduced SFD by value 2.5%, 6.3%, and 8.8 %, respectively, compared to that of control mix. For the addition of Q LP by value (50,75, and100) kg, the reduction was 11.9%,

10%, and 8%, respectively, compared to SFD of control mix. Finally, addition of 4% NC with QLP by value (50, 75, and100) kg, the decrease was 12.5%, 8.8%, and 6.3%, respectively, compared to SFD of control mix.

The SFD results for adding NC alone in SCC mixtures reduced the SFD values from 780 mm to 720 mm which were lower than the reference specimen (SCC0). It is mainly because of the effect of NC paste nanoparticles on increase the surface area of cementitious paste compared to the cement paste control, where the macron particles causing increased water demand to absorb water, leaving less free water contributing to the flow ability that makes the mixes drier than the control mix **[157]**.

The other reason is the stiffening effect of NC also caused to reduces the SFD of SCC mixes **[158]**. At the same time, QLP alone in SCC caused to increase in the SFD of SCC mixes, but still lower than the reference SCC mix (SCC0). In general, two reasons for this phenomena can be hypothesized. The first is that the size of QLP is finer than cement, and as a filler, it increases the overall surface area of the powder. The second is that the pozzolanic reaction of QLP containing more CaO than cement, which can induce a hydration reaction that causes a substantial decrease in water content. $Ca(OH)_2$ is formed by the reaction where CaO particles react with water, which is very fresh and more soluble than the factory-produced slacked lime and contributes to better workability **[159]**.

 Higher QLP dosages lead to greater hydration reactions so that the slump flow steadily rises but remain lower than the reference SCC mix. Moreover, the combined effect of both NC (4% only) and different contents of QLP (50, 75 and 100) on SFD of SCC mixes showed an increase in the results, but still lower than the SFD for the reference SCC mix (SCC0). It is mainly due to the existence of more voids in the paste, which was created by the larger surface area of NC and quicklime particles compared to that of SRC particles, and thus, there was a greater rise in demand for water to keep consistency **[160]**.

The increase in the CaO content produced from the NC and the production of calcium hydroxide or slackened lime from the added dosage of QLP was the suggested reasons to enhance the workability. Overall, reasons such as higher temperatures, higher initial

slump, higher cement quality, high alkali, and low cement sulfate content as in the Sulfate resistance cement (SRC) used in this study were suggested by several experiments as the reasons behind the decrease in slump flow **[161]**.

4.3.2. T_{500} Slump Flow and V-funnel Flow Times Results

Figure (4-12) shows the results of the T_{500} slump flow, and the obtained values were ranged between (2.15-3.28) sec.
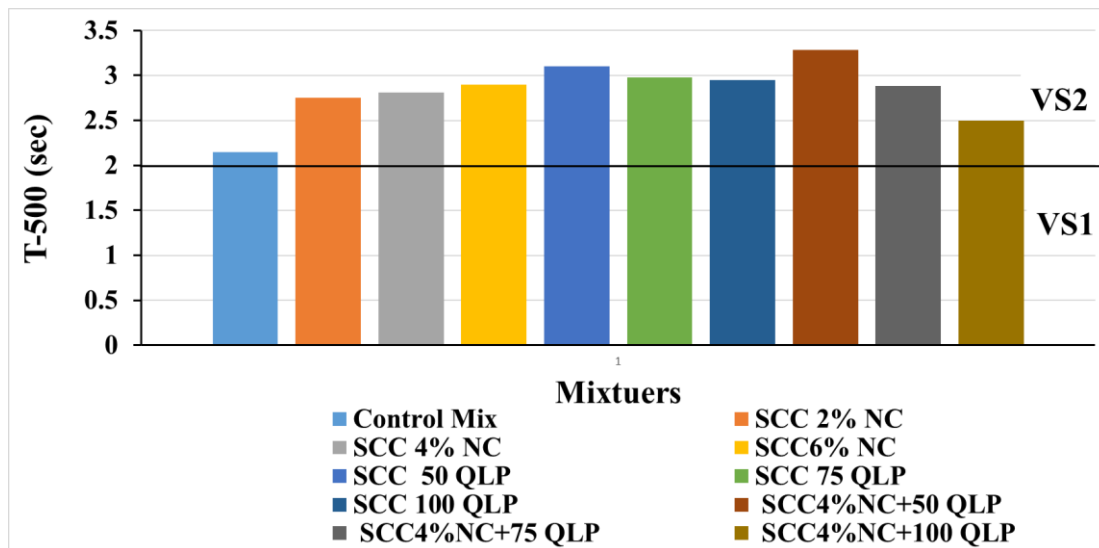
Figure (4-12): T_{500} values of all mixes

Moreover, the V-funnel flow time results are shown in Figure (4-13), and the obtained values were ranged from 10.2 sec to 21.1 sec. Both obtained results can therefore be categorized into the VS2 / VF2 category as per EFNARC viscosity guidelines. The lowest value of V-funnel flow time and $T5_{00}$ slump flow was achieved at 10.2 sec and 2.15 sec, respectively, for the control mix.

Furthermore, the highest values of V-funnel flow time and T_{500} slump flow were achieved as 21.1sec and 3.8 sec, respectively, for the SCC 4% NC -50 QLP. The interaction between V-funnel flow and T_{500} flow time is shown in Figure (4-14), and it indicates the viscosity scale recommended by EFNARC 2005.
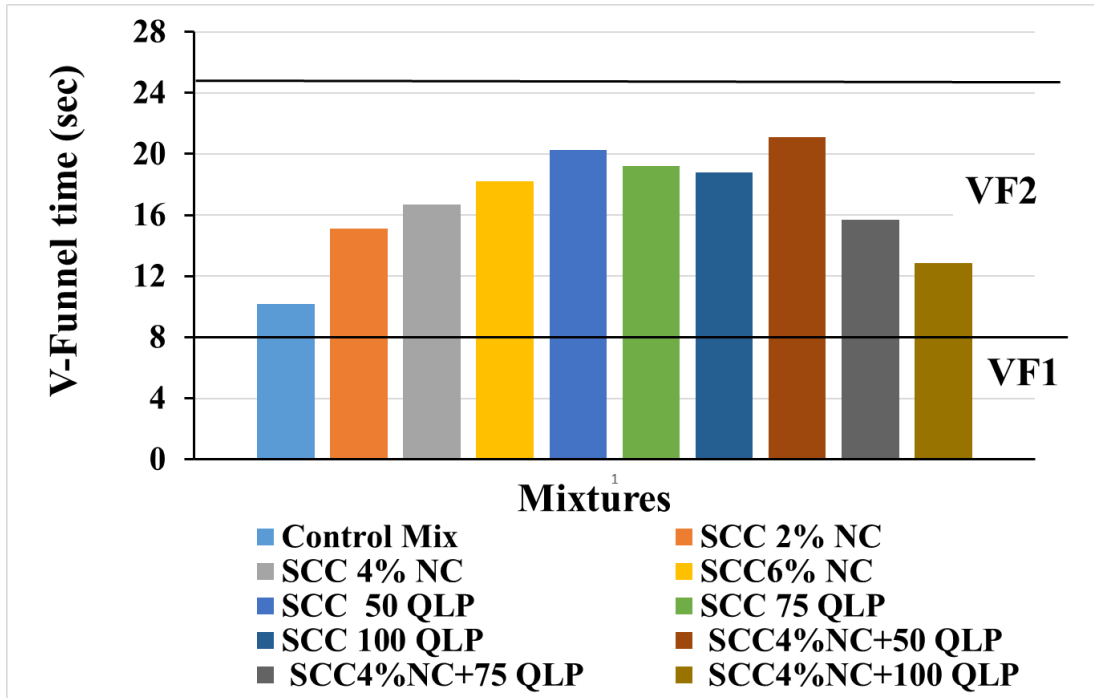
Figure (4-13): V- funnel time values of all mixes
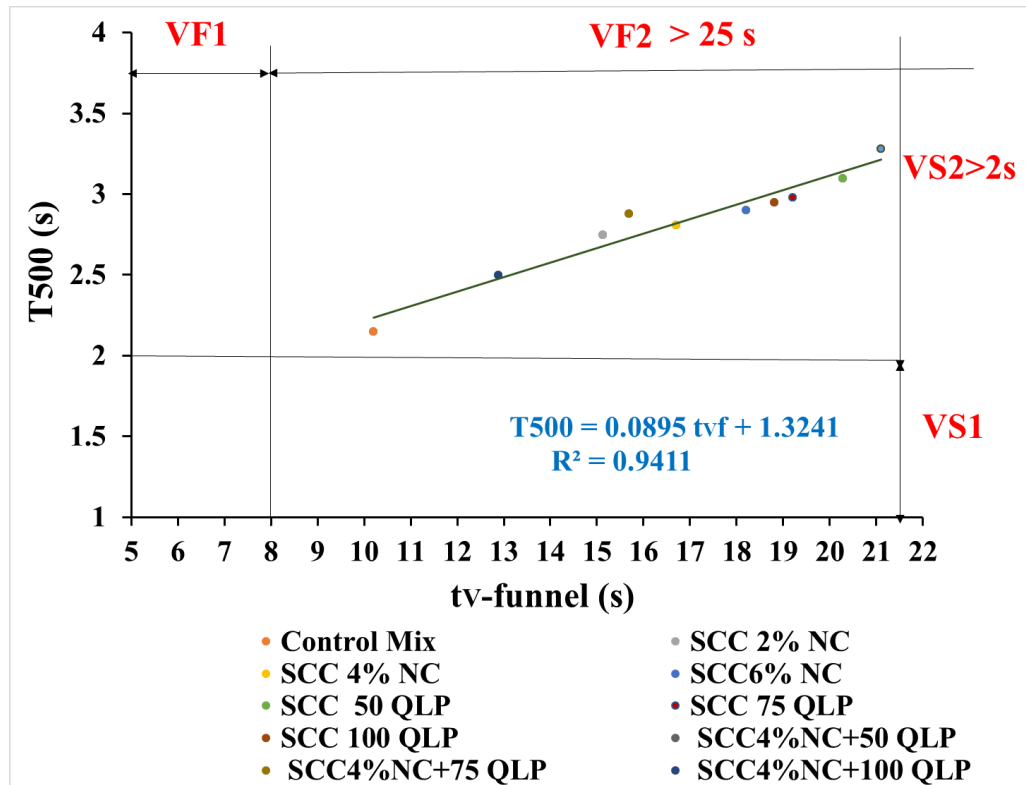
Figure (4-14): Correlation between V-funnel time flow and T_{500} slump flow for all mixes.

The V-funnel flow time of mixes demonstrated nearly the same pattern with T_{500} flow time by excellent relevant linear relationship ($R^2 = 0.9411$) of all mixtures between T_{500} and V-funnel flow times. It can also be inferred that comparing to control mix, the addition of (2, 4, and 6%) NC leads to a rise in the viscosity of mixed SCCs by approximately (48.24, 63.7, and 78.43%).

The flocculation mechanism can be related to this pattern, leading to a thickened fresh mix since NC particles increase the flocculation power of fresh cement mixtures. Flocculation strength is identified as the resistance of the flow to breakdown under a given shear condition. The actual effect of flocculation is to trap particles into the water, raising the fraction of the solid volume and, therefore, stiffening the fresh mix **[161,162]**.

Compared with the reference mixture, V-funnel flow time was raised by 98.8% when adding 50 kg of QLP. After that, by applying 75 and 100 kg of QLP, the V-funnel flow time was continued to decline with rates of 88.2 and 84.4%, respectively.

These findings are probably due to the increase in the production of $Ca(OH)_2$, which represents the result of the reaction of the quicklime with water in the cement paste.

When 4% NC with 50 kg QLP were added into the mixture, the highest viscosity was obtained with a rise of 106.86% compared to that of the reference viscosity, which may be due to the higher content of fines of QLP particles and ultra-fines as NC particles in the mixtures which can lead to a local blocking effect.

Owing to the relatively high solid content and high packing density, the effective diameters of the granular pore structure are very limited so that the fluid process can hardly pass. The temporary vacuum will only be filled with fluid before the distance between two larger grains is wide enough to be filled with medium-sized grains, which significantly reduces the velocity of the larger grains. In general, this effect is one of the causes of shear thickening behaviour **[163]**, in addition to the active pozzolanic reaction of both NC and QLP, which increases the demand for water absorption and reduces workability.

The V-funnel flow time dropped rapidly and significant at the mix of 4% NC with 75 and 100 kg QLP, but it remains higher than the reference viscosity by 53.73% and 26.72%, respectively.

That was due to the increase of CaO content from NC and the increase of QLP dosage; an increase in $Ca(OH)_2$ production was revealed and lead to improved viscosity.

4.3.3. Blocking Ratio (L-Box test) Results

Figure (4-15) shows the L-Box ratio results for all the SCC specimens. The Highest value of L-Box's was obtained as 0.94 for control mix and SCC 2%NC, and the lowest value of 0.86 was obtained for SCC 4% NC-50 QLP. The addition of NC gradually reduced the L-Box ratio results, whereas QLP alone and together with NC caused increasing the L-Box results of the SCC mixture. However, all the values were ranged from 0.94 to 0.86 and were within a reasonable range for SCC on the EFNARC 2005 based passing ability. Thus, it can be remarked that the addition of NC and QLP significantly affects the SCC mixture's passing ability. Furthermore, the relation between V-funnel flow and L-Box ratio is shown in Figure (4-16). The interaction between V-funnel flow time and L-Box ratio depicted that there is a strong meaningful polynomial relationship ($R^2 = 0.8616$) between passing ability and viscosity which is described by the results of the V-funnel flow time test.
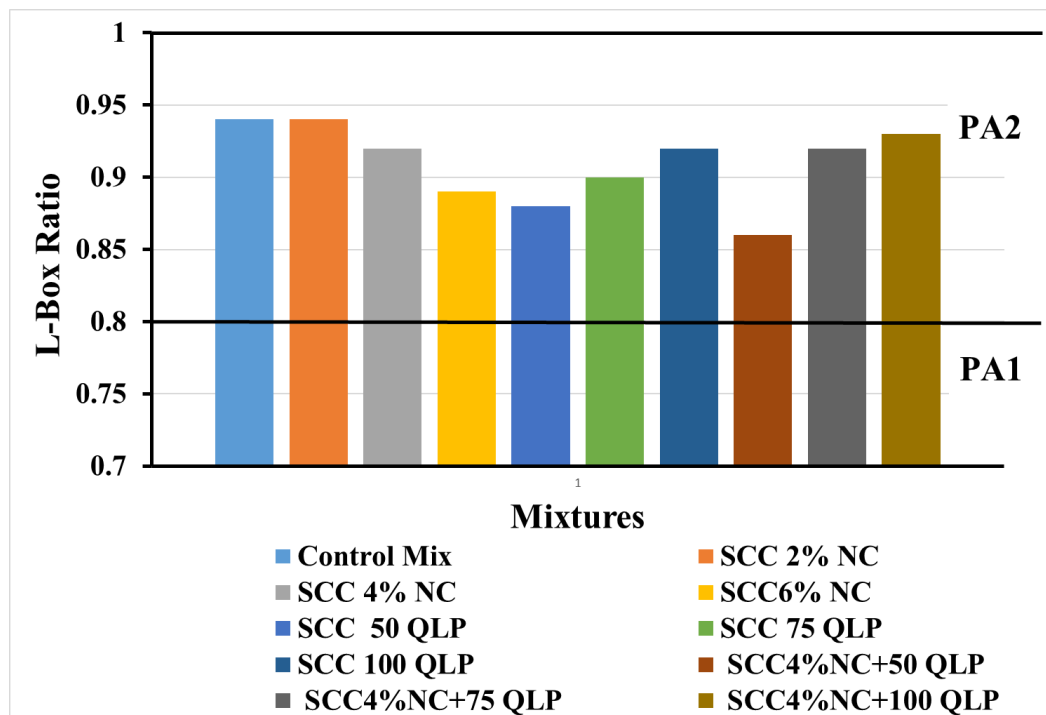
Figure (4-15): L-Box ratio values of all mixes

The chart shows: $Passing\ ability = -0.0001tv^3 + 0.0046tv^2 - 0.0623tv + 1.2199$, $R^2 = 0.8616$. Y-axis: L-Box ratio %. X-axis: tv-funnel flow (sec). Legend: Control Mix, SCC 2% NC, SCC 4% NC, SCC6% NC, SCC 50 QLP, SCC 75 QLP, SCC 100 QLP, SCC4%NC+50 QLP, SCC4%NC+75 QLP, SCC4%NC+100 QLP.
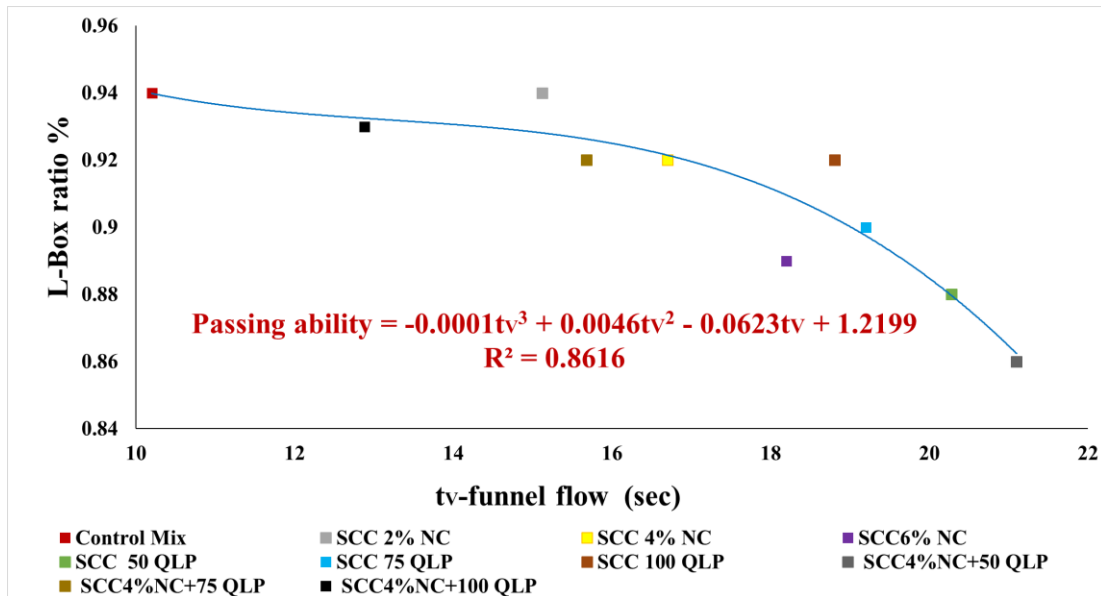
Figure (4-16): Correlation between V-funnel and L-Box ratio for all mixes

4.3.4. Sieve Segregation Resistance Test Results

Figure (4-17) illustrates the segregation ratio (SR) of all the SCC mixes. The SR results demonstrated that the addition of NC gradually reduced the SR by increasing the content of NC. This is owing to NC's large specific surface area, ease of formation of a flocculent network structure, and the ability to absorb more free water during wetting **[73]**. Further, the addition of QLP and NC-QLP gradually reduced the SR of the SCC mixtures. The control mixture and SCC 2% NC mixture have the highest SR value, whereas the lowest value was achieved for SCC 50 QLP. However, all the obtained values of SR for SCC mixtures are in SR_2 classification as per ENFARC 2005.
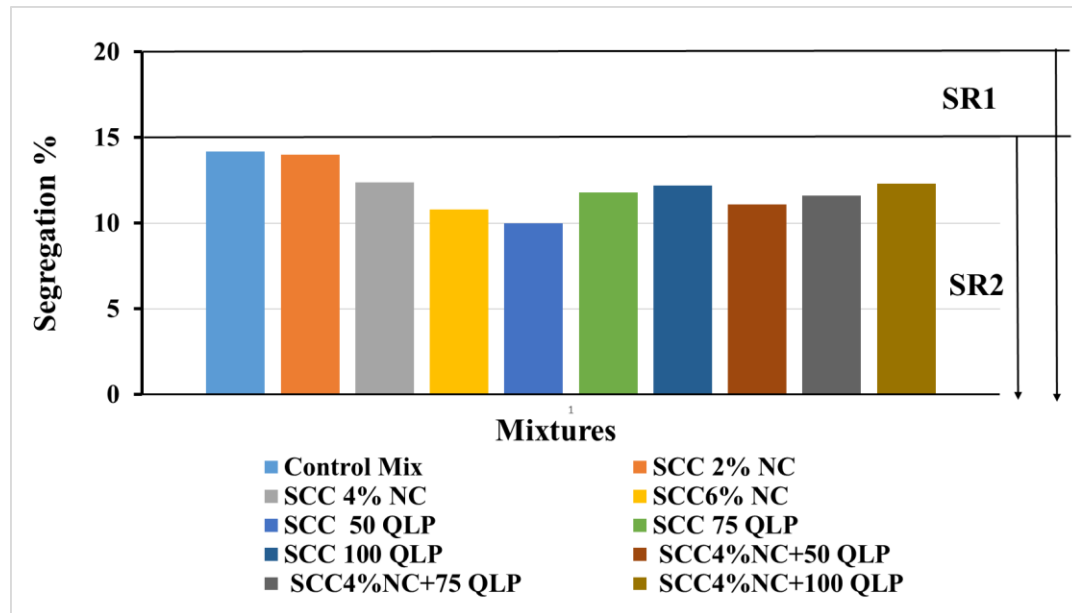
Figure (4-17): Sieve segregation resistance values of mixes

4.3.5. Fresh Density Test Results

Figure (4-18) shows the fresh density of the SCCs mixed with NC and QLP. The fresh density of SCC mainly affected due to several parameters such as cement specific gravity, aggregates and cementitious content additives. However, the specific gravity is the main source to impact the flow ability and workability of SCC. In this study, the water-to-binder ratio (w/b), coarse and fine aggregate content and superplasticizer content were kept constant, with except for cement content, which was supplemented by different proportions of NC as 2, 4 and 6%, QLP as 16, 23.4 and 29% or both (NC and QLP) as 20, 27.4, and 33% by cement weight. The results showed a reduction in the fresh density with NC and QLP. The addition of NC and QLP gradually reduced the fresh density of SCC specimens. Moreover, the highest fresh density value of 2320 g/ cm^3 was obtained by the SCC0, while for SCC 4% NC-100 QLP recorded the lowest value of 2110 g/ cm^3. The decrease in density was due to the lower specific gravities values of NC particles (2.6 g/cm^3) and QLP (2.68 g/cm^3) as compound with specific gravities values of cement (3.15 g/cm^3) **[164]**. Therefore, increasing the quantity of NC and QLP caused a reduction in the fresh density of the SCC mixtures.
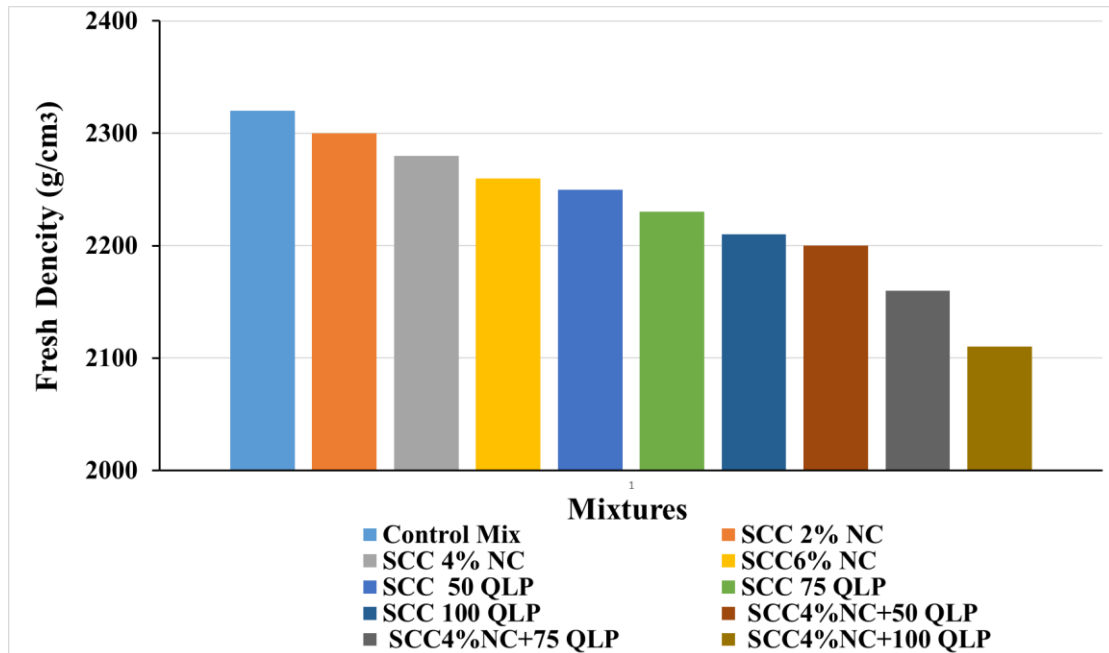
Figure (4-18): Fresh density values of all mixes

4.4. Hardened Concrete Results

Many parameters, such as the inclusion of reinforcement, weight percentages and kind of reinforcement, can affect the hardened properties of SCC. Different weight percentages of NC and QLP were mixed in SCC. The NC and QLP were refined and replaced with different cement weight percentages to prepare SCC specimens. Hypothetically, the refined size and the inclusion of NC and QLP significantly affect the hardened properties of the SCC. The SCC specimens were cured for 7, 28, 56, 90, and 120 days for conducting hardened properties. Mechanical tests (compressive strength, splitting tensile strength, flexural strength, modulus of elasticity), Physical tests (Ultra Pulse Velocity (UPV), the dry density of concrete, the volume of permeable pores (Voids), water absorption), and Durability tests (the burning effects, and resistance to sulfate attack by solutions $MgSO_4$) of SCC specimens were found.

4.4.1. Mechanical Tests Results

4.4.1.1. Compressive Strength Test Results

Table (4-4) (see Appendix A) and figure (4-19) show the compressive strength of control and SCC mixtures incorporating various weight percentages of NC and QLP.
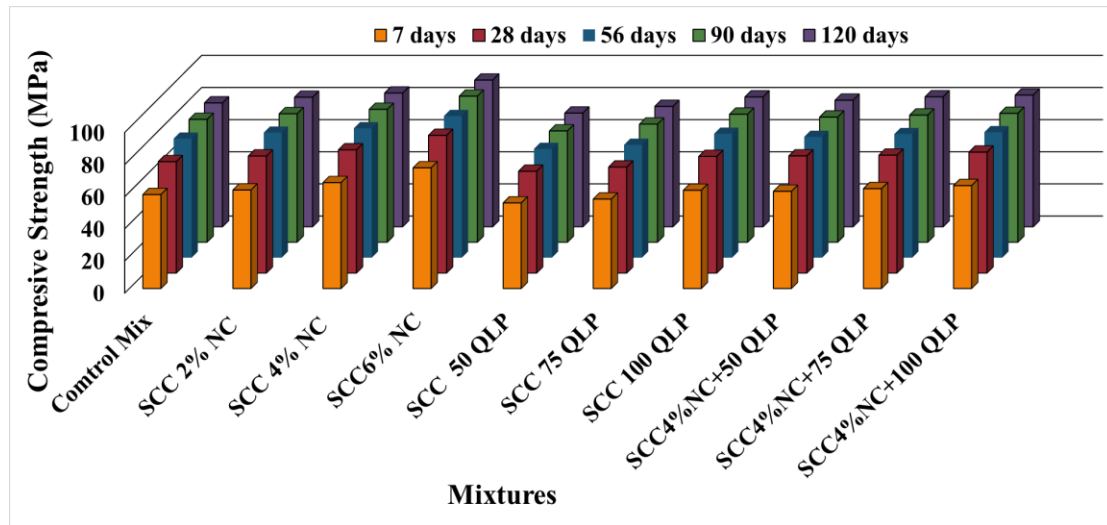
Figure (4-19): Compressive strength for specimens mixed

The results revealed that the inclusion of Nano clay (NC) and quicklime (QLP) increased the compressive strength of the SCC mixtures. Additionally, the compressive strength increased by increasing the curing age at respective weight percentages of NC and QLP. Moreover, the compressive strength values for NC and QLP (SCC 100 QLP) were higher than the reference SCC specimen's compressive strength (SCC0).

Furthermore, the lower weight percentages of QLP caused to have compressive strength lower than control mix, whereas all the contents of NC in SCC have higher compressive strength.

The compressive strength for 2, 4 and 6% of NC mixed in SCC was higher than control mix (SCC0) by 4.9%, 12.7% and 28.5% at 7 days curing age, 5.1%, 10.6% and 23.6% at 28 days curing age, 5%, 8.7% and 19% at 56 days curing, 4.6%, 8.2% and 19% at 90 days curing, and 4.6%, 8% and 18.4% at 120 days curing age.

However, the overall maximum value of compressive strength was achieved for SCC 6% NC at 120 days curing age. This means that a higher percentage of NC and the most upper curing age provided the maximum compressive strength value.

The growth in compressive strength of SCC mixed with NC is mainly due to NC particles that exhibit pozzolanic behaviour in the cementitious matrix and react with $Ca(OH)_2$ crystals to create a dense Calcium Silicate-Hydrate (C-S-H) gel.

In addition, NC particles can occupy the micro-pores and bind firmly with the bulk volume of the matrix to build a more compact and incorporated microstructure **[165]**. The C-S - H gel is the main hydration component contributing to the stability, strength, and improved cement-based materials' durability **[162]**.

The compressive strength values of 50 QLP and 75 QLP mixes in SCC were less than of reference SCC by about 8.9%, 8.6%, 8.7%, 9.4% and 8.2%, and 4.8%, 4.9%, 5.2%, 3.4% and 3.8% at 7, 28, 56, 90 and 120 days curing ages respectively.

While the 100 QLP mix in SCC provided higher compressive strength than SCC0 by about 4.3%, 4.5%, 3.9%, 4.1% and 4.6% 7, 28, 56, 90 and 120 days curing ages respectively. It is well known that when pozzolans are used partially in concrete, its strength is generally influenced by (i) cement hydration effect, (ii) chemical or pozzolanic effect resulting from the reaction between amorphous silica and cement hydration product $Ca(OH)_2$, and (iii) finer pozzolan particle filler effect.

In this study, the water-cement ratio was kept constant to avoid the water-cement ratio's influence on the SCC mixtures' strength. Therefore, the SCC QLP mixes' strength should only depend on the available cement content and the QLP filler effect **[166]**.

Finally, SCC specimens' compressive strength values mixed with 50, 75 and 100QLP and 4% NC were higher than the reference SCC specimen (SCC0). The compressive strength values were higher than SCC0 by 3.4%, 6.3% and 9.6% at 7 days curing age, 5.2%, 5.9% and 8.6% at 28 days curing age, 1.4%, 3.8% and 5.4% at 56 days curing age, 1.9%, 3.5% and 5% at 90 days curing age and 2.2%, 4.9% and 6.3% at 120 days curing age for SCC specimens mixed with 4% NC-50 QLP, 4% NC-75 QLP and 4% NC-100 QLP mixes respectively.

Moreover, the main reason for obtaining the best value of compressive strength for this mixture is NC and QLP inclusion's combined effect. Based on the obtained results in this research, it can be concluded that NC and QLP have a significant effect on the compressive strength of SCC. Furthermore, as comparing the NC to QLP, NC has a more significant effect on the compressive strength of SCC. However, higher values of

QLP replacement can provide significant compressive strength. Thus, the utilization of both NC and QLP as replacing the cement positively impacts the manufacture of SCC.

4.4.1.2. Splitting Strength Test Results

The splitting strength was experimentally found for all SCC specimens cured at 28, 56, 90, and 120 -days. Table (4-5) (see Appendix A) and Figure (4-20) describe the splitting strength of reference SCC (SCC0) and SCC specimens mixed with Nano clay (NC) and quicklime (QLP). The results revealed that the splitting strength gradually increased with increasing the content of NC and QLP in SCC.
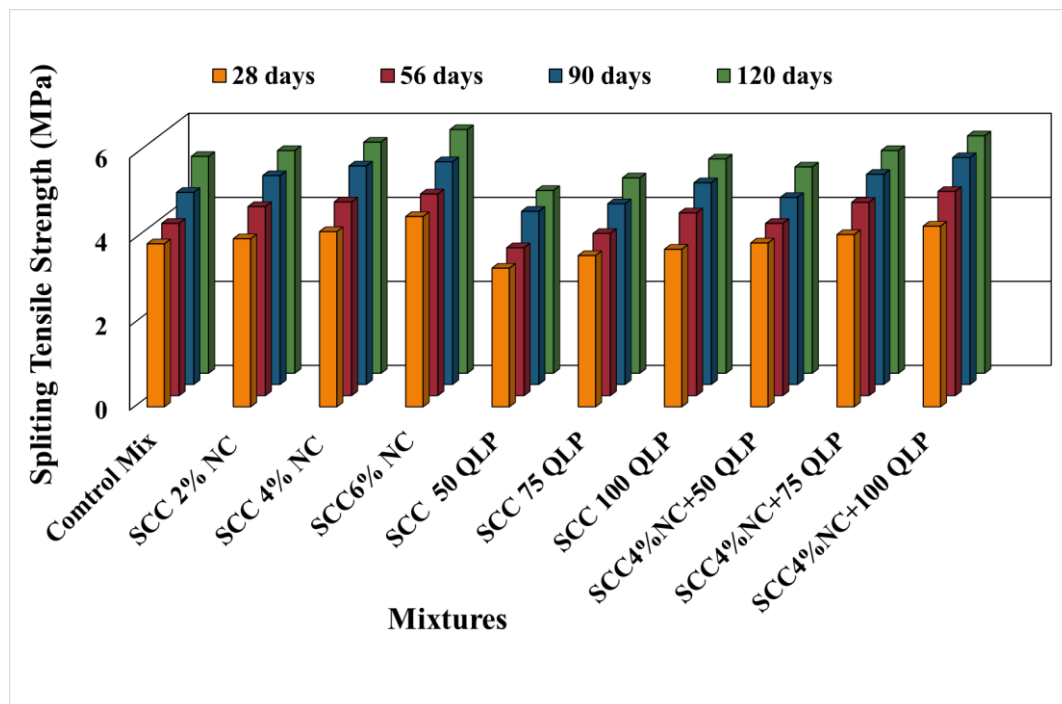
Figure (4-20): Splitting tensile strength for specimens

Furthermore, the addition of NC alone has a more significant effect on SCC specimens' splitting strength and produced higher values than reference SCC (SCC0) and QLP addition. The best value was obtained at SCC 6% NC as compared to QLP addition and SCC0. This is due to the finer size and a specific gravity of NC, which improved the specimens' bonding and hydration **[13, 57, 90]**.

The splitting strength values of SCC 6% NC was higher than reference SCC by about 16.8%, 17.1%, 16% and 12.4% at 28, 56, 90 and 120 days curing ages, respectively. Whereas the addition of QLP alone in SCC caused a gradual increase in splitting strength of the SCC specimens. However, at lower weight percentages (50 and 75QLP), the splitting strength values were lower than reference SCC (SCC0) specimens.

 The splitting strength values of 50QLP and 75QLP mixes in SCC were less than of reference SCC by about 14.9%, 14.1%, 9.8% and 15.7%, and 7.2%, 5.6%, 5.9% and 9.9% at 28, 56, 90 and 120 days curing ages respectively.

Also, the addition of NC and QLP together in SCC progressively increased the splitting SCC specimens' strength. The highest value (4.9 MPa) of splitting strength was obtained for SCC 4% NC-100 QLP. However, based on the obtained results, it can be remarked that the addition of NC has a more significant effect on the splitting strength of SCC as compared to QLP addition in SCC. Also, the combined addition of NC and QLP has noticeable values for splitting the SCC specimens' strength.

4.4.1.3. Flexural Strength Test Results

Table (4-6) (see Appendix A) and figure (4-21) shows the flexural strength results for reference SCC (SCC0) and SCC specimens mixed with Nano clay (NC) and quicklime (QLP).
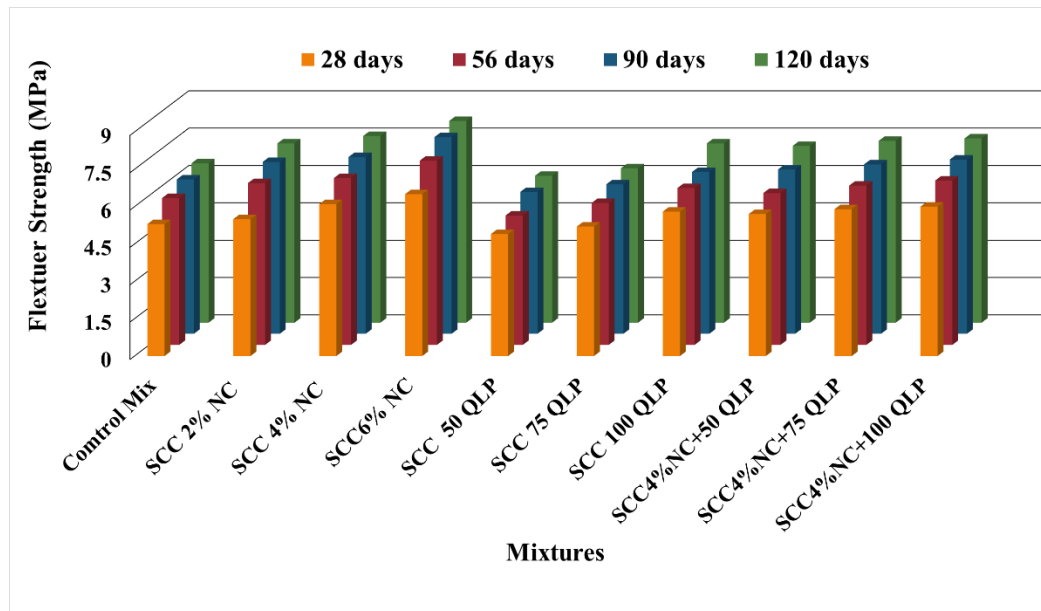
Figure (4-21): Flexural strength for SCCs mixtures

The flexural strength was experimentally investigated for all the specimens cured at 28, 56, 90 and 120 days. The results revealed that flexural strength increased with increasing the curing age at any respective weight percentage of NC and QLP. Moreover, the addition of both NC and QLP caused a gradual increase in the flexural strength of the specimens as is consistent with previous researches **[62, 66]**.

The flexural strength values for SCC specimens mixed with NC only were higher than other mixture. This is the reason that the best value of flexural strength was achieved for SCC 6% NC specimens at any respective curing age. The flexural strength of 6%NC was higher than SCC0 by about 22.6, 25.4, 27.4, 26.5% at 28, 56, 90 and 120 days, respectively. The main reason for such observation is the fine size of NC, which offered better hydration in the mixture specimens.

Whereas the addition of QLP caused an increase in flexural strength of the specimens, but at a lower weight percentage (50 and 75 QLP), the flexural strength was lower than the reference SCC (SCC0) specimen at any respective curing age. The flexural strength values of 50 QLP and 75 QLP mixes in SCC were less than of reference SCC by about 7.5%, 11.9%, 8.1% and 7.8%, and 1.9%, 3.4%, 3.2% and 3.1% at 28, 56, 90 and 120 days curing ages respectively. Furthermore, 100 QLP mix in SCC provided also higher values than SCC0 by about 8.6%, 6.4%, 4.6% and 11% at 28, 56, 90 and 120 days curing ages, respectively.

While in combined addition effect, the NC and QLP produced a gradual increase in the flexural strength, and the values were higher than the flexural strength of reference SCC (SCC0). Thus, it can be concluded that NC has a more significant effect on the flexural strength of SCC specimens as compared to that of QLP.

4.4.1.4. Modules of Elasticity Test Results

Modulus of elasticity is mainly related to the compressive strength of concrete **[167]**. The modulus of elasticity was experimentally found for all the specimens cured at 90 days, as shown in Table (4-7) (see Appendix A) and figure (4-22).

The results clearly showed that the modulus of elasticity of SCC specimens increased with an increase in NC content than control mix by 6.83%, 19.77, and 26.1 of 2%, 4%, and 6%NC, respectively. Moreover, the addition of 100 QLP and hybrid (4% Nano clay+ (50, 75, and100) QLP) as a partial replacement of cement showed an increase of modulus of elasticity than that of SCC0 by about 3.25%, 4.9%, 12.1% and17%, respectively.

Some critical parameters affect the modulus of elasticity of concrete such as, the coarse aggregate properties, mix design, curing age, the aggregate-paste bond(transition zone), density and porosity of cement paste matrix **[168, 169]**.

In the concrete mixture, the Nano clay content also exhibits higher density, which reduces the mixture's void content, which increases the elasticity module of the hardened concrete **[170]**.

While in combined addition effect, the NC and QLP produced a gradual increase in the modulus of elasticity, and the values were higher than the modulus of elasticity of reference SCC (SCC0). Thus, it can be concluded that NC has a more significant effect on SCC specimens' modulus' elasticity compared to that of QLP.
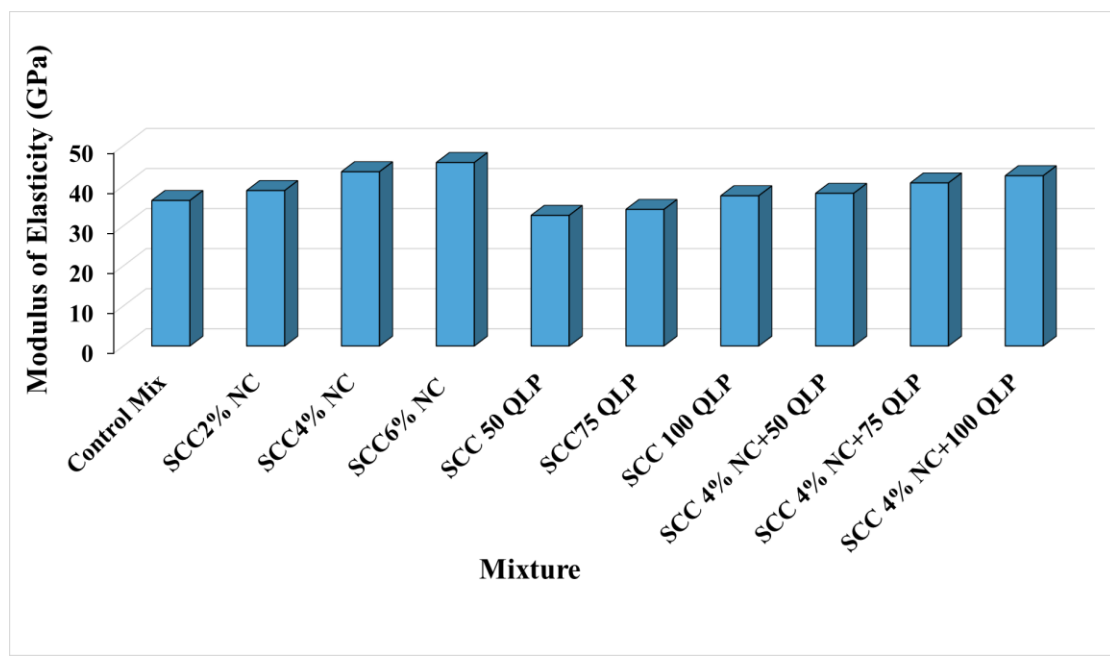
Figure (4-22): Modulus of elasticity for specimens mixed

4.4.2. Physical Tests Results

4.4.2.1. Dry Density Test Results

The dry density results of reference SCC (SCC0) and SCC mixed with NC and QLP at 7, 28, 56, 90 and 120 days curing ages are shown in Table (4-8) (see Appendix A) and Figure (4-23).
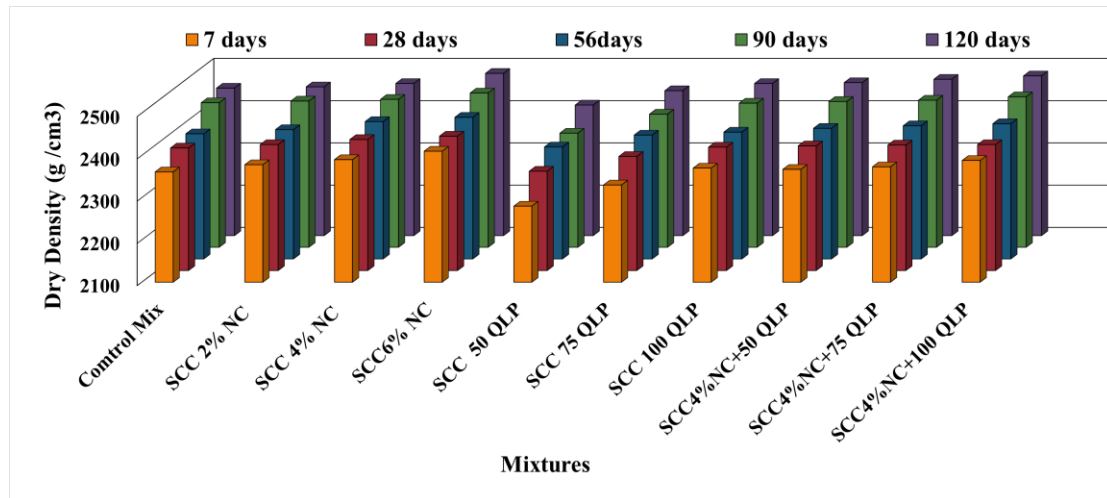
Figure (4-23): Dry density of SCC samples

The values are varied from 2280 to 2410 g/cm^3, 2335 g/cm^3 to 2418 g/cm^3, 2365 g/cm^3 to 2435 g/cm^3, 2370 g/cm^3 to 2465 g/cm^3 and 2409 g/cm^3 to 2484 g/cm^3 for 7, 28, 56, 90 and 120 days curing ages respectively.

The results depicted that increasing the content of NC and QLP, the hardened concrete density increased. Also, the hardened concrete density increased by increasing the curing age at respective weight percentages of NC and QLP. Further, in comparison of NC with QLP, the inclusion of NC provided higher values of the hardened concrete density than SCC-QLP mixtures and reference SCC (SCC0) at respective curing age.

The main reason for it is because ettringite and calcium hydroxide filling the empty space between the structure produced by the big ettringite and calcium hydroxide crystals. This tends to increase the density and hence the transition zone's strength between aggregate and cement paste [166].

For QLP inclusion in SCC, the lower weight percentages of QLP (50 and 75) mixed in SCC provided lower the hardened concrete density values as compared to that of reference SCC (SCC0). The main reason for it is due to the specific gravity value of QLP as compared to the specific gravity value of cement.

For the combined effect of NC and QLP in SCC, the weight percentages of QLP (50, 75 and 100) with 4% NC mixed in SCC provided the gradual increase in the hardened concrete density of the specimens. Further, the hardened concrete density values of such mixture specimens were higher than the hardened concrete density value of SCC0. However, at SCC 100 QLP with 4% NC has best values of the hardened concrete density at respective age and were higher than the hardened concrete density values for reference SCC (SCC0).

Moreover, the same pattern of results was also observed for compressive strength of SCC 50 QLP and SCC 75 QLP with SCC0. It may be important to highlight that the compressive strength and density of SCC are proportioned with each other irrespective of any parameters.

The correlation between compressive strengths and density can be seen in Figure (4-24).The results indicate that the mixing density showed almost the same compressive strength pattern by an outstanding significant polynomial relationship with a coefficient correlation of R^2 = 0.9857, 0.9496, 0.9077, 0.8405 and 0.8142 at 7, 28, 56, 90 and 120 days of age, respectively.
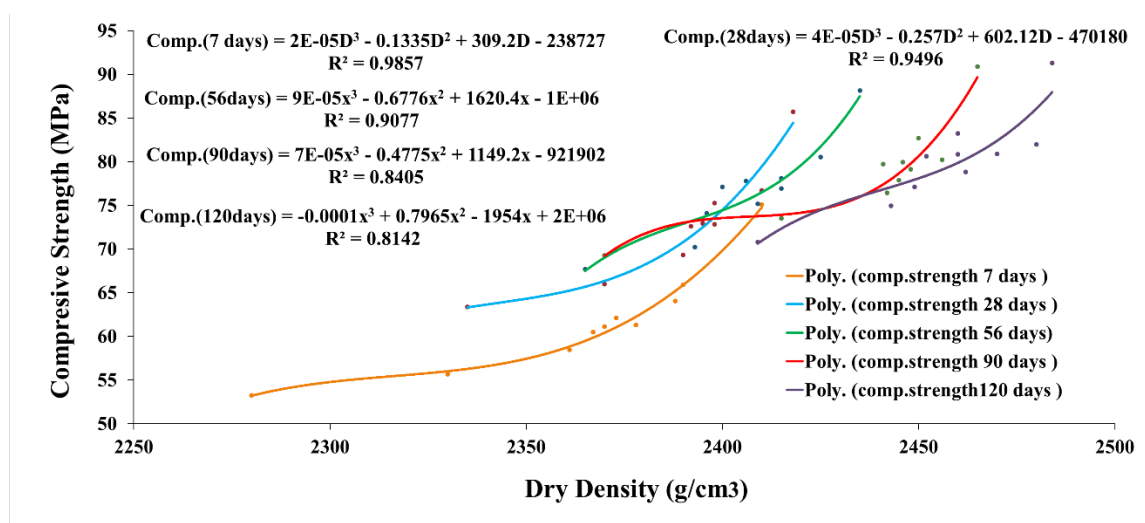
Figure (4-24) Relationship between compressive strength and dry density for all mixes

4.4.2.2. Ultra Pulse Velocity (UPV) Test Results

Table (4-9) (see Appendix A) and figure (4-25) shows the UPV results for reference SCC specimen and SCC specimens mixed with NC and QLP. The UPV of all specimens was calculated at 7, 28, 56, 90, and 120 days curing ages.
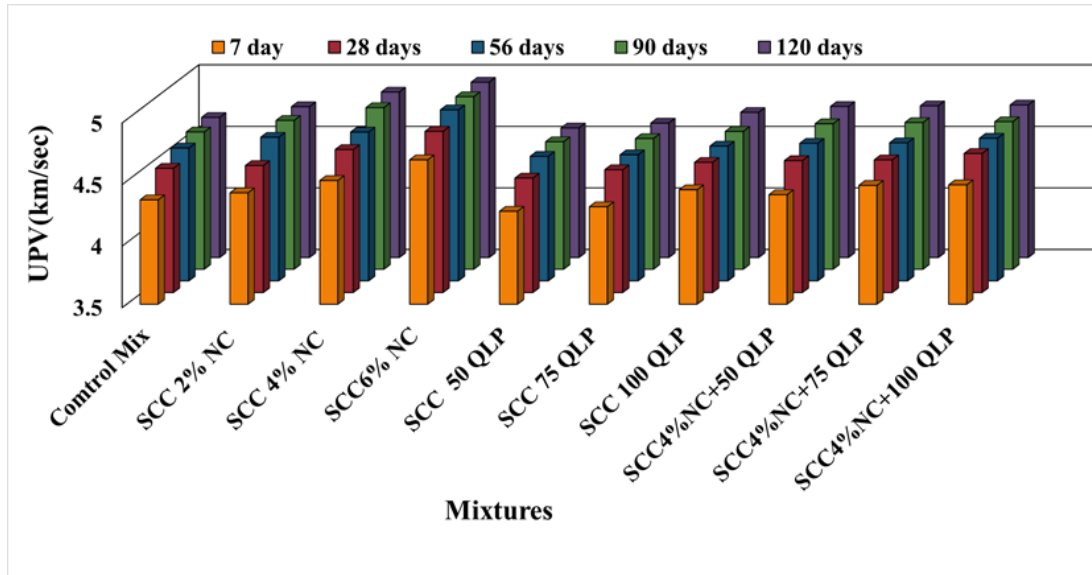
Figure (4-25): Ultra Pulse Velocity for SCC specimens

 The UPV values were obtained in the range of 4.255 to 4.673 km/s, 4.43 to 4.81 km/s, 4.512 to 4.89 km/s, 4.536 to 4.902 km/s and 4.553 to 4.925 km/s for 7, 28, 56, 90 and 120 days curing ages respectively. The results pattern defined that the UPV increased by increasing the curing age.

 It must be supposed that UPV is mainly dependent on concrete density, moisture content, and curing duration. This is the reason that higher values of UPV were obtained at the upper curing age period at any respective weight percentages of both NC and QLP inclusion. In the comparison of NC to QLP, NC addition produced higher UPV results than reference SCC (SCC0) and QLP mixed in SCC specimens. It is mainly because of the improvement in NC density as compared to cement (for SCC0) and QLP.

The highest value of UPV was obtained at higher content of NC (SCC 6% NC) with respect to curing age. Furthermore, the smaller content of QLP (50 and 75 QLP)

provided less and or the same values of UPV as compared to that of reference SCC (SCC0). However, these obtained results depicted a very high quality of concrete according to IS: 13311 quality criteria **[171]**.

Moreover, the UPV results showed the same pattern of compressive strengths as obtained in the mechanical compressive strength. The main reason for it is because of the polynomial relationship between both. Due to it the correlation illustrated in Figure (4-26) showed that the UPV of mixes displayed the same compressive intensity pattern with an outstanding positive exponential correlation coefficient relationship R^2 = 0.9855, 0.9402, 0.9217, 0.8838 and 0.909at ages 7, 28, 56, 90 and 120 days, respectively.
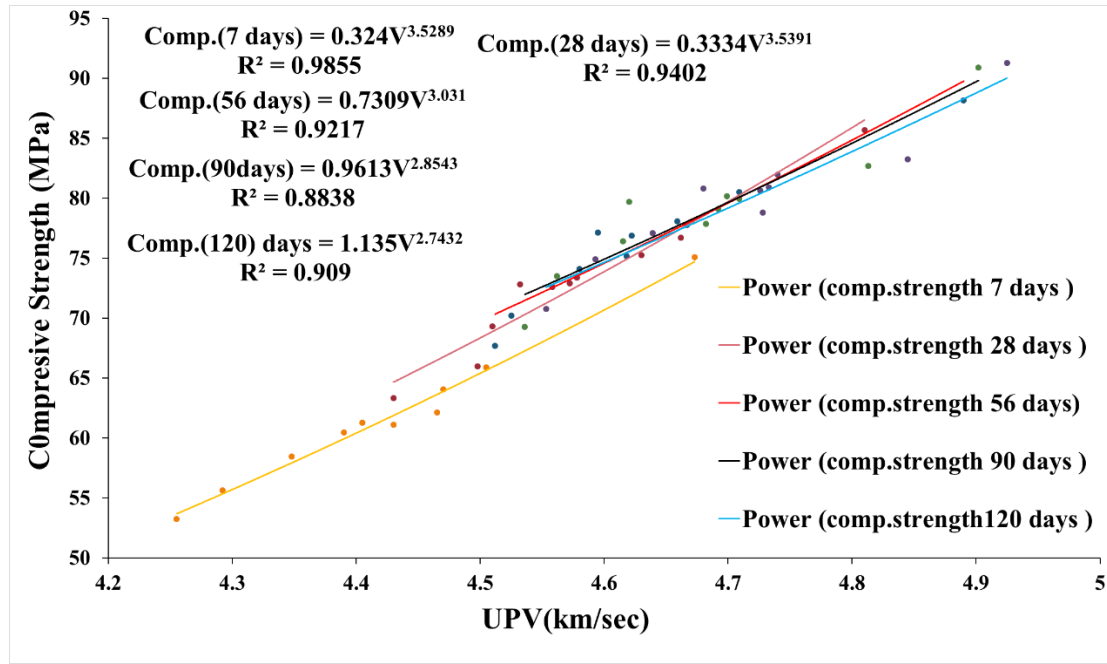
Figure (4-26): Relationship between compressive strength and ultra-pulse velocity for all mixes

4.4.2.3. Volume of Permeable Pores (Voids)Test Results

Table (4-10) (see Appendix A) and Figure (4-27) show the voids results of reference SCC (SCC0) and SCC mixed with NC and QLP at 28, 56, 90 and 120 days curing ages.
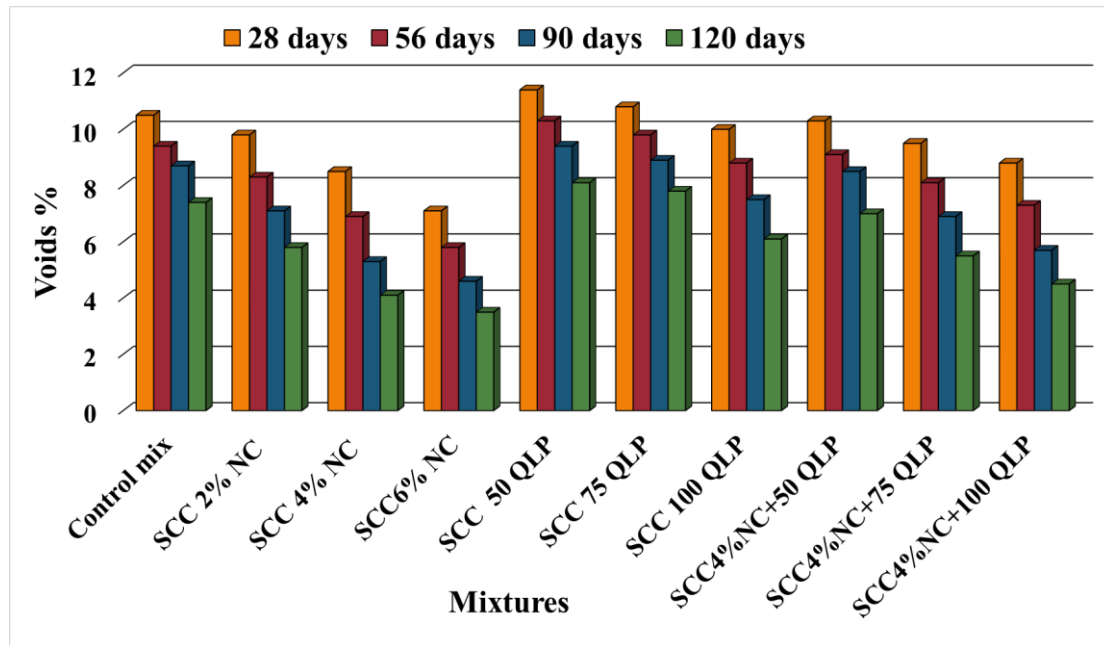
Figure (4-27): Volume of permeable pores (Voids) for specimens mixed

The results describe that the increase of content NC and QLP leads to a decrease the permeable voids. Also, it decreased by increasing the curing age at respective weight percentages of NC and QLP. Furthermore, the addition of both NC and QLP caused a gradual decrease in the voids of the specimens.

The volume of permeable pores values of SCC specimens mixed with NC only was lower than that of reference SCC (SCC0) and SCC specimens mixed with QLP. The reason is that the best value of reduction in voids was achieved for SCC 6% NC specimens at ay respective curing age. The voids of 6% NC were lower than SCC0 by about 32.38, 38.3, 47.12, 52.7% at 28, 56, 90 and 120 days.

The addition of nanomaterials has been reported to refine the pore structure of cement paste or concrete, decrease the amount of mixed cement, and improve the mechanical properties and durability of concrete **[172,173]**. Decreased voids are coherent with the corresponding trend of bulk density, where density increased with time.

The reduction of voids leads to a denser hardened SCC with time associated with the continuous hydration and pozzolanic reaction of NC, which takes place at a later age. These two reactions give a similar product, i.e. calcium silicate hydrates, which refine the pores of hardened SCC. For QLP inclusion in SCC, the lower weight percentages

111

of QLP (50 and 75) mixed in SCC provided higher voids values as compared to that of reference SCC (SCC0) by about (7.9 and 2.8) %, (8.7 and 4.1) %, (7.4 and 2.2) %, (8.6 and 5.13) % at 28, 56, 90 and 120 days, respectively.

In combining the addition effect, both NC and QLP produced a gradual decrease in the volume of permeable pores, and the values were lower than the volume of permeable pores of reference SCC (SCC0). Thus, it can be concluded that NC has a more significant effect on the voids of SCC specimens as compared to that of QLP.

4.4.2.4. Water Absorption Test Results

Table (4-11) (see Appendix A) and Figure (4-28) indicates the water absorption of control and SCC mixtures incorporating various weight percentages of NC and QLP.
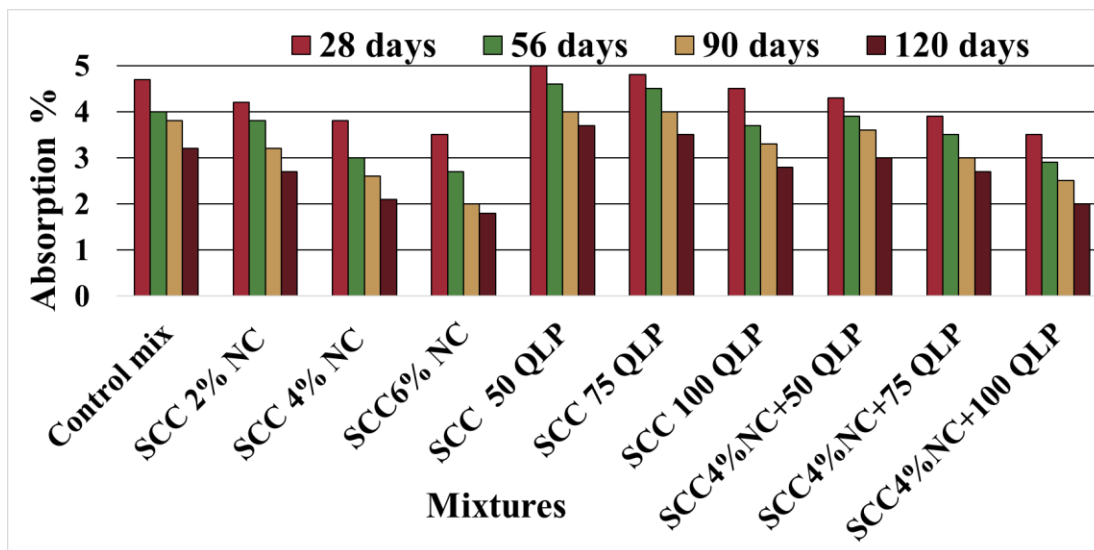
Figure (4-28): Water absorption of specimens.

The results revealed that the inclusion of NC and QLP decreased the water absorption of the SCC mixtures. Additionally, the water absorption decreased by increasing the curing age at respective weight percentages of NC and QLP.

Moreover, the water absorption values for NC and QLP (SCC 100 QLP) were lower than that of the reference SCC. Further, the lower weight percentages of QLP caused to have water absorption higher than SCC0, whereas all the contents of NC in SCC have lower water absorption.

Porosity in concrete is affected by the size of the interface zone between aggregates and paste, which has control over the number of pore openings. Compared to bulk paste, the porosity of this zone is higher **[174]**. The pores can appear as macro-pores, capillary pores and gel pores in the concrete. Together with the macro-pores, pores of (0.01-1) μm in size have a real effect on ionic transport properties. For ionic transport by capillary suction, as measured by water absorption, only pores about 0.5μm in size can be accessed by water **[175]**.

In SCC, the proportion in which finer components tend to be higher while the coarser components are lower than conventional concrete which is critical in achieving moderate viscosity. A higher surface area of the solid particles with a higher finer proportion will hold free water in the mixture. Also, in the absence of a compacting process, free water is not disrupted. Therefore, there is a lower tendency to bleed and accumulate water around aggregates, leading to lower pores in the ITZ **[174, 175]**.

A higher addition of fillers or pozzolanic materials such as NC and QLP to the SCC mix results in lower absorption of water **[174]**, which may be associated with the enhanced distribution of particles, reduction of inter-particle friction, and higher packing density.

From what was mentioned previously, the water absorption of 6% NC was lower than that of SCC0 by about 25.5, 32.5, 47.4, 43.75% at 28, 56, 90 and 120 days, respectively. Moreover, as comparing the NC to QLP, NC has a more significant effect on the water absorption of SCC. However, higher values of QLP replacement can provide lower water absorption. Thus, the utilization of both NC and QLP to replace the cement positively impacts On SCC.

4.4.3. Durability Tests of Self-Compacting Concrete

4.4.3.1. Influence of High-Temperature Environment on SCC Properties

I – Compressive Strength Results

The test results of the compressive strength values at (200, 400, 600, 800) °C under 3 hours heating time for all mixes at 56, 90 and 120 days curing ages are shown in Tables

(4-12), (4-13) and (4-14), respectively (see Appendix A). The results revealed that the loss of compressive strength ratio decreased by the inclusion of NC and QLP and increasing the curing age. For all mixtures, compressive strength increases at 200 °C and then decreases as the temperature rises above 200 °C. The SCC 6% NC mix achieved the maximum gain in compressive strengths than its control mix (SCC0). The gain in compressive strength at 200 °C is 6.23%, 6.49%, and 6.34%, while the corresponding minimum loss in compressive strength at 800 °C is 64.39%, 61.02%, and 55.8% at ages 56, 90, and 120 days, respectively.

Figures (4-29), (4-30), and (4-31) showed that the heating conditions can be divided into two stages (at room temperature to 200) °C, and (200 to 800) °C from the perspective of SCC specimens' compressive strength at curing ages 56, 90 and 120 days.
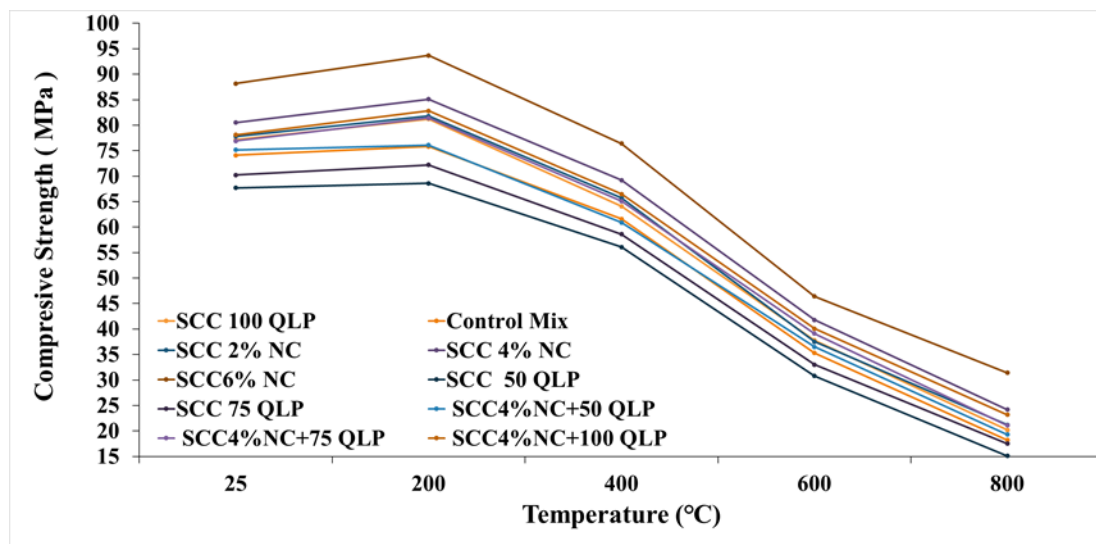
Figure (4-29): Residual compressive strength of SCCs containing NC and QLP after exposure to a temperature at age 56 days

114
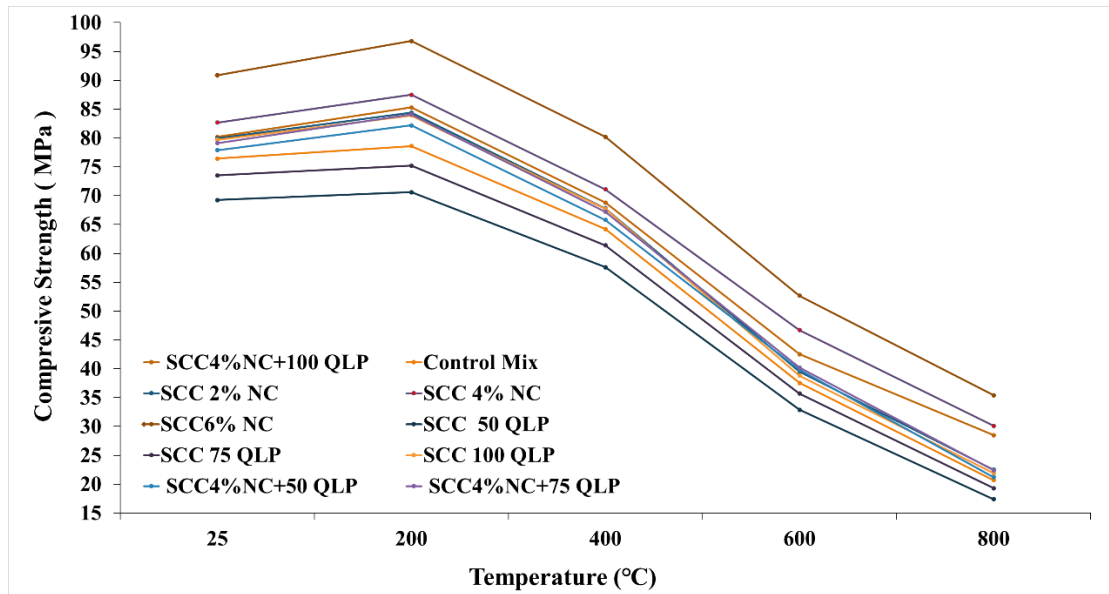
Figure (4-30): Residual compressive strength of SCCs containing NC and QLP after exposure to a temperature at age 90 days
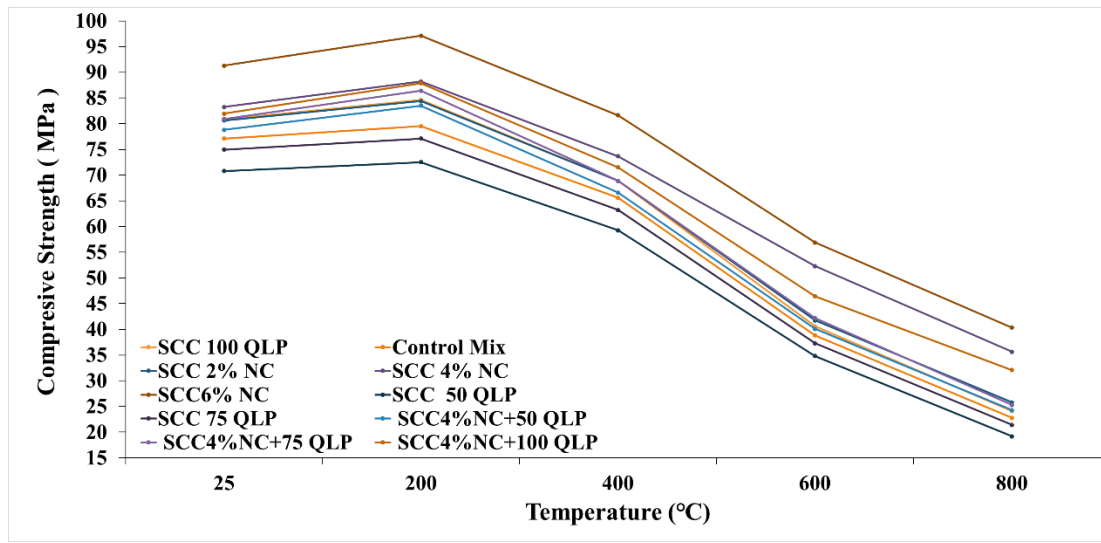
Figure (4-31): Residual compressive strength of SCCs containing NC and QLP after exposure to a temperature at age 120 days

The results stated that the Nano clay improved the compressive strength under heating temperatures because the specimens of Nano clay are denser as is consistent with previous researches **[86,102]**. There is a decrease in the amount and extent of micro cracking in the transition zone.

Furthermore, the lower weight percentages of the mixtures containing QLP (50 and 75) kg achieved a minimum gain at 200 °C and a maximum loss at 800 °C in compressive strength. While higher values of QLP replacement can reduce the compressive strength loss ratio. Finally, SCC specimens' compressive strength values hybrid (4% Nano clay+ (50, 75 and 100QLP)) as a partial replacement of cement were higher than reference SCC specimen(SCC0) under burning temperatures. Thus, the utilization of both NC and QLP to replace the cement, has a clear effect on the production of SCC.

From above Figures can see that there is little increase in strength from (at room temperature to 200) °C for the control mix, followed by a sharp decrease in the higher heating degrees. As a result of the steam effect, the increase in strength up to 250 C may well be due to the continuous hydration of un hydrated cement grains under the so-called internal autoclaving effect condition. On the other hand, the specimens with Nano Clay and QLP showed an increase in compressive strength higher than that of control specimens at (at room temperature to 200) °C stage.

The increase in strength of blended cement mortars may be due to the pozzolanic the reaction of amorphous aluminosilicate (Al_2O_3 $2SiO_2$) present in NC and QLP with CH freed during SRC hydration. That could be form an additional amount of C-S-H that has low Ca/Si ratio with high resistance as well as calcium aluminates hydrate (C-A-H) phases that deposit in the pore system [176, 177].

The thermal effect might cause water migration at high temperatures, whereas dehydration of moisture supply from outside is insufficient. Due to the heterogeneous volume dilatations of ingredients and the buildup of vapor in the pores, internal stress micro, and macro cracks are generated. Therefore, the observed decrease in compressive strength of mixtures concrete containing nanomaterials and QLP at higher temperatures, especially above 200 °C, may be due to internal thermal stress generated around pores, which generate micro-cracks [177].

The decrease in SCC mixtures' compressive strength at (200 to 800) °C is attributed to the break-down of interfacial bond due to incompatible volume change between cement paste and aggregate during heating and dehydration of the calcium-silica hydrate in cement paste [57].

Results showed remarkable enhancement for mixes that have Nano additives in their composition with different ratios.

II-Mass Loss Results

The mass loss results of reference mix (SCC0) and SCC mixed with NC and QLP at 56, 90 and 120 days curing ages at (200, 400, 600, 800) °C under 3 hours heating time are shown in Tables (4-15), (4-16) and (4-17) (see Appendix A) and Figures (4-32), (4-33) and (4-34) respectively.

The results revealed that the mass loss ratio decreased by increasing the replacement ratio of NC and QLP and increasing the curing age. Moreover, the mass loss values of NC and QLP (SCC 100 QLP) were lower than the mass loss of reference SCC specimen (SCC0). Furthermore, the lower weight percentages of QLP caused mass loss higher than that of SCC0, whereas all the contents of NC in SCC have a lower mass loss.

However, the overall minimum value of mass loss ratio was achieved for SCC 6% NC at 120 days curing age at (200, 400, 600, 800) °C under 3 hours heating time. This means that at the higher percentage of NC associated with the most upper curing age provided the minimum value of mass loss ratio.
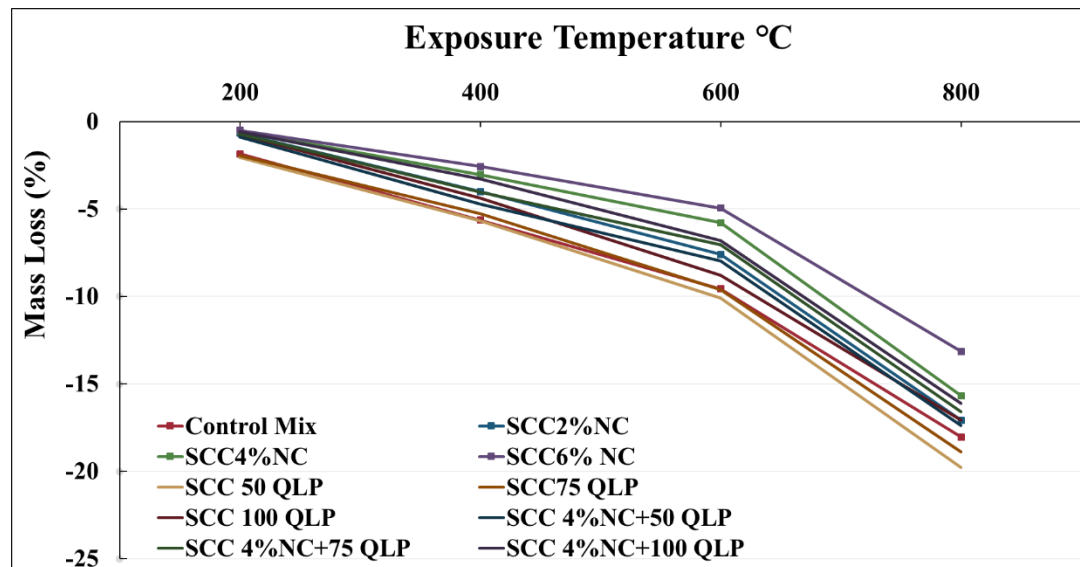
Figure (4-32): Mass loss of mixtures after exposure to a burning temperature at age 56 days
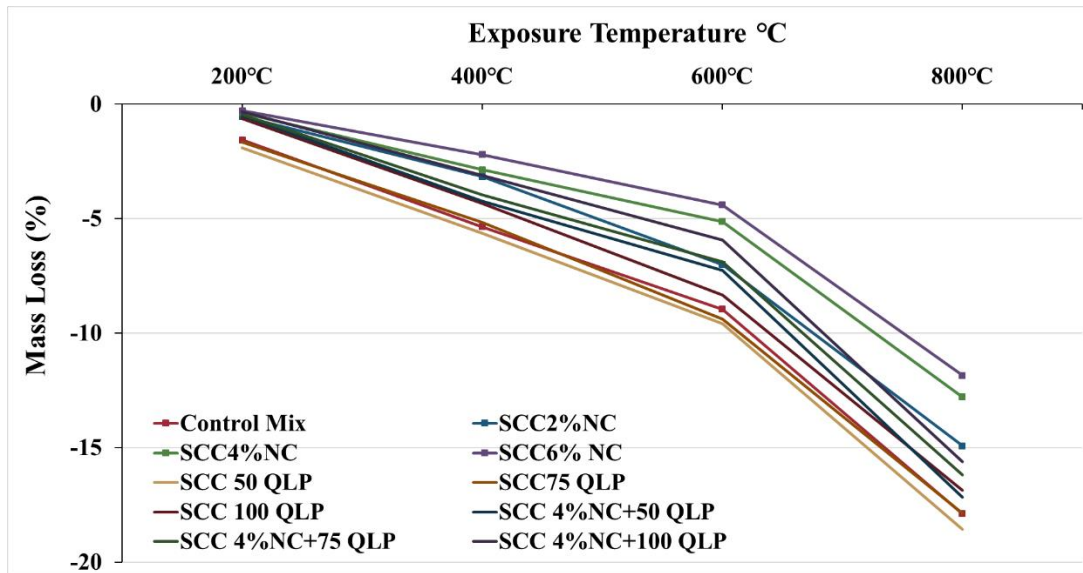
Figure (4-33): Mass loss of mixtures after exposure to a burning temperature at age 90 days
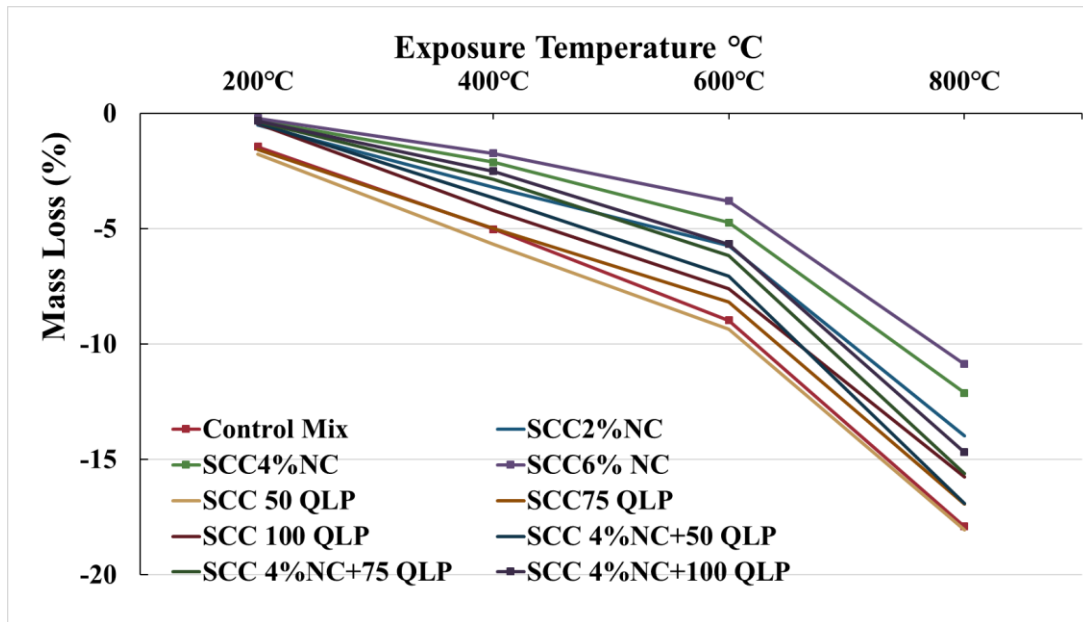
Figure (4-34): Mass loss of mixtures after exposure to a burning temperature at age 120 days

The temperature ranges of (200 to 400) °C is the most favorable for the dehydration of general cement paste components (tobermorite gel, ettringite, and C-S-H gel); this could explain the mass loss in this temperature region. Portlandite decomposes to CaO above 400 °C and escaping water vapor causes another loss of mass.

 Temperatures above 600 °C lead to calcite decomposition, and the CO_2 originates from the cement paste escapes, thus reducing its mass. Anhydrite decomposition may be one of the causes of higher mass loss at temperatures of 800 °C **[178]**.

Figure (4-35) showed the shape of the cement paste after subjecting it to a 600 °C burning through the compressive strength test.

Figure (4-35): The specimen failure at age 90-day under temperature 600°C at 3 hours heating duration.

4.4.3.2. Influence of a Magnesium Sulfate Attack Environment on SCC Properties.

I- Visual Observation.

There was no change in the dimensions of the SCC specimens. Still, efflorescence was observed on the surface of the specimens immersed in both 5%,10%, and 20%

MgSO$_4$ solutions for 30, 60 and 90 days' immersion, and it increased with an increase in the concentration and days of immersion. The photograph of the specimens was shown in Figure (4-36).

Figure (4-36): Specimens exposed to magnesium sulfate attack

II-Mass Loss Results

After immersion in cycles wet and dry 5%, 10% and 20% MgSO$_4$ solution for 30, 60 and 90 days, the ratio of loss mass was determined. The results were compared with those of specimens stored at the same ages in ordinary curing water at ages 56, 90, and 120 days.

 The resulting specimen's deterioration is presented in Tables (4-18), (4-19), and (4-20) (see Appendix A) and Figures (4-37), (4-38), and (4-39), respectively.

The results showed the mass loss values for NC, QLP (SCC 100 QLP) and inclusion of NC and QLP were lower than the mass loss of reference SCC specimen (SCC0). Furthermore, the lower weight percentages of QLP caused to have mass loss higher than SCC0, whereas, all the contents of NC in SCCs have a lower mass loss. However, the overall minimum values of the loss of mass were achieved for SCC 6% NC.
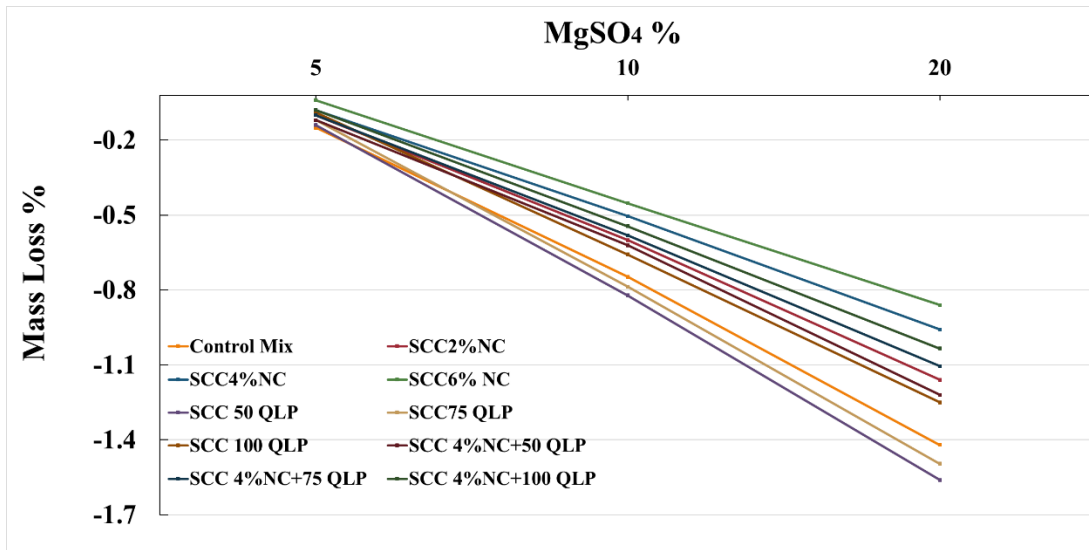
Figure (4-37): Percentage loss of mass after immersion in cycles wet and dry magnesium sulfate for 30 days.
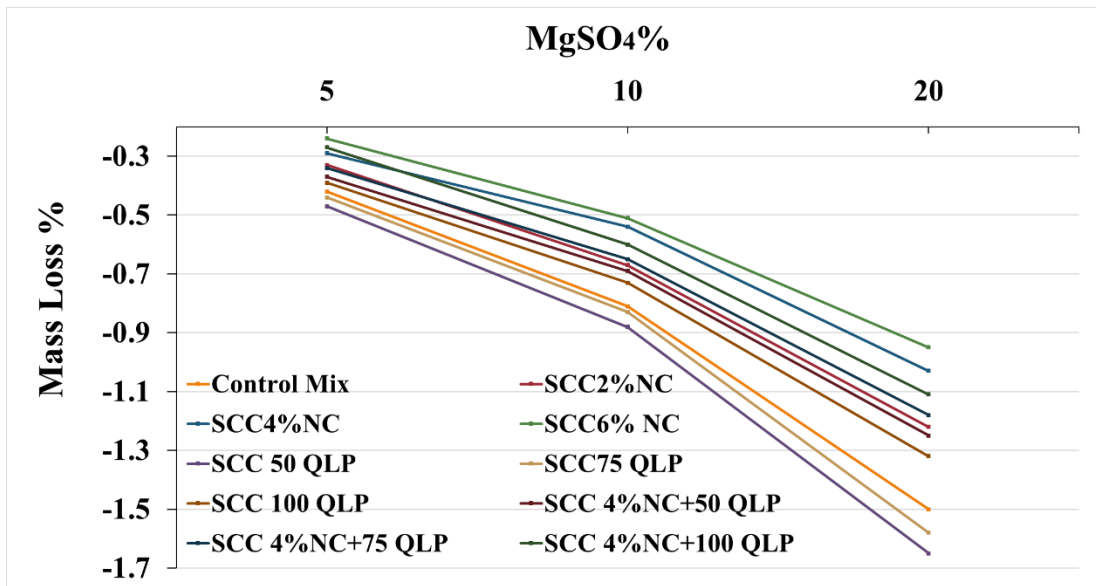
Figure (4-38): Percentage loss of mass after immersion in cycles wet and dry magnesium sulfate for 60 days.
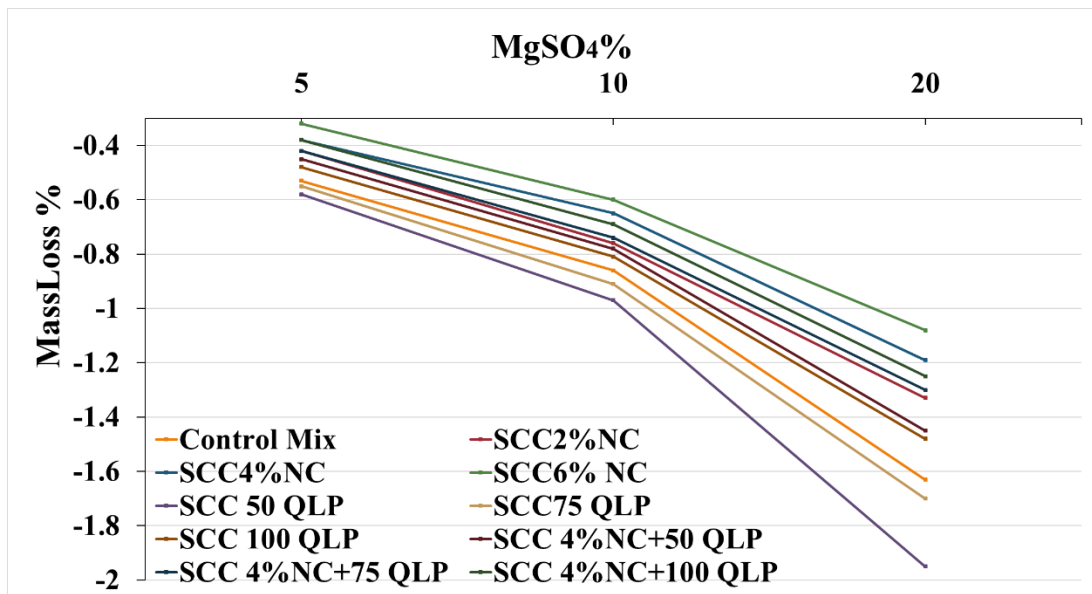
Figure (4-39): Percentage loss of mass after immersion in cycles wet and dry magnesium sulfate for 90 days.

Finally, SCC specimens' mass loss values mixed with 50, 75 and 100 QLP, and 4% NC were lower than reference SCC specimen (SCC0). Moreover, for most mixtures, the rate of mass loss was low due to low porosity, the low content of C_3S as a result of the use of sulfate resistant cement and the pozzolanic reaction of nanomaterials that consume this compound. Generally, exposure to sulphate causes an increase in the volume of cement paste in concrete or motor. It can be explained that sulfate ions in the soil, groundwater and seawater diffuse into the hydrated cement paste and react with C_3A in the presence of $Ca(OH)_2$ to form ettringite and gypsum, causing concrete expansion and deterioration **[179]**.

The degradation mechanism can be explained due to magnesium sulfate attack, brucite $(Mg(OH)_2)$ is also formed and brucite retards the adverse effects of sulfate attack at a preliminary stage. In the following stages, however, the decomposition of C-S-H gel to M-S-H gel occurs; thus, the binder is softened, and mechanical strength is reduced **[180]**.

III- Variation in UPV After Exposure to Magnesium Sulfate Results

The experimental results from the cube specimens (100 x 100 x 100) mm with w/c of 0.38 achieved a lower loss of UPV for period 30,60, and 90 days after immersion in cycles wet and dry 5%, 10% and 20% $MgSO_4$ solution. The results were compared with those of specimens stored at the same ages in ordinary curing water at ages 56, 90, and 120 days. The ultrasonic test methodology is based on the fact that the time of propagation expresses the material density that could be correlated with the mechanical properties, such as the compressive strength and the elasticity module **[181]** .

Tables (4-21), (4-22), and (4-23) (see Appendix A) and Figures (4-40), (4-41) and (4-42), respectively, present results of UPV losses.
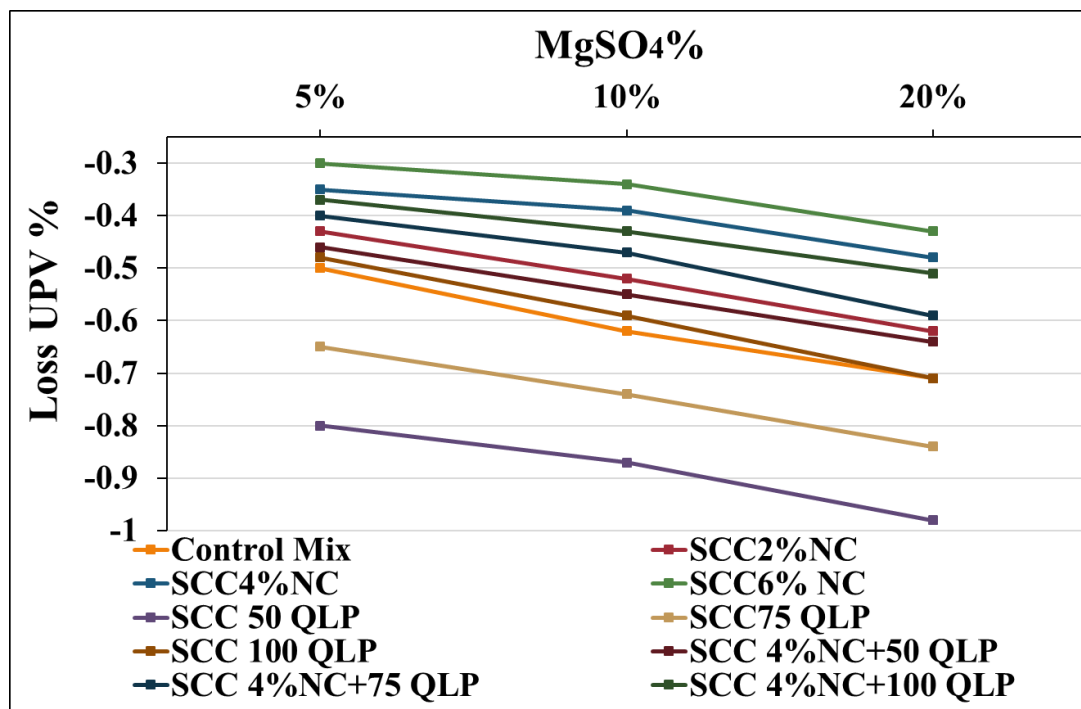
Figure (4-40): Change in UPV after immersion in cycles wet and dry magnesium sulfate for 30 days.
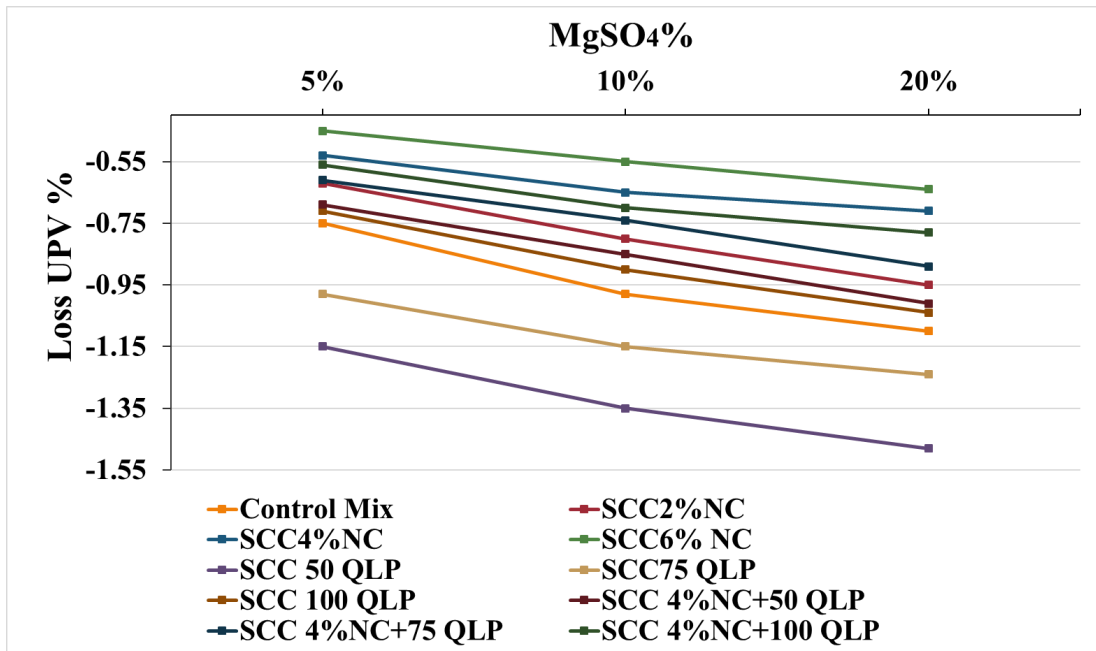
Figure (4-41): Change in UPV after immersion in cycles wet and dry magnesium sulfate for 60 days.
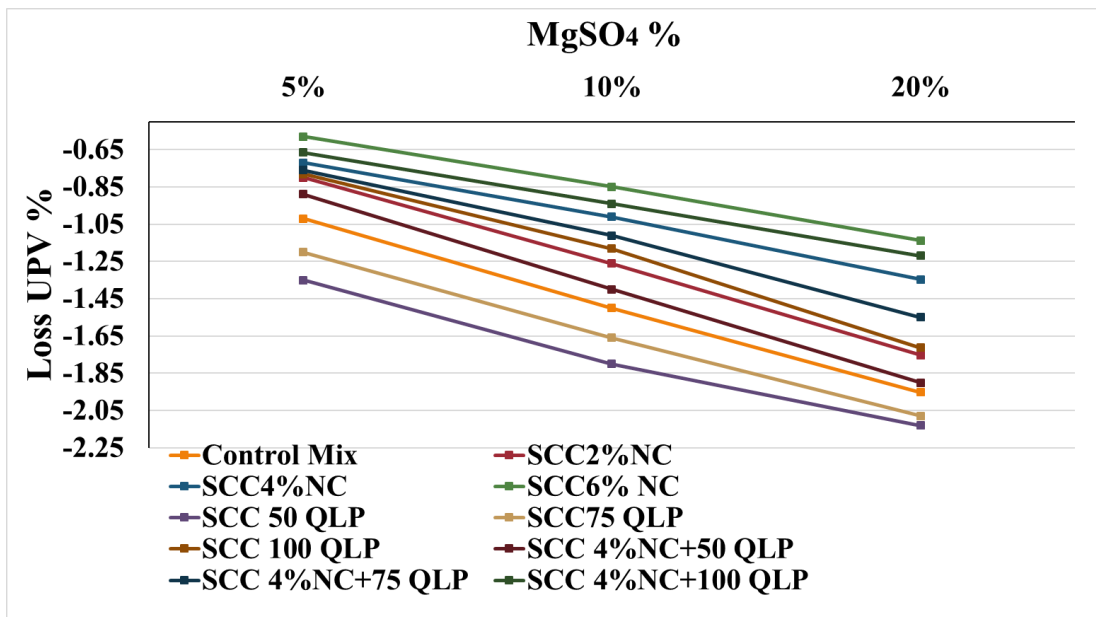
Figure (4-42): Change in UPV after immersion in cycles wet and dry magnesium sulfate for 90 days.

The results showed that UPV loss values for NC, QLP (SCC 100 QLP), NC and QLP inclusion were lower than that of the reference SCC specimen UPV loss (SCC0). Besides, UPV loss greater than that of control mix which was caused by the lower weight percentages of QLP, whereas all NC contents in SCCs have a lower loss of UPV.

For SCC 6 % NC, however, the overall minimum values of UPV loss were achieved. Finally, the UPV loss values of SCC specimens mixed with 50, 75 and 100 QLP, and 4 % NC were lower than that of the reference SCC specimen values (SCC0).

The low loss of UPV of the samples can be explained for several reasons, including (1) using self-compaction concrete known for its high durability. (2) using sulfate-resistant cement increases the loss resistance of the mass. (3) using Nano clay increases the density of concrete to the severity of its pozzolanic reaction, thus reduces the voids inside the concrete, which in turn reduces the permeability of the sulfate ion inside the concrete.

IV- Compressive Strength Loss Results

Tables (4-24), (4-25), and (4-26) (see Appendix A) and Figures (4-43), (4-44), and (4-45) indicates the compressive strength of control and SCC mixtures incorporating various weight percentages of NC and QLP which was studied after 30, 60, and 90 day of immersion in 5%, 10%, and 20% magnesium sulfate solution.

The results were compared with those of specimens stored in fresh water at the same ages. Additionally, the percentage loss of compressive strength was observed to be increased with increasing time at 5,10 and 20 respective weight percentages of sulfate solutions. Moreover, the compressive strength loss values for NC, QLP (SCC 100 QLP) and inclusion of NC and QLP were lower than the compressive strength loss of reference SCC. Furthermore, the lower weight percentages of QLP caused to have compressive strength loss higher than SCC0, whereas, all the contents of NC in SCC have lower compressive strength loss.
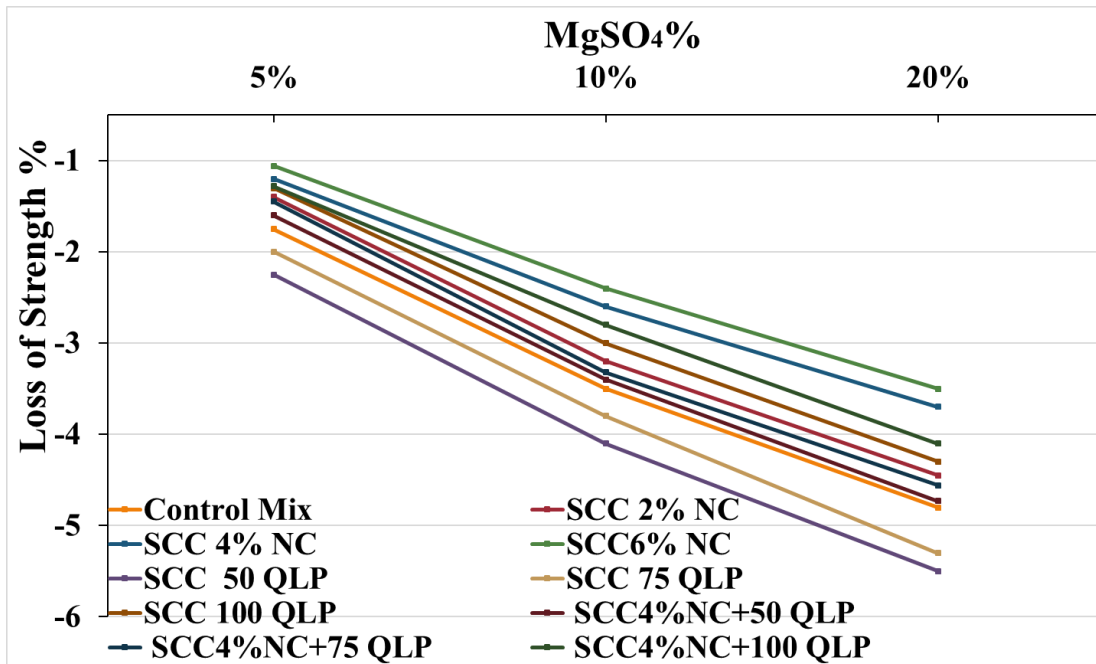
Figure (4-43): Loss of compressive strength for mixtures after immersion in cycles wet and dry in magnesium sulfate for 30 days
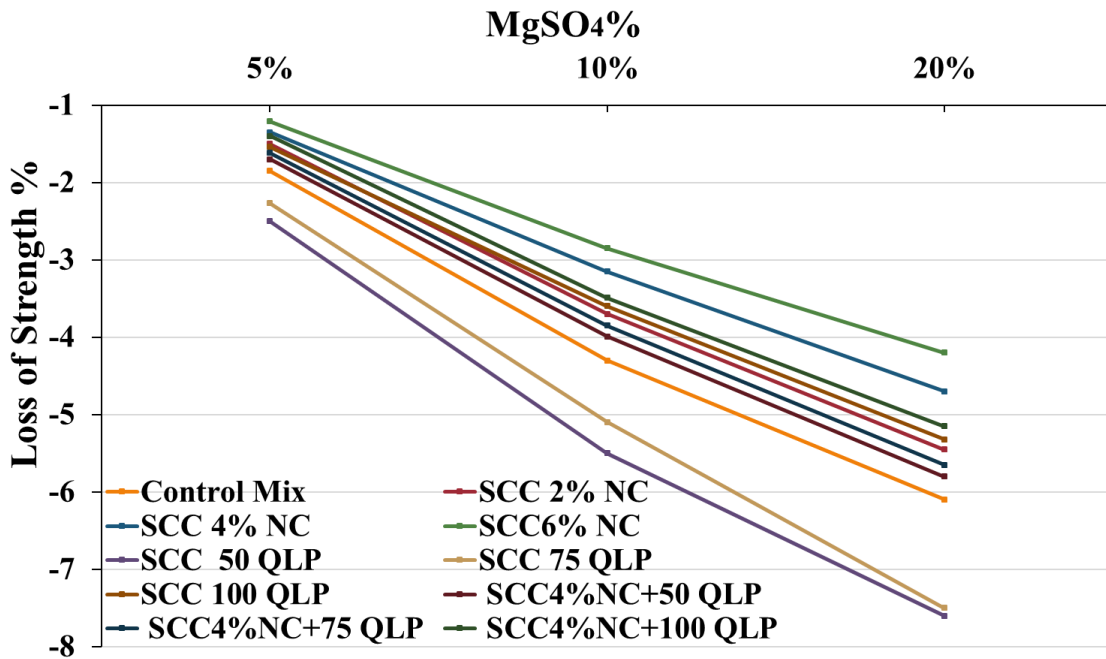
Figure (4-44): Loss of compressive strength for mixtures after immersion in cycles wet and dry in magnesium sulfate for 60 days
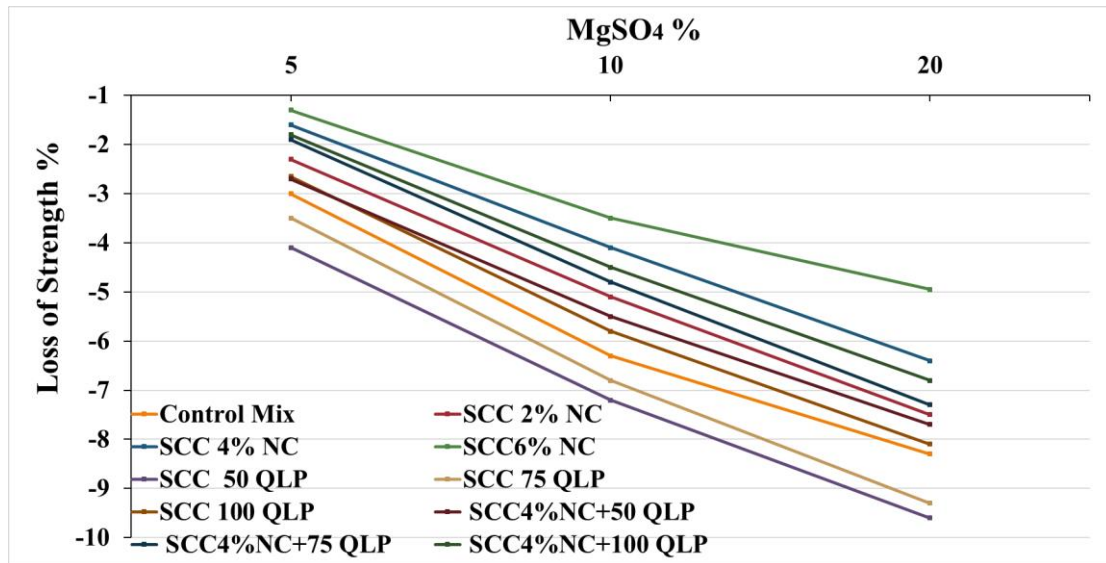
Figure (4-45): Loss of compressive strength for mixtures after immersion in cycles wet and dry in magnesium sulfate for 90 days

The strength loss at 30 days of sulfate immersion was lower than that of control mix (SCC0) by 20%, 31.43% and 39.43% at 5% $MgSO_4$, 17.14%, 25.71% and 31.43% at 10% $MgSO_4$, 14.6%, 22.9% and 27.1% at 20% $MgSO_4$ for 2, 4 and 6% of NC mixed in SCCs respectively.

At 60 days of sulfate immersion, the strength loss was lower than SCC0 by 18.92%, 27% and 34.6% at 5% $MgSO_4$, and 13.9%, 24.4% and 30% at 10% $MgSO_4$, and 10.7%, 21.3% and 29.5% at 20% $MgSO_4$ for 2, 4 and 6% of NC mixed in SCCs respectively.

Finally, the strength loss at 90 days of sulfate immersion was lower than SCC0 by 23.34%, 46.7% and 56.7% at 5% $MgSO_4$, 19%, 34.9% and 44.5% at 10% $MgSO_4$, 9.6%, 22.9% and 40.4 % at 20% $MgSO_4$ for 2, 4 and 6% of NC mixed in SCCs respectively.

However, the overall minimum values of the compressive strength loss were achieved for SCC 6%NC. The lower loss of concrete strength with Nano clay shows that it serves as a filler to increase the micro's density and acts as an activator in the hydration reaction. Nano clay freely mixes with free calcium oxide resulting in further reactions that form new cement paste and chemically stable. This affects the relationship between

the mortars, and the inter-surface zone which becomes stronger and increases the bonds between coarse aggregate and mortar.

The impermeability of concrete is enhanced, leading to a smaller amount of water-soluble $SO4^{-2}$ content in concrete under the sulfate attack. The nanomaterial can also reduce calcium aluminate (C_3A) content in cementitious material, leading to increase sulfate resistance of concrete **[182]** .

The compressive strength loss values of QLP 50 and QLP 75 mixes in SCC were higher than that of reference SCC, While the 100 QLP mix in SCC provided lower the strength loss than SCC0 due to the gypsum and ettringite content which were reduced under sulfate attack by using the large amount replacement of cement by pozzolans materials. Finally, SCC specimens' compressive strength loss values mixed with 50, 75 and 100 QLP and 4% NC were lower than reference SCC specimen (SCC0).

The strength loss values were lower than the SCC0 at 30 days of sulfate immersion by 8.6%, 17.14% and 26.86% at 5% $MgSO_4$, 2.9%, 5.1% and 20% at 10% $MgSO_4$, 1.5%, 5% and 14.6% at 20% $MgSO_4$ for SCC specimens mixed with 4% NC-50 QLP, 4% NC-75 QLP and 4% NC-100 QLP mixes respectively.

At 60 days of sulfate immersion, the strength loss was lower than SCC0 by 8.1%, 12.43% and 24.32% at 5% $MgSO_4$, and 6.97%, 11.63% and 18.84% at 10% $MgSO_4$, and 6.23%,7.37%, and 15.6% at 20% $MgSO_4$, for SCC specimens mixed with 4% NC and (50 QLP, 75 QLP, 100 QLP) mixes respectively.

Finally, the strength loss at 90 days of sulfate immersion was lower than SCC0 by 10%, 36.7% and 40% at 5% $MgSO_4$, 12.7%, 23.8% and 28.6% at 10% $MgSO_4$, 7.23%, 12% and 18.1 % at 20% $MgSO_4$ for SCC specimens mixed with 50, 75 and 100 QLP and 4% NC respectively.

 Furthermore, at a higher weight percentage of QLP (100 QLP) and 4% NC has the best value of compressive strength loss compared to reference SCCs. The main reason for obtaining the best value of this mixture's strength loss is NC and QLP inclusion's combined effect. Although the samples did not significantly degrade compared to the high concentration of magnesium sulfate of 20% in the most extended curing period at

90 days due to the use of sulfate-resistant cement containing a low amount of C_3A the primary source of attack sulfate.

However, the highest resistance loss was 9.6% for the mixture SCC 50 QLP, but NC roughly halved the loss for the same concentration and same duration and was 4.95%. Based on the obtained results in this research, it can be concluded that the NC and QLP have a significant effect on the resistance of sulfate of the SCC. Moreover, as comparing the NC to QLP, NC has a more significant effect on the resistance.

However, higher values of QLP replacement can provide significant resistance of sulfate. Thus, the utilization of both NC and QLP to replace the cement positively impacts fabrication SCC. Figure (4-46) shows the sample of SCC0 after exposed to 10% MgSO4 solution at age 120 days.

Figure (4-46): Sample of control mix (SCC0) after immersion cycles wet and dry in 10% MgSO₄ solution at 120 days.

CHAPTER FIVE

CONCLUSIONS

and

RECOMMENDATIONS

Chapter Five

Conclusions and Recommendations

5.1. Conclusions:

Based on the obtained results in this experimental research, the following conclusions have been drawn as presented below:

1- After upgrading the clay (enrichment) by sulfuric acid leaching at room temperature and intensive mechanical treatment, Nanoclay was successfully obtained by ultrafine grinding (Ball milling) method after (40) hours with a particle size of less than 100 nm.

2- The Nano clay characterization reveals spherical particles with odd forms and fusible agglomerates.

3- The results confirmed that the NC served as cement replacement and an activator to improve the hydration process and absorb Ca $(OH)_2$ calcium hydroxide crystals to create more C-S-H that filling the pores to intensify the strength.

4- The wet mixing technique is a better method for appropriately dispersing NC which used a mixer motor of NC with water.

5- Fresh properties outcomes were within the limitations of EFNARC 2005 for SCC.

6- By increasing the viscosity of SCCs, the injection of NC into SRC mixtures reduced the fresh properties and thus avoided the isolation and bleeding of fresh mixtures. Correspondingly, more viscous properties obtained when utilized NC and QLP together in SCC mixtures.

7- Hardened characteristics of SCC mixtures were developed by NC incorporation increased up to 6%.

8- Using of the higher amount of QLP can improved the hardened properties of SCC but utilization of the small quantity obtained lower hardened results than that of the reference mix.

9- Similarly, the combined use of NC and QLP led to improve hardened properties.

10- Exposure to 800 ℃ temperature degree for 3 hours causes SCC0 (control mix) to lose about 75.44 %, 72.92 %, and 70.43 % of its strength at ages 56, 90, and 120 days, respectively, those ratios are very dangerous and can cause building structure failure, this must be a strong motive for researchers to continue their research in this field.

11- The 6 % of Nano clay, and hybrid (4% Nano clay+100 QLP)) as a partial replacement of cement found to be the best ratios to improve concrete resistance to fire at 800 ℃ under 3 hours for ages 56, 90, 120 days. The improvement percent were 14.6 %, 16.32 % and 20.74 % for SCC specimens mixed with 6% NC, and 6.83%, 11.6%, and13.62% for SCC specimens mixed with 4% NC-100 QLP. Moreover, it was found to be the best percent to improve concrete resistance for 20% $MgSO_4$ solution at 30, 60, and 90 days, the improvement percent were 27%, 29.5, and 40.36% for SCC specimens mixed with 6% NC and 14.6%,15.6%, and 18% for SCC specimens mixed with 4% NC-100 QLP.

12- The reduction compressive strength for the SCC0 due to immersion in 20% solution of $MgSO_4$ was about 4.8%, 6.1%, and 8.3% at 30, 60 and 90 days, respectively. Increase percent with time of exposure to periodic immersion and drying, which decrease in the structure's service lifetime and early maintenance of parts exposed to sulfate attacks, that resulting in great economic losses.

13- Incorporating of NC and QLP in SCC positively effect on improved UPV results.

14- The utilization of NC alone provided better results as compared to QLP. Therefore, to obtain environmentally sustainable concrete, it seems fitting to use a limited volume of NC to make significant improvements in the properties of SCC mixtures.

15- Since NC particles are finer and have a larger surface area, the specimens with them were denser, reducing porosity in concrete. Therefore, the use of Nano

clay should be widespread to extend the lifespan of the structures under severe chemical environments.

5.2. Recommendations for Future Work.

5.2.1. Recommendations for (NC) Manufacture

1- To avoid environmental pollution such as dust collectors, provide a controlled system for manufacturing NC.

2- Nano clay obtained by ball milling Kaolinite clay which can be produced in large quantities, at low costs, and in a sustainable manner, allowing for widespread use in concrete. It can replace cement in concrete mixes, which is the most expensive and environmentally unfriendly component.

5.2.2. Recommendations for Future Research Work

1- Using the same or different types of NC (kaolinite) but different mineral admixtures and fillers, more research could be done to produce SCC using the same or different methods. To increase the strength target for the produced SCC, silica fume, fly ash and rice husk ash can be used.

2- Using higher percentages of NC such as 8%, 10% and studying its properties on fresh and hardened SCC mixture.

3- Conducting chemical durability tests, especially for the sulfuric acid and rapid chloride permeability.

4- Examining the structural behaviour of SCC constructed with various structural elements (beams, slabs and columns).

REFERENCE

[1] M. Ventra, S. Evoy, and J. R. Heflin, *Introduction to nanoscale science and technology*. Springer Science & Business Media, 2006.

[2] J. F. Mongillo, "Nanotechnology 101 Greenwood Press," *Westport, CT*, pp. 4–13, 2007.

[3] L. Fiiipponi and D. Sutherland, *Nanotechnologies: principles, applications, implications and hands-on activities: A compendium for educators*. European Union, Directorate General for Research and Innovation, 2012.

[4] A. Hunashyal, N. Banapurmath, A. Jain, S. Quadri, and A. Shettar, "Experimental investigation on the effect of multiwalled carbon nanotubes and nano-SiO2 addition on mechanical properties of hardened cement paste," *Adv. Mater.*, vol. 3, no. 5, pp. 45–51, 2014.

[5] E. Drexler, C. Peterson, G. Pergamit, and S. Brand, "Unbounding the future: the nanotechnology revolution," 1991.

[6] F. Sanchez and K. Sobolev, "Nanotechnology in concrete–a review," *Constr. Build. Mater.*, vol. 24, no. 11, pp. 2060–2071, 2010.

[7] A. El Mir and S. G. Nehme, "Utilization of industrial waste perlite powder in self-compacting concrete," *J. Clean. Prod.*, vol. 156, pp. 507–517, 2017.

[8] W.-J. Long, Y. Gu, J. Liao, and F. Xing, "Sustainable design and ecological evaluation of low binder self-compacting concrete," *J. Clean. Prod.*, vol. 167, pp. 317–325, 2017.

[9] I. Flores-Vivian, R. Pradoto, M. Moini, and K. Sobolev, "The use of nanoparticles to improve the performance of concrete," in *Nano Conference*, 2013.

[10] H. H. Alghazali, "Behavior and temporal-based effects of sustainable self-consolidating concrete in bridge structures," 2018.

[11] S. A. Shakrani, A. Ayob, and M. A. A. Rahim, "A review of nanoclay applications in the pervious concrete pavement," in *AIP Conference Proceedings*, 2017, vol. 1885, no. 1, p. 20049.

[12] A. Hakamy, F. U. A. Shaikh, and I. M. Low, "Characteristics of nanoclay and calcined nanoclay-cement nanocomposites," *Compos. Part B Eng.*, vol. 78, pp. 174–184, 2015.

[13] A. M. Ibrahem, "The effect of nano metakaolin material on some properties of concrete," *Diyala J. Eng. Sci.*, vol. 6, no. 1, pp. 50–61, 2013.

[14] A. M. Fadzil, M. S. M. Norhasri, M. S. Hamidah, M. R. Zaidi, and J. M. Faizal, "Alteration of nano metakaolin for ultra high performance concrete," in *InCIEC 2013*, Springer, 2014, pp. 887–894.

[15] D. Lau, W. Jian, Z. Yu, and D. Hui, "Nano-engineering of construction materials using molecular dynamics simulations: Prospects and challenges," *Compos. Part B Eng.*, vol. 143, no. October 2017, pp. 282–291, 2018.

[16] B. Birgisson, A. K. Mukhopadhyay, G. Geary, M. Khan, and K. Sobolev, "Nanotechnology in concrete materials: A synopsis," *Transp. Res. Circ.*, no. E-C170, 2012.

[17] P. Kannan, C. F. Jerin, and D. K. Murali, "A Review on Self Compacting Concrete," *Int. J. Adv. Res. Eng. Manag.*, vol. 1, pp. 64–68, 2015.

[18] P. Niewiadomski, D. Stefaniuk, and J. Hoła, "Microstructural Analysis of Self-compacting Concrete Modified with the Addition of Nanoparticles," *Procedia Eng.*, vol. 172, pp. 776–783, 2017.

[19] R. W. Kelsall, I. W. Hamley, and M. Geoghegan, *Nanoscale science and technology*. Wiley Online Library, 2005.

[20] B. Domènech, J. Bastos-Arrieta, A. Alonso, J. Macanás, M. Muñoz, and D. N. Muraviev, "Bifunctional polymer-metal nanocomposite ion exchange materials," *Ion Exch. Technol.*, pp. 35–72, 2012.

[21] G. L. Hornyak, J. Dutta, H. F. Tibbals, and A. Rao, *Introduction to nanoscience*. CRC press, 2008.

[22] K. K. Chattopadhyay, *Introduction To Nanoscience And Nenotechnology*. PHI Learning Pvt. Ltd., 2009.

[23] Z. Rizlan and O. Mamat, "Process parameters optimization of silica sand nanoparticles production using low speed ball milling method," *Chinese J. Eng.*, vol. 2014, 2014.

[24] H. J. H. Brouwers and H. J. Radix, "Self-compacting concrete: theoretical and experimental study," *Cem. Concr. Res.*, vol. 35, no. 11, pp. 2116–2136, 2005.

[25] M. Ouchi, "Self-compacting concrete-development, applications and investigations," *Nord. Concr. Res.*, vol. 23, pp. 29–34, 2000.

[26] H. Okamura and M. Ouchi, "Self-compacting concrete," *J. Adv. Concr. Technol.*, vol. 1, no. 1, pp. 5–15, 2003.

[27] P. K. Mehta, "Advancements in concrete technology," *Concr. Int.*, vol. 21, no. 6, pp. 69–76, 1999.

[28] S.-C. C. E. P. Group, *The European guidelines for self-compacting concrete: Specification, production and use*. International Bureau for Precast Concrete (BIBM), 2005.

[29] M. Ouchi, S. A. Nakamura, T. Osterberg, S. Hallberg, and M. Lwin, "Applications of self-compacting concrete in Japan, Europe and the United States," *Kochi Univ. Technol. Kochi, Japan*, 2003.

[30] N. K. E. GARG, "Self-Compacted Concrete," *Int. J. Recent Res. Asp.*, vol. 3,

pp. 116–117, 2016.

[31] J. S. Damtoft, J. Lukasik, D. Herfort, D. Sorrentino, and E. M. Gartner, "Sustainable development and climate change initiatives," *Cem. Concr. Res.*, vol. 38, no. 2, pp. 115–127, 2008.

[32] S. Zhang, D. Hughes, A. A. Jeknavorian, T. Nishimura, and K. Yang, "88. Self-compacting concrete, worldwide experience," in *2nd Int. symposium on design, performance and use of self consolidating concrete*, 2009, pp. 831–840.

[33] Ó. H. Wallevik and I. Níelsson, *PRO 33: 3rd International RILEM Symposium on Self-Compacting Concrete*, vol. 33. RILEM publications, 2003.

[34] J. J. Assaad, "Influence of recycled aggregates on dynamic/static stability of self-consolidating concrete," *J. Sustain. Cem. Mater.*, vol. 6, no. 6, pp. 345–365, 2017.

[35] S. P. Shah, R. Ferron, N. Tregger, L. Ferrara, and M. Beakraft, "Self-consolidating concrete: now and future," in *2nd International RILEM Symposium on Design, performance and use of Self-Consolidating Concrete*, 2009, pp. 3–15.

[36] N. Al-Bayati, "SELF COMPACTING CONCRETE WITH TESTS," Mar. 2017.

[37] B. B. Sabir, S. Wild, and J. Bai, "Metakaolin and calcined clays as pozzolans for concrete: a review," *Cem. Concr. Compos.*, vol. 23, no. 6, pp. 441–454, 2001.

[38] M. Zhang, "The effect of clay minerals on copper and gold flotation," 2016.

[39] Z. Adamis, R. B. Williams, and J. Fodor, *Bentonite, kaolin, and selected clay minerals*, no. 231. World health organization, 2005.

[40] B. N. Rolfe, R. F. Miller, and I. S. McQueen, "Dispersion characteristics of montmorillonite, kaolinite, and illite clays in waters of varying quality, and their control with phosphate dispersants," 1960.

[41] H. Z. Harraz, "Nano clay and it ' s applications By :," no. April 2016, 2017.

[42] S. Sperinck, P. Raiteri, N. Marks, and K. Wright, "Dehydroxylation of kaolinite to metakaolin—a molecular dynamics study," *J. Mater. Chem.*, vol. 21, no. 7, pp. 2118–2125, 2011.

[43] A. Chakchouk, L. Trifi, B. Samet, and S. Bouaziz, "Formulation of blended cement: Effect of process variables on clay pozzolanic activity," *Constr. Build. Mater.*, vol. 23, no. 3, pp. 1365–1373, 2009.

[44] P. Blanchart, S. Deniel, and N. Tessier-Doyen, "Clay structural transformations during firing," in *Advances in Science and Technology*, 2010, vol. 68, pp. 31–37.

[45] C. Belver and M. Á. Vicente, "Porous silica gel by acid leaching of metakaolin," in *Materials Syntheses*, Springer, 2008, pp. 47–51.

[46] S. M. A. El-Gamal, M. S. Amin, and M. Ramadan, "Hydration characteristics and compressive strength of hardened cement pastes containing nano-metakaolin," *HBRC J.*, vol. 13, no. 1, pp. 114–121, 2017.

[47] C. Chen and W. Tuan, "Evolution of mullite texture on firing tape-cast kaolin bodies," *J. Am. Ceram. Soc.*, vol. 85, no. 5, pp. 1121–1126, 2002.

[48] E. Berodier and K. Scrivener, "Impact of filler on hydration kinetics," in *32nd Cement and Concrete Science Conference*, 2012.

[49] D. Zhang, C.-H. Zhou, C.-X. Lin, D.-S. Tong, and W.-H. Yu, "Synthesis of clay minerals," *Appl. Clay Sci.*, vol. 50, no. 1, pp. 1–11, 2010.

[50] A. M. Rashad, "Metakaolin as cementitious material: History, scours, production and composition–A comprehensive overview," *Constr. Build. Mater.*, vol. 41, pp. 303–318, 2013.

[51] J. A. Kostuch, G. V Walters, and T. R. Jones, "High performance concretes incorporating metakaolin: a review," *Concrete*, vol. 2, no. 1993, pp. 1799–1811, 2000.

[52] M. A. Caldarone, K. A. Gruber, and R. G. Burg, "High reactivity metakaolin (HRM): a new generation mineral admixture for high performance concrete," *Concr. Int.*, vol. 16, no. 11, pp. 37–41, 1994.

[53] J. M. Khatib and S. Wild, "Pore size distribution of metakaolin paste," *Cem. Concr. Res.*, vol. 26, no. 10, pp. 1545–1553, 1996.

[54] E. Ghafari, H. Costa, and E. Júlio, "Critical review on eco-efficient ultra high performance concrete enhanced with nano-materials," *Constr. Build. Mater.*, vol. 101, pp. 201–208, 2015.

[55] M. A. Fadzil, M. S. M. Nurhasri, M. A. Norliyati, M. S. Hamidah, M. H. W. Ibrahim, and R. Z. Assrul, "Characterization of Kaolin as Nano Material for High Quality Construction," in *MATEC Web of Conferences*, 2017, vol. 103, p. 9019.

[56] M. S. M. Norhasri, M. S. Hamidah, and A. M. Fadzil, "Inclusion of nano metaclayed as additive in ultra high performance concrete (UHPC)," *Constr. Build. Mater.*, vol. 201, pp. 590–598, 2019.

[57] M. S. Morsy, S. H. Alsayed, and M. Aqel, "Effect of nano-clay on mechanical properties and microstructure of ordinary Portland cement mortar," *Int. J. Civ. Environ. Eng. IJCEE-IJENS*, vol. 10, no. 01, pp. 23–27, 2010.

[58] M. S. Morsy, H. Shoukry, M. M. Mokhtar, A. M. Ali, and S. A. El-Khodary, "Facile production of nano-scale metakaolin: An investigation into its effect on compressive strength, pore structure and microstructural characteristics of mortar," *Constr. Build. Mater.*, vol. 172, pp. 243–250, 2018.

[59] R. Gopalakrishnan, "Mechanical and microsturcture studies on nano-clay admixtured cement mortar," *Rasayan J. Chem.*, vol. 9, pp. 331–334, 2016.

[60] H. Shoukry, "Development of Nano Modified Eco-Friendly Green Binders for Sustainable Construction Applications," *Nano Hybrids Compos.*, vol. 24, pp. 25–36, 2019.

[61] S. M. A. El-Gamal, F. S. Hashem, and M. S. Amin, "Influence of carbon nanotubes, nanosilica and nanometakaolin on some morphological-mechanical properties of oil well cement pastes subjected to elevated water curing temperature and regular room air curing temperature," *Constr. Build. Mater.*, vol. 146, pp. 531–546, 2017.

[62] K. Al-Jabri and H. Shoukry, "Influence of nano metakaolin on thermo-physical, mechanical and microstructural properties of high-volume ferrochrome slag mortar," *Constr. Build. Mater.*, vol. 177, pp. 210–221, 2018.

[63] G. Xiaoyu, F. Yingfang, and L. Haiyang, "The compressive behavior of cement mortar with the addition of nano metakaolin," *Nanomater. Nanotechnol.*, vol. 8, p. 1847980418755599, 2018.

[64] M. M. Hassaan, H. M. Khater, M. S. El-Mahllawy, and A. M. El Nagar, "Production of geopolymer composites enhanced by nano-kaolin material," *J. Adv. Ceram.*, vol. 4, no. 4, pp. 245–252, 2015.

[65] X. F. Li and H. Q. Chen, "The influence of nano-kaolin to cement performance," in *Applied Mechanics and Materials*, 2012, vol. 174, pp. 1208–1213.

[66] H. Shoukry, M. F. Kotkata, S. A. Abo-EL-Enein, M. S. Morsy, and S. S. Shebl, "Enhanced physical, mechanical and microstructural properties of lightweight vermiculite cement composites modified with nano metakaolin," *Constr. Build. Mater.*, vol. 112, pp. 276–283, 2016.

[67] H. Shoukry, M. F. Kotkata, S. A. Abo-el-Enein, and M. S. Morsy, "Flexural strength and physical properties of fiber reinforced nano metakaolin cementitious surface compound," *Constr. Build. Mater.*, vol. 43, pp. 453–460, 2013.

[68] S. M. A. El-Gamal, F. S. Hashem, and M. S. Amin, "Thermal resistance of hardened cement pastes containing vermiculite and expanded vermiculite," *J. Therm. Anal. Calorim.*, vol. 109, no. 1, pp. 217–226, 2012.

[69] A. E. Al-Salami, M. S. Morsy, S. Taha, and H. Shoukry, "Physico-mechanical characteristics of blended white cement pastes containing thermally activated ultrafine nano clays," *Constr. Build. Mater.*, vol. 47, pp. 138–145, 2013.

[70] P. min Zhan *et al.*, "Utilization of nano-metakaolin in concrete: A review," *J. Build. Eng.*, vol. 30, p. 101259, 2020.

[71] S. Aiswarya, A. G. Prince, and A. Narendran, "Experimental investigation on concrete containing nano-metakaolin," *IRACST. Eng. Sci. Technol*, vol. 3, no. 1, pp. 180–187, 2013.

[72] L. Senff, J. A. Labrincha, V. M. Ferreira, D. Hotza, and W. L. Repette, "Effect of nano-silica on rheology and fresh properties of cement pastes and mortars,"

Constr. Build. Mater., vol. 23, no. 7, pp. 2487–2491, 2009.

[73] M. Amin and K. Abu el-Hassan, "Effect of using different types of nano materials on mechanical properties of high strength concrete," *Constr. Build. Mater.*, vol. 80, pp. 116–124, 2015.

[74] Y. Knop and A. Peled, "Setting behavior of blended cement with limestone: influence of particle size and content," *Mater. Struct.*, vol. 49, no. 1–2, pp. 439–452, 2016.

[75] M. S. M. Norhasri, M. S. Hamidah, and A. M. Fadzil, "Applications of using nano material in concrete: A review," *Constr. Build. Mater.*, vol. 133, pp. 91–97, 2017.

[76] B. Bhuvaneshwari, S. Sasmal, and N. R. Iyer, "Nanoscience to nanotechnology for civil engineering—proof of concepts," in *Proceedings of the 4th WSEAS International Conference on Recent Researches in Geography, Geology, Energy, Environment and Biomedicine (GEMESED'11)*, 2011, pp. 230–235.

[77] M. Heikal and N. S. Ibrahim, "Hydration, microstructure and phase composition of composite cements containing nano-clay," *Constr. Build. Mater.*, vol. 112, pp. 19–27, 2016.

[78] S. A. Abo-El-Enein, M. S. Amin, F. I. El-Hosiny, S. Hanafi, T. M. ElSokkary, and M. M. Hazem, "Pozzolanic and hydraulic activity of nano-metakaolin," *HBRC J.*, vol. 10, no. 1, pp. 64–72, 2014.

[79] A. D. Salman, "Studying The Effect of Nano-Metakaolin Admixture Material On Mechanical Properties of Oil Well Cement (OWC)," *Eng. Technol. J.*, vol. 35, no. 9 Part A, 2017.

[80] K. Al-Jabri, H. Shoukry, and A. Abdel Aal, "Physico-mechanical properties of lime–silica fume pastes modified with nano-metakaolin," *Proc. Inst. Civ. Eng. Build.*, vol. 173, no. 9, pp. 627–634, 2020.

[81] M. Kaur, J. Singh, and M. Kaur, "Microstructure and strength development of fly ash-based geopolymer mortar: Role of nano-metakaolin," *Constr. Build. Mater.*, vol. 190, pp. 672–679, 2018.

[82] M. F. Ghazy, M. A. A. Elaty, and R. S. Elkhoriby, "Performance of blended cement mortars incorporating nano-metakaolin particles at elevated temperatures," in *Proceeding of the International Conference on Advances in Structural and Geotechnical Engineering, Hurghada, Egypt*, 2015, pp. 6–9.

[83] M. Heikal and N. S. Ibrahim, "Hydration, microstructure and phase composition of composite cements containing nano-clay," *Constr. Build. Mater.*, vol. 112, pp. 19–27, 2016.

[84] M. S. Morsy, Y. Al-Salloum, T. Almusallam, and H. Abbas, "Effect of nano-metakaolin addition on the hydration characteristics of fly ash blended cement mortar," *J. Therm. Anal. Calorim.*, vol. 116, no. 2, pp. 845–852, 2014.

[85]   M. S. Morsy, S. H. Alsayed, and M. Aqel, "Hybrid effect of carbon nanotube and nano-clay on physico-mechanical properties of cement mortar," *Constr. Build. Mater.*, vol. 25, no. 1, pp. 145–149, 2011.

[86]   M. S. Morsy, Y. A. Al-Salloum, H. Abbas, and S. H. Alsayed, "Behavior of blended cement mortars containing nano-metakaolin at elevated temperatures," *Constr. Build. Mater.*, vol. 35, pp. 900–905, 2012.

[87]   G. M. Habeeb, J. M. Al-Jeabory, and M. H. Majeed, "Sustainable performance of reactive powder concrete by using nano meta kaolin," *J. Eng. Sustain. Dev.*, vol. 22, no. 02 Part-6, pp. 96–106, 2019.

[88]   Z. H. A. Alsallami, "Effect of sulfate in sand on some mechanical properties of nano metakaolin normal concrete," *J. Babylon Univ. Sci.*, vol. 24, no. 2, p. 1, 2016.

[89]   M. A. Mirgozar Langaroudi and Y. Mohammadi, "Effect of nano-clay on workability, mechanical, and durability properties of self-consolidating concrete containing mineral admixtures," *Constr. Build. Mater.*, vol. 191, pp. 619–634, 2018.

[90]   B. Alrashedi and M. Hassan, "Effects of nano and micro size of clay particles on the compressive and tensile strength properties of self-consolidating concrete," *MATEC Web Conf.*, vol. 162, pp. 1–5, 2018.

[91]   K.-Y. Liao, P.-K. Chang, Y.-N. Peng, and C.-C. Yang, "A study on characteristics of interfacial transition zone in concrete," *Cem. Concr. Res.*, vol. 34, no. 6, pp. 977–989, 2004.

[92]   H. A. Abdel Gawwad, S. Abd El-Aleem, and A. S. Faried, "Influence of nano-silica and-metakaolin on the hydration characteristics and microstructure of air-cooled slag-blended cement mortar," *Geosystem Eng.*, vol. 20, no. 5, pp. 276–285, 2017.

[93]   A. Nadeem, S. A. Memon, and T. Y. Lo, "The performance of fly ash and metakaolin concrete at elevated temperatures," *Constr. Build. Mater.*, vol. 62, pp. 67–76, 2014.

[94]   A. M. Diab, M. Abd Elmoaty, and A. A. Aly, "Long term study of mechanical properties, durability and environmental impact of limestone cement concrete," *Alexandria Eng. J.*, vol. 55, no. 2, pp. 1465–1482, 2016.

[95]   A. M. El Nagar and H. M. Khater, "Development of High Thermal Stability Geopolymer Composites Enhanced by Nano Metakaolin," *J. Build. Mater. Struct.*, vol. 6, no. 1, pp. 10–19, 2019.

[96]   M. S. Morsy and H. A. Aglan, "Development and characterization of nanostructured-perlite-cementitious surface compounds," *J. Mater. Sci.*, vol. 42, no. 24, pp. 10188–10195, 2007.

[97]   Y. Reches, "Nanoparticles as concrete additives: Review and perspectives," *Constr. Build. Mater.*, vol. 175, pp. 483–495, 2018.

[98] R. Siddique and J. Klaus, "Influence of metakaolin on the properties of mortar and concrete: A review," *Appl. Clay Sci.*, vol. 43, no. 3–4, pp. 392–400, 2009.

[99] A. M. Diab, H. E. Elyamany, M. Abd Elmoaty, and M. M. Sreh, "Effect of nanomaterials additives on performance of concrete resistance against magnesium sulfate and acids," *Constr. Build. Mater.*, vol. 210, pp. 210–231, 2019.

[100] M. Zhang and H. Li, "Pore structure and chloride permeability of concrete containing nano-particles for pavement," *Constr. Build. Mater.*, vol. 25, no. 2, pp. 608–616, 2011.

[101] I. Z. Saaid, A. H. Osama, and F. E. Omar, " Compration between the effect of addition of nano-calcium carbonate and nano-kaoline on developing the properties of reinforced," *Intellekt. Sist. Proizv.*, vol. 16, no. 3, pp. 147–159, 2018.

[102] W. C. Wang, "Compressive strength and thermal conductivity of concrete with nanoclay under Various High-Temperatures," *Constr. Build. Mater.*, vol. 147, pp. 305–311, 2017.

[103] S.-H. Han and J.-K. Kim, "Effect of temperature and age on the relationship between dynamic and static elastic modulus of concrete," *Cem. Concr. Res.*, vol. 34, no. 7, pp. 1219–1227, 2004.

[104] T. Zadražil, F. Vodák, and O. Kapičková, "Effect of temperature and age of concrete on strength–porosity relation," *Acta Polytech.*, vol. 44, no. 1, 2004.

[105] K. Sakr and E. El-Hakim, "Effect of high temperature or fire on heavy weight concrete properties," *Cem. Concr. Res.*, vol. 35, no. 3, pp. 590–596, 2005.

[106] A. Nadeem, S. A. Memon, and T. Y. Lo, "Mechanical performance, durability, qualitative and quantitative analysis of microstructure of fly ash and Metakaolin mortar at elevated temperatures," *Constr. Build. Mater.*, vol. 38, pp. 338–347, 2013.

[107] F. P. Glasser, J. Marchand, and E. Samson, "Durability of concrete—Degradation phenomena involving detrimental chemical reactions," *Cem. Concr. Res.*, vol. 38, no. 2, pp. 226–246, 2008.

[108] B. Luca, B. Elsener, P. Pietro, R. Elena, and P. Rob, "Corrosion of Steel in Concrete-Prevention, Diagnosis, Repair second edition in chinese language," 2019.

[109] O. S. B. Al-Amoudi, "Attack on plain and blended cements exposed to aggressive sulfate environments," *Cem. Concr. Compos.*, vol. 24, no. 3–4, pp. 305–316, 2002.

[110] G. W. Scherer, "Crystallization in pores," *Cem. Concr. Res.*, vol. 29, no. 8, pp. 1347–1358, 1999.

[111] G. W. Scherer, "Stress from crystallization of salt," *Cem. Concr. Res.*, vol. 34,

no. 9, pp. 1613–1624, 2004.

[112] R. J. Flatt and G. W. Scherer, "Thermodynamics of crystallization stresses in DEF," *Cem. Concr. Res.*, vol. 38, no. 3, pp. 325–336, 2008.

[113] B. Tian and M. D. Cohen, "Does gypsum formation during sulfate attack on concrete lead to expansion?," *Cem. Concr. Res.*, vol. 30, no. 1, pp. 117–123, 2000.

[114] W. Müllauer, R. E. Beddoe, and D. Heinz, "Sulfate attack expansion mechanisms," *Cem. Concr. Res.*, vol. 52, pp. 208–215, 2013.

[115] K. Van Tittelboom, N. De Belie, and R. D. Hooton, "Test methods for resistance of concrete to sulfate attack–a critical review," in *Performance of Cement-Based Materials in Aggressive Aqueous Environments*, Springer, 2013, pp. 251–288.

[116] A. Hendi, A. Behravan, D. Mostofinejad, H. Akhavan Kharazian, and A. Sedaghatdoost, "Performance of two types of concrete containing waste silica sources under MgSO4 attack evaluated by durability index," *Constr. Build. Mater.*, vol. 241, p. 118140, 2020.

[117] S. Kawashima, P. Hou, D. J. Corr, and S. P. Shah, "Modification of cement-based materials with nanoparticles," *Cem. Concr. Compos.*, vol. 36, pp. 8–15, 2013.

[118] Z. Guo *et al.*, "Comparison study on the sulfate attack resistivity of cement-based materials modified with nanoSiO2 and conventional SCMs: Mechanical strength and volume stability," *Constr. Build. Mater.*, vol. 211, pp. 556–570, 2019.

[119] P. Mondal, "Nanomechanical properties of cementitious materials." Northwestern University, 2008.

[120] P. Hosseini, A. Afshar, B. Vafaei, A. Booshehrian, E. Molaei Raisi, and A. Esrafili, "Effects of nano-clay particles on the short-term properties of self-compacting concrete," *Eur. J. Environ. Civ. Eng.*, vol. 21, no. 2, pp. 127–147, 2017.

[121] A. Kheloufi, Y. Berbar, A. Kefaifi, S. A. Medjahed, and F. Kerkar, "Improvement of ImpuritiesRemoval from Silica Sand by Leaching Process," *Alger. Silicon Technol. Dev. Unit*, pp. 1–6, 2009.

[122] T. Ahmad and O. Mamat, "The development and characterization of zirconia-silica sand nanoparticles composites," *World J. Nano Sci. Eng.*, vol. 1, no. 01, p. 7, 2011.

[123] A. G. King, *Ceramic technology and processing: a practical working guide*. William Andrew, 2001.

[124] C. Suryanarayana, "Mechanical alloying and milling," *Prog. Mater. Sci.*, vol. 46, no. 1–2, pp. 1–184, 2001.

[125] H. Stanjek and W. Häusler, "Basics of X-ray Diffraction," *Hyperfine Interact.*,

vol. 154, no. 1, pp. 107–119, 2004.

[126] Y. Amemiya, T. Matsushita, A. Nakagawa, Y. Satow, J. Miyahara, and J. Chikawa, "Design and performance of an imaging plate system for X-ray diffraction study," *Nucl. Instruments Methods Phys. Res. Sect. A Accel. Spectrometers, Detect. Assoc. Equip.*, vol. 266, no. 1–3, pp. 645–653, 1988.

[127] W. Zhou, R. Apkarian, Z. L. Wang, and D. Joy, "Fundamentals of scanning electron microscopy (SEM)," in *Scanning microscopy for nanotechnology*, Springer, 2006, pp. 1–40.

[128] L. Reimer, "Scanning electron microscopy: physics of image formation and microanalysis." IOP Publishing, 2000.

[129] "Iraqi Specifications, No. 5, 2019. Properties of Portland Cement." .

[130] A. C33/C33M, "Standard specification for concrete aggregates." ASTM international West Conshohocken, PA, 2013.

[131] B. Statements and T. Size, "ASTMC128-88 'Standard Test Method for Density , Relative Density (Specific Gravity), and Absorption,'" pp. 1–6.

[132] A. Machine and B. Statements, "C131/C131M − 14 ' StandardStandard Test Method for Resistance to Degradation of Small-Size Coarse Aggregate by Abrasion and Impact in the Los Angeles Machine,'" vol. i, pp. 1–5, 2014.

[133] F. Series and C. Series, "ASTM C 88 - 76 'Standard Test Method for soundness of aggregates by use of sodium sulfate or magnesium sulfate,'" no. November, pp. 3–8, 1976.

[134] Sika.manual, "'High Performance Superplasticiser Concrete Admixture'., Version No. 12.2014., Date of product sheet (02,2015).," no. 12, pp. 1–2, 2019.

[135] C. ASTM, "C494, A. Standard Specification for Chemical Admixtures for Concrete, in Standard Specification for Chemical Admixtures for Concrete2004, ASTM International West Conshohocken, PA." American Society for Testing and Materials, West Conshohocken, PA, 1916.

[136] A. Bes, "Dynamic process simulation of limestone calcination in normal shaft kilns," 2006.

[137] D. K. Ashish and S. K. Verma, "An overview on mixture design of self-compacting concrete," *Struct. Concr.*, vol. 20, no. 1, pp. 371–395, 2019.

[138] A. Siva and G. Ravindiran, "A Review on Self Compacting Concrete," *Int. J. ChemTech Res.*, vol. 10, pp. 62–68, Oct. 2018.

[139] C. ASTM, "311-04,'Standard Test Methods for Sampling and Testing Fly Ash or Natural Pozzolans for Use in Portland-Cement Concrete.,'" *Annu. B. ASTM Stand*, 2005.

[140] A. ASTM, "ASTM C109/C109M 'Standard test method for compressive strength of hydraulic cement mortars (using [50-mm] cube specimens),'" *Annu.*

B. ASTM Stand. B. ASTM Stand., vol. 4, no. 1, pp. 1–9, 2013.

[141] British Standards Institution, "BS EN 12350-10:2010.Testing fresh concrete - Part 10: Self-compacting concrete - L-Box test," p. 16, 2013.

[142] British Standards Institution, "BSI Standards Publication Testing concrete –BS EN 12350-9:2010.Self-compacting concrete — Vfunnel test," p. 18, 2013.

[143] BS EN 12350-10, "Testing fresh concrete Part 10 : Self-compacting concrete — L box test," *BSI Stand. Publ.*, 2010.

[144] K. H. Khayat, "Workability, testing, and performance of self-consolidating concrete," *Mater. J.*, vol. 96, no. 3, pp. 346–353, 1999.

[145] 2010 BS EN12350-11:, "BSI Standards Publication Testing fresh concrete Part 11: Self-compacting concrete -- sieve Segregation test," *BSI Stand. Publ.*, 2010.

[146] T. O. Standard, "ASTM-C138 / C138 M − 14 'Standard Test Method for Density (Unit Weight), Yield , and Air Content (Gravimetric),'" vol. i, pp. 1–4, 2014.

[147] S. Jamle, N. Delmiya, and R. Singh, "Efficient Use of UPV Meter: A Non Destructive Test of Concrete by Fragmentation Analysis," *J. Xi'an Univ. Archit. Technol. ISSN*, pp. 1006–7930, 2020.

[148] C. Astm, "597, Standard test method for pulse velocity through concrete," *ASTM Int. West Conshohocken, PA*, 2009.

[149] F. Saint-Pierre, A. Philibert, B. Giroux, and P. Rivard, "Concrete quality designation based on ultrasonic pulse velocity," *Constr. Build. Mater.*, vol. 125, pp. 1022–1027, 2016.

[150] ASTM C642, "Standard Test Method for Density, Absorption, and Voids in Hardened Concrete, ASTM International, United States," *Annu. B. ASTM Stand.*, no. March, pp. 1–3, 1997.

[151] B. Standard, "BS EN 12390-3 2002 'British Standard Testing hardened concrete,'" no. August, 2003.

[152] ASTM C496/C496M - 11, "Standard Test Method for Splitting Tensile Strength of Cylindrical Concrete Specimens," *ASTM Int.*, vol. i, p. 5, 2011.

[153] A. C78-15a, "C78C78M − 15a"Standard Test Method forFlexural Strength of Concrete (Using Simple Beam withThird-Point Loading)"," *ACI Struct. JournalIranian J. Polym. Sci. Tchnology*, vol. 4, no. Reapproved, pp. 1–7, 1995.

[154] I. Kett, "Static Modulus of Elasticity and Poisson's Ratio of Concrete in Compression.ASTM C 469.," *Eng. Concr.*, pp. 131–137, 2009.

[155] ASTM C39, "Compressive Strength of Cylindrical Concrete Specimens," *ASTM Stand.*, pp. 1–7, 2015.

[156] K. S. W. Sing, "The use of gas adsorption for the characterization of porous solids," *Colloids and Surfaces*, vol. 38, no. 1, pp. 113–124, 1989.

[157] M. A. Kwalramani and Z. I. Syed, "Application of nanomaterials to enhance microstructure and mechanical properties of concrete," *Int. J. Integr. Eng.*, vol. 10, no. 2, 2018.

[158] S. Kawashima, J. H. Kim, D. J. Corr, and S. P. Shah, "Study of the mechanisms underlying the fresh-state response of cementitious materials modified with nanoclays," *Constr. Build. Mater.*, vol. 36, pp. 749–757, 2012.

[159] C. Shi, "Studies on several factors affecting hydration and properties of lime-pozzolan cements," *J. Mater. Civ. Eng.*, vol. 13, no. 6, pp. 441–445, 2001.

[160] M. J. Mohd Faizal, M. S. Hamidah, and M. S. Muhd Norhasri, "Strength and Chloride Content of Nanoclayed Ultra-High Performance Concrete," in *Proceeding on Structure, Materials and Construction Engineering Conference (CONS ENG'14), DAKAM, pg*, pp. 99–111.

[161] J. Newman and B. S. Choo, *Advanced concrete technology 2: concrete properties*. Elsevier, 2003.

[162] N. A. Tregger, M. E. Pakula, and S. P. Shah, "Influence of clays on the rheology of cement pastes," *Cem. Concr. Res.*, vol. 40, no. 3, pp. 384–391, 2010.

[163] K. H. Khayat and D. Feys, *Design, Production and Placement of Self-consolidating Concrete: Proceedings of SCC2010, Montreal, Canada, September 26-29, 2010*, vol. 1. Springer Science & Business Media, 2010.

[164] Z. Li, *Advanced concrete technology*. John Wiley & Sons, 2011.

[165] P. Hosseini, R. Hosseinpourpia, A. Pajum, M. M. Khodavirdi, H. Izadi, and A. Vaezi, "Effect of nano-particles and aminosilane interaction on the performances of cement-based composites: An experimental study," *Constr. Build. Mater.*, vol. 66, pp. 113–124, 2014.

[166] M. N. N. Khan, M. Jamil, M. R. Karim, M. F. M. Zain, and A. Kaish, "Filler effect of pozzolanic materials on the strength and microstructure development of mortar," *KSCE J. Civ. Eng.*, vol. 21, no. 1, pp. 274–284, 2017.

[167] P. Dinakar, M. K. Reddy, and M. Sharma, "Behaviour of self compacting concrete using Portland pozzolana cement with different levels of fly ash," *Mater. Des.*, vol. 46, pp. 609–616, 2013.

[168] M. H. Zhang and O. E. Gjvorv, "Mechanical properties of high-strength lightweight concrete," *Mater. J.*, vol. 88, no. 3, pp. 240–247, 1991.

[169] L. K. Crouch, J. Pitt, and R. Hewitt, "Aggregate effects on pervious Portland cement concrete static modulus of elasticity," *J. Mater. Civ. Eng.*, vol. 19, no. 7, pp. 561–568, 2007.

[170] B. Vakhshouri and S. Nejadi, "Empirical models and design codes in prediction of modulus of elasticity of concrete," *Front. Struct. Civ. Eng.*, vol. 13, no. 1, pp. 38–48, 2019.

[171] P. K. Mehta and P. J. M. Monteiro, *Concrete microstructure, properties and*

materials. 2017.

[172] U. Sharma, L. P. Singh, B. Zhan, and C. S. Poon, "Effect of particle size of nanosilica on microstructure of CSH and its impact on mechanical strength," *Cem. Concr. Compos.*, vol. 97, pp. 312–321, 2019.

[173] R. Liu, H. Xiao, J. Geng, J. Du, and M. Liu, "Effect of nano-CaCO3 and nano-SiO2 on improving the properties of carbon fibre-reinforced concrete and their pore-structure models," *Constr. Build. Mater.*, vol. 244, p. 118297, 2020.

[174] S. A. Kristiawan and G. Y. Murti, "Porosity of Self-Compacting Concrete (SCC) incorporating high volume fly ash," in *IOP Conference Series: Materials Science and Engineering*, 2017, vol. 176, no. 1, p. 12043.

[175] M. Valcuende, C. Parra, E. Marco, A. Garrido, E. Martínez, and J. Cánoves, "Influence of limestone filler and viscosity-modifying admixture on the porous structure of self-compacting concrete," *Constr. Build. Mater.*, vol. 28, no. 1, pp. 122–128, 2012.

[176] G. V. Walters and T. R. Jones, "Effect of metakaolin on alkali-silica reaction (asr) in concrete manufactured with reactive aggregate," *Spec. Publ.*, vol. 126, pp. 941–954, 1991.

[177] A. A. Elsayd and I. N. Fathy, "Experimental Study of Fire Effects on Compressive Strength of Normal-Strength Concrete Supported With Nanomaterials Additives," vol. 09, no. 2, pp. 17–26, 2019.

[178] M. Vyšvařil, P. Bayer, M. Chromá, and P. Rovnaníková, "Physico-mechanical and microstructural properties of rehydrated blended cement pastes," *Constr. Build. Mater.*, vol. 54, pp. 413–420, 2014.

[179] D. Bondar, C. J. Lynsdale, N. B. Milestone, and N. Hassani, "Sulfate resistance of alkali activated pozzolans," *Int. J. Concr. Struct. Mater.*, vol. 9, no. 2, pp. 145–158, 2015.

[180] F. Türker, F. Aköz, S. Koral, and N. Yüzer, "Effects of magnesium sulfate concentration on the sulfate resistance of mortars with and without silica fume," *Cem. Concr. Res.*, vol. 27, no. 2, pp. 205–214, 1997.

[181] S. Popovics, *Strength and related properties of concrete: A quantitative approach*. John Wiley & Sons, 1998.

[182] A. Nasution, I. Imran, and M. Abdullah, "Improvement of concrete durability by nanomaterials," *Procedia Eng.*, vol. 125, pp. 608–612, 2015.

Appendix A

Table (4-3): Fresh properties results.

Mix ID	Slump Flow		V-funnel time (t_v) (sec)	L-Box	Segregation Resistance (%)	Fresh Density (k/cm^3)
	D (mm)	T$_{500}$ (sec)				
Control Mix	800	2.15	10.2	0.94	14.2	2320
SCC 2% NC	780	2.75	15.12	0.94	14	2300
SCC 4% NC	750	2.81	16.7	0.92	12.4	2280
SCC6% NC	730	2.9	18.2	0.89	10.8	2260
SCC 50 QLP	705	3.1	20.28	0.88	10	2250
SCC 75 QLP	720	2.98	19.2	0.9	11.8	2230
SCC 100 QLP	735	2.95	18.81	0.92	12.2	2210
SCC4%NC+50 QLP	700	3.28	21.1	0.86	11.1	2200
SCC4%NC+75 QLP	730	2.88	15.68	0.92	11.6	2160
SCC4%NC+100 QLP	750	2.5	12.88	0.93	12.3	2110

Table (4-4): Compressive strength results

Mix ID	Compressive Strength (MPa)				
	7 day	28 day	56 day	90 day	120 day
Control Mix	58.46	69.32	74.1	76.44	77.1
SCC 2% NC	61.3	72.85	77.8	79.97	80.63
SCC 4% NC	65.89	76.7	80.52	82.69	83.25
SCC6% NC	75.1	85.7	88.16	90.9	91.31
SCC 50 QLP	53.25	63.36	67.68	69.26	70.79
SCC 75 QLP	55.66	65.98	70.24	73.51	74.94
SCC 100 QLP	61.1	72.6	77.13	79.7	80.83
SCC4%NC+50 QLP	60.47	72.91	75.17	77.88	78.8
SCC4%NC+75 QLP	62.13	73.39	76.91	79.13	80.9
SCC4%NC+100 QLP	64.05	75.27	78.1	80.2	81.97

Table (4-5): Splitting tensile strength of SCC specimens.

Mix ID	Splitting Tensile Strength(MPa)			
	28 day	56 day	90 day	120 day
Control Mix	3.88	4.1	4.57	5.16
SCC 2% NC	4	4.5	4.97	5.3
SCC 4% NC	4.17	4.61	5.2	5.5
SCC6% NC	4.53	4.8	5.3	5.8
SCC 50 QLP	3.3	3.52	4.12	4.35
SCC 75 QLP	3.6	3.86	4.3	4.65
SCC 100 QLP	3.75	4.35	4.8	5.1
SCC4%NC+50 QLP	3.9	4.1	4.45	4.91
SCC4%NC+75 QLP	4.1	4.6	5	5.3
SCC4%NC+100 QLP	4.3	4.86	5.4	5.65

Table (4-6): Flexural strength results.

Mix ID	Flexural Strength (MPa)			
	28 day	56 day	90 days	120 day
Control Mix	5.3	5.9	6.2	6.4
SCC 2% NC	5.5	6.5	6.9	7.2
SCC 4% NC	6.1	6.7	7.1	7.5
SCC6% NC	6.5	7.4	7.9	8.1
SCC 50 QLP	4.9	5.2	5.7	5.9
SCC 75 QLP	5.2	5.7	6	6.2
SCC 100 QLP	5.8	6.3	6.5	7.2
SCC4%NC+50 QLP	5.7	6.1	6.6	7.1
SCC4%NC+75 QLP	5.9	6.4	6.8	7.3
SCC4%NC+100 QLP	6	6.6	7	7.4

Table (4-7): Modulus of elasticity results.

Mix	E_C (GPa)
Control Mix	36.32
SCC 2% NC	38.8
SCC 4% NC	43.5
SCC6% NC	45.8
SCC 50 QLP	32.6
SCC 75 QLP	34.1
SCC 100 QLP	37.5
SCC4%NC+50 QLP	38.1
SCC4%NC+75 QLP	40.7
SCC4%NC+100 QLP	42.5

Table (4-9): Results of dry density for SCCs

Mix ID	Dry Density (g /cm^3)				
	7 day	28 day	56 day	90 day	120 day
Control Mix	2361	2390	2396	2442	2449
SCC 2% NC	2378	2398	2406	2446	2452
SCC 4% NC	2390	2410	2425	2450	2460
SCC6% NC	2410	2418	2435	2465	2484
SCC 50 QLP	2280	2335	2365	2370	2409
SCC 75 QLP	2330	2370	2393	2415	2443
SCC 100 QLP	2370	2392	2400	2441	2460
SCC4%NC+50 QLP	2367	2395	2409	2445	2462
SCC4%NC+75 QLP	2373	2395	2415	2448	2470
SCC4%NC+100 QLP	2388	2398	2420	2456	2478

Table (4-8): Ultrasonic pulse velocity results.

Mix ID	UPV km/sec				
	7 day	28 day	56 day	90 day	120 day
Control Mix	4.348	4.510	4.580	4.615	4.639
SCC 2% NC	4.405	4.532	4.667	4.709	4.726
SCC 4% NC	4.505	4.662	4.709	4.813	4.845
SCC6% NC	4.673	4.810	4.890	4.902	4.925
SCC 50 QLP	4.255	4.430	4.512	4.536	4.553
SCC 75 QLP	4.292	4.498	4.525	4.562	4.593
SCC 100 QLP	4.430	4.558	4.595	4.620	4.680
SCC4%NC+50 QLP	4.390	4.572	4.618	4.682	4.728
SCC4%NC+75 QLP	4.465	4.578	4.622	4.692	4.733
SCC4%NC+100 QLP	4.470	4.630	4.659	4.699	4.740

Table (4-10): Permeable pores voids results.

Mix ID	Permeable Pores Voids (%)			
	28 day	56 day	90 day	120 day
Control Mix	10.5	9.4	8.7	7.4
SCC 2% NC	9.8	8.3	7.1	5.8
SCC 4% NC	8.5	6.9	5.3	4.1
SCC6% NC	7.1	5.8	4.6	3.5
SCC 50 QLP	11.4	10.3	9.4	8.1
SCC 75 QLP	10.8	9.8	8.9	7.8
SCC 100 QLP	10	8.8	7.5	6.1
SCC4%NC+50 QLP	10.3	9.1	8.5	7
SCC4%NC+75 QLP	9.5	8.1	6.9	5.5
SCC4%NC+100 QLP	8.8	7.3	5.7	4.5

Table (4-11): Water absorption results

Mix ID	Water Absorption %			
	28 day	56 day	90 day	120 day
Control Mix	4.7	4	3.8	3.2
SCC 2% NC	4.2	3.8	3.2	2.7
SCC 4% NC	3.8	3	2.6	2.1
SCC6% NC	3.5	2.7	2	1.8
SCC 50 QLP	5	4.6	4.3	3.7
SCC 75 QLP	4.8	4.3	4	3.5
SCC 100 QLP	4.5	3.7	3.3	2.8
SCC4%NC+50 QLP	4.3	3.9	3.6	3
SCC4%NC+75 QLP	3.9	3.5	3	2.7
SCC4%NC+100 QLP	3.6	2.9	2.5	2

Table (4-12): Results of the compressive strength at elevated temperatures under 3 hours heating time for all mixes at 56 days.

Mix ID	Compressive Strength (MPa) Temperature (°C)								
	25	200	Increase Ratio %	400	Reduction Ratio %	600	Reduction Ratio %	800	Reduction Ratio %
Control Mix	74.1	75.8	2.29	61.6	16.87	35.3	52.36	18.2	75.44
SCC 2% NC	77.8	81.8	5.14	65.7	15.55	37.5	51.8	21.2	72.75
SCC 4% NC	80.5	85.1	5.71	69.2	14.04	41.8	48.08	24.2	69.94
SCC6% NC	88.2	93.7	6.24	76.4	13.38	46.4	47.39	31.4	64.4
SCC 50 QLP	67.7	68.6	1.33	56.1	17.13	30.8	54.51	15.1	77.7
SCC 75 QLP	70.2	72.2	2.85	58.6	16.52	33	52.99	17.2	75.5
SCC 100 QLP	77.1	81.2	5.32	64.1	16.86	37.8	50.97	20.2	73.8
SCC4%NC+50 QLP	72.2	76.1	5.40	60.9	15.65	36.5	49.45	19.3	73.27
SCC4%NC+75 QLP	76.9	81.4	5.85	65.1	15.35	39.1	49.16	21.1	72.56
SCC4%NC-100 QLP	78.1	82.8	6.02	66.5	14.85	40.1	48.66	23.2	70.29

Table (4-13): Results of the compressive strength at elevated temperatures under 3 hours heating time for all mixes at 90 days.

Mix ID	Compressive Strength (MPa)								
	Temperature (°C)								
	25	200	Increase Ratio %	400	Reduction Ratio %	600	Reduction Ratio %	800	Reduction Ratio %
Control Mix	76.44	78.6	2.83	64.21	15.99	37.56	50.86	20.7	72.92
SCC 2% NC	79.97	84.4	5.54	67.8	15.22	39.5	50.61	22.5	71.86
SCC 4% NC	82.69	87.5	5.82	71.1	14.02	46.7	43.52	30.1	63.6
SCC6% NC	90.9	96.8	6.49	80.2	11.77	52.65	42.08	35.43	61.02
SCC 50 QLP	69.26	70.6	1.93	57.6	16.84	32.9	52.5	17.4	74.88
SCC 75 QLP	73.51	75.2	2.3	61.4	16.47	35.7	51.44	19.3	73.75
SCC 100 QLP	79.7	83.9	5.27	67.7	15.06	38.8	51.32	21.9	72.52
SCC4%NC+50 QLP	77.88	82.2	5.55	65.8	15.51	39.8	48.9	21.2	72.78
SCC4%NC+75 QLP	79.13	84.1	6.28	67.2	15.08	40.2	49.2	22.4	71.69
SCC4%NC-100 QLP	80.2	85.3	6.36	68.8	14.21	42.53	46.97	28.5	64.46

Table (4-14): Results of the compressive strength at elevated temperatures under 3 hours heating time for all mixes at 120 days.

Mix ID	Compressive Strength (MPa)								
	Temperature (°C)								
	25	200	Increase Ratio %	400	Reduction Ratio %	600	Reduction Ratio %	800	Reduction Ratio %
Control Mix	77.1	79.5	3.11	65.59	14.93	38.85	49.61	22.8	70.43
SCC 2% NC	80.63	84.4	4.68	68.9	14.55	41.74	48.23	25.8	68
SCC 4% NC	83.25	88.2	5.95	73.66	11.52	52.3	37.18	35.68	57.2
SCC6% NC	91.31	97.1	6.34	81.63	10.60	56.88	37.71	40.34	55.82
SCC 50 QLP	70.79	72.5	2.42	59.28	16.26	34.8	50.84	19.2	72.88
SCC 75 QLP	74.94	77.1	2.88	63.2	15.67	37.3	50.23	21.4	71.44
SCC 100 QLP	80.83	84.6	4.66	68.9	14.76	40.6	49.77	24.11	70.17
SCC4%NC+50 QLP	78.8	83.5	5.97	66.6	15.48	40.1	49.11	24.3	69.16
SCC4%NC+75 QLP	80.9	86.4	6.8	68.9	14.83	42.2	47.84	25.3	68.73
SCC4%NC-100 QLP	81.97	87.9	7.23	71.5	12.77	46.46	43.32	32.1	60.84

Table(4-15) : Results of the mass (gm) at elevated temperatures under 3 hours heating time for all mixes at 56 days age.

Mix ID	200°C			400°C			600°C			800°C		
	Mass (gm) at 110 °C	Mass (gm) at 200	Mass Loss %	Mass (gm) at 110 °C	Mass (gm) at 400	Mass Loss %	Mass (gm) at 110 °C	Mass (gm) at 600	Mass Loss %	Mass (gm) at 110 °C	Mass (gm) at 800	Mass Loss %
Control Mix	2386	2342	1.844	2384	2250	5.621	2383	2155	9.568	2379	1950	18.03
SCC 2% NC	2397	2381	0.668	2395	2299	4.008	2397	2215	7.593	2400	1990	17.08
SCC 4% NC	2415	2402	0.538	2418	2345	3.019	2420	2280	5.785	2425	2045	15.67
SCC6% NC	2425	2413	0.495	2422	2360	2.56	2430	2310	4.938	2435	2115	13.14
SCC 50 QLP	2355	2307	2.038	2331	2199	5.663	2333	2098	10.07	2338	1876	19.76
SCC 75 QLP	2383	2337	1.930	2370	2245	5.274	2374	2146	9.604	2373	1925	18.88
SCC 100 QLP	2390	2372	0.753	2418	2312	4.384	2412	2200	8.789	2418	2005	17.08
SCC4%NC+50 QLP	2400	2379	0.875	2406	2293	4.697	2403	2212	7.948	2409	1990	17.39
SCC4%NC+75 QLP	2405	2388	0.707	2431	2333	4.031	2428	2257	7.043	2422	2020	16.59
SCC4%NC-100 QLP	2410	2396	0.581	2440	2360	3.279	2437	2271	6.812	2438	2045	16.12

Table(4-16) : Results of the mass (gm) at elevated temperatures under 3 hours heating time for all mixes at 90 days age.

Mix ID	200°C			400°C			600°C			800°C		
	Mass (gm) at 110 °C	Mass (gm) at 200	Mass Loss %	Mass (gm) at 110 °C	Mass (gm) at 400	Mass Loss %	Mass (gm) at 110 °C	Mass (gm) at 600	Mass Loss %	Mass (gm) at 110 °C	Mass (gm) at 800	Mass Loss %
Control Mix	2432	2394	1.563	2430	2300	5.35	2425	2208	8.948	2427	1993	17.88
SCC 2% NC	2436	2423	0.534	2432	2355	3.166	2430	2260	6.996	2433	2070	14.92
SCC 4% NC	2440	2431	0.369	2443	2373	2.865	2440	2315	5.123	2442	2130	12.78
SCC6% NC	2455	2448	0.285	2454	2400	2.2	2453	2345	4.403	2450	2160	11.84
SCC 50 QLP	2360	2315	1.907	2362	2229	5.631	2360	2134	9.576	2358	1920	18.58
SCC 75 QLP	2405	2365	1.663	2403	2279	5.16	2400	2175	9.375	2402	1973	17.86
SCC 100 QLP	2431	2416	0.617	2430	2325	4.321	2433	2230	8.344	2430	2020	16.87
SCC4%NC+50 QLP	2435	2423	0.493	2433	2330	4.233	2437	2260	7.263	2436	2018	17.16
SCC4%NC+75 QLP	2437	2426	0.451	2434	2338	3.944	2430	2263	6.872	2438	2043	16.20
SCC4%NC-100 QLP	2448	2440	0.327	2445	2369	3.108	2442	2297	5.938	2440	2059	15.62

Table(4-17) : Results of the mass (gm) at elevated temperatures under 3 hours heating time for all mixes at 120 days age.

Mix ID	Mass (gm) at 110 °C	200°C		400°C			600°C			800°C		
		Mass (gm) at 200	Mass Loss %	Mass (gm) at 110 °C	Mass (gm) at 400	Mass Loss %	Mass (gm) at 110 °C	Mass (gm) at 600	Mass Loss %	Mass (gm) at 110 °C	Mass (gm) at 800	Mass Loss %
Control Mix	2435	2400	1.437	2430	2308	5.021	2433	2215	8.96	2436	2000	17.89
SCC 2% NC	2442	2430	0.491	2444	2366	3.191	2440	2300	5.738	2441	2100	13.97
SCC 4% NC	2455	2448	0.285	2458	2406	2.116	2456	2340	4.723	2452	2155	12.11
SCC6% NC	2485	2480	0.201	2483	2440	1.732	2481	2387	3.789	2486	2216	10.86
SCC 50 QLP	2395	2353	1.754	2396	2260	5.676	2394	2170	9.357	2392	1960	18.06
SCC 75 QLP	2433	2395	1.562	2430	2309	4.979	2435	2236	8.172	2432	2020	16.94
SCC 100 QLP	2450	2439	0.449	2453	2350	4.199	2452	2266	7.586	2455	2068	15.76
SCC4%NC+50 QLP	2452	2442	0.408	2455	2365	3.666	2455	2282	7.047	2454	2039	16.91
SCC4%NC+75 QLP	2462	2453	0.366	2460	2390	2.846	2463	2311	6.171	2465	2080	15.62
SCC4%NC+100 QLP	2471	2463	0.324	2472	2410	2.508	2475	2335	5.657	2473	2110	14.68

Table (4-18): Mass (gm) of mixtures after immersion in cycles wet and dry magnesium sulfate for 30 days.

Mix ID	Mass 0% MgSO$_4$ at 56 days	Mass 5% MgSO$_4$	Loss %	Mass 10% MgSO$_4$	Loss %	Mass 20% MgSO$_4$	Loss %
Control Mix	2396	2392	0.15	2378	0.75	2362	1.42
SCC 2% NC	2406	2404	0.1	2392	0.6	2378	1.16
SCC 4% NC	2425	2423	0.08	2413	0.5	2402	0.958
SCC6% NC	2435	2434	0.04	2424	0.45	2414	0.88
SCC 50 QLP	2365	2362	0.14	2346	0.82	2328	1.561
SCC 75 QLP	2393	2390	0.12	2374	0.79	2357	1.495
SCC 100 QLP	2400	2398	0.09	2384	0.66	2370	1.249
SCC4%NC+50 QLP	2409	2406	0.12	2394	0.62	2380	1.22
SCC4%NC+75 QLP	2415	2413	0.1	2401	0.58	2388	1.105
SCC4%NC+100 QLP	2420	2418	0.08	2407	0.54	2395	1.034

Table (4-19): Mass (gm) of mixtures after immersion in cycles wet and dry magnesium sulfate for 60 days.

Mix ID	Mass 0% MgSO$_4$ at 90 days	Mass 5% MgSO$_4$	Loss %	Mass 10% MgSO$_4$	Loss %	Mass 20% MgSO$_4$	Loss %
Control Mix	2442	2432	0.42	2422	0.81	2405	1.5
SCC 2% NC	2446	2438	0.33	2430	0.67	2416	1.22
SCC 4% NC	2450	2443	0.29	2437	0.54	2425	1.03
SCC6% NC	2465	2459	0.24	2452	0.51	2442	0.97
SCC 50 QLP	2370	2359	0.47	2349	0.88	2331	1.65
SCC 75 QLP	2415	2404	0.44	2395	0.83	2377	1.58
SCC 100 QLP	2441	2431	0.39	2423	0.73	2409	1.32
SCC4%NC+50 QLP	2445	2436	0.37	2428	0.69	2414	1.25
SCC4%NC+75 QLP	2448	2440	0.34	2432	0.65	2419	1.18
SCC4%NC+100 QLP	2456	2449	0.27	2441	0.6	2429	1.11

Table (4-20): Mass (gm) of mixtures after immersion in cycles wet and dry magnesium sulfate for 90 days.

Mix ID	Mass 0% MgSO₄ at 120 days	Mass 5% MgSO₄	Loss %	Mass 10% MgSO₄	Loss %	Mass 20% MgSO₄	Loss %
Control Mix	2449	2436	0.53	2428	0.86	2409	1.63
SCC 2% NC	2452	2442	0.42	2433	0.76	2419	1.33
SCC 4% NC	2460	2451	0.38	2444	0.65	2431	1.21
SCC6% NC	2484	2476	0.32	2469	0.6	2457	1.15
SCC 50 QLP	2409	2395	0.58	2386	0.97	2362	1.95
SCC 75 QLP	2443	2430	0.55	2421	0.91	2401	1.7
SCC 100 QLP	2460	2448	0.48	2440	0.81	2424	1.48
SCC4%NC+50 QLP	2462	2451	0.45	2443	0.78	2426	1.45
SCC4%NC+75 QLP	2470	2460	0.42	2452	0.74	2438	1.3
SCC4%NC+100 QLP	2478	2469	0.38	2461	0.69	2447	1.25

Table (4-21): UPV results for the mixtures after immersion in cycles wet and dry magnesium sulfate for 30 days.

Mix ID	UPV(km/sec)						
	0% MgSO₄ at 56 days	5% MgSO₄	Loss %	10% MgSO₄	Loss %	20% MgSO₄	Loss %
Control Mix	4.58	4.557	0.5	4.552	0.62	4.547	0.71
SCC 2% NC	4.667	4.647	0.43	4.643	0.52	4.638	0.62
SCC 4% NC	4.709	4.693	0.35	4.691	0.39	4.686	0.48
SCC6% NC	4.89	4.875	0.3	4.873	0.34	4.869	0.43
SCC 50 QLP	4.512	4.476	0.8	4.473	0.87	4.468	0.98
SCC 75 QLP	4.525	4.496	0.65	4.492	0.74	4.487	0.84
SCC 100 QLP	4.595	4.573	0.48	4.568	0.59	4.562	0.71
SCC4%NC+50 QLP	4.618	4.597	0.46	4.593	0.55	4.588	0.64
SCC4%NC+75 QLP	4.622	4.604	0.4	4.6	0.47	4.595	0.59
SCC4%NC+100 QLP	4.659	4.642	0.37	4.639	0.43	4.635	0.51

Table (4-22): UPV results for the mixtures after immersion in cycles wet and dry magnesium sulfate for 60 days

Mix ID	UPV(km/sec)						
	0% MgSO₄ at 90 days	5% MgSO₄	Loss %	10% MgSO₄	Loss %	20% MgSO₄	Loss %
Control Mix	4.615	4.58	0.75	4.569	0.98	4.519	1.1
SCC 2% NC	4.709	4.68	0.62	4.671	0.8	4.627	0.95
SCC 4% NC	4.813	4.787	0.53	4.782	0.65	4.748	0.71
SCC6% NC	4.902	4.88	0.45	4.875	0.55	4.844	0.64
SCC 50 QLP	4.536	4.484	1.15	4.475	1.35	4.408	1.48
SCC 75 QLP	4.562	4.517	0.98	4.51	1.15	4.453	1.24
SCC 100 QLP	4.62	4.587	0.71	4.578	0.9	4.53	1.04
SCC4%NC+50 QLP	4.682	4.65	0.69	4.642	0.85	4.595	1.01
SCC4%NC+75 QLP	4.692	4.663	0.61	4.657	0.74	4.616	0.89
SCC4%NC+100 QLP	4.699	4.673	0.56	4.666	0.7	4.629	0.78

Table (4-23): UPV results for the mixtures after immersion in cycles wet and dry magnesium sulfate for 90 days

Mix ID	UPV(km/sec)						
	0% MgSO₄ at 120 days	5% MgSO₄	Loss %	10% MgSO₄	Loss %	20% MgSO₄	Loss %
Control Mix	4.639	4.592	1.02	4.569	1.5	4.548	1.95
SCC 2% NC	4.726	4.688	0.8	4.666	1.26	4.643	1.75
SCC 4% NC	4.845	4.81	0.72	4.796	1.01	4.78	1.35
SCC6% NC	4.925	4.896	0.58	4.883	0.85	4.869	1.14
SCC 50 QLP	4.553	4.492	1.35	4.471	1.8	4.456	2.13
SCC 75 QLP	4.593	4.543	1.08	4.517	1.66	4.497	2.08
SCC 100 QLP	4.68	4.643	0.78	4.625	1.18	4.6	1.71
SCC4%NC+50 QLP	4.728	4.686	0.89	4.662	1.4	4.638	1.9
SCC4%NC+75 QLP	4.733	4.697	0.76	4.68	1.11	4.66	1.55
SCC4%NC+100 QLP	4.74	4.708	0.67	4.695	0.94	4.682	1.22

Table (4-24): Compressive strength of mixtures after immersion in cycles wet and dry magnesium sulfate for 30 days.

Mix ID	Compressive Strength (MPa)						
	0% MgSO₄ at 60 days	5% MgSO₄	Loss %	10% MgSO₄	Loss %	20% MgSO₄	Loss %
Control Mix	74.1	72.8	1.75	71.51	3.5	70.54	4.8
SCC 2% NC	77.8	76.71	1.4	75.54	2.9	74.61	4.1
SCC 4% NC	80.52	79.55	1.2	78.43	2.6	77.54	3.7
SCC6% NC	88.16	87.23	1.06	86.04	2.4	85.07	3.5
SCC 50 QLP	67.68	66.16	2.25	64.91	4.1	63.96	5.5
SCC 75 QLP	70.24	68.84	2	67.57	3.8	66.52	5.3
SCC 100 QLP	77.13	76.13	1.3	74.82	3	73.81	4.3
SCC4%NC+50 QLP	75.17	73.97	1.6	72.61	3.4	71.61	4.73
SCC4%NC+75 QLP	76.91	75.79	1.45	74.36	3.32	73.4	4.56
SCC4%NC+100 QLP	78.1	77.1	1.28	75.91	2.8	74.9	4.1

Table (4-25): Compressive strength of mixtures after immersion in cycles wet and dry magnesium sulfate for 60 days.

Mix ID	Compressive Strength (MPa)						
	0% MgSO₄ at 90 days	5% MgSO₄	Loss %	10% MgSO₄	Loss %	20% MgSO₄	Loss %
Control Mix	76.44	75.03	1.85	73.15	4.3	71.78	6.1
SCC 2% NC	79.97	78.77	1.5	77.01	3.7	75.61	5.45
SCC 4% NC	82.69	81.57	1.35	80.0	3.25	78.72	4.8
SCC6% NC	90.9	89.8	1.21	88.17	3	86.9	4.3
SCC 50 QLP	69.26	67.53	2.5	65.45	5.5	64	7.6
SCC 75 QLP	73.51	71.84	2.27	69.76	5.1	68	7.5
SCC 100 QLP	79.7	78.47	1.54	76.83	3.6	75.46	5.32
SCC4%NC+50 QLP	77.88	76.56	1.7	74.77	4	73.36	5.72
SCC4%NC+75 QLP	79.13	77.85	1.62	76.08	3.8	74.66	5.65
SCC4%NC+100 QLP	80.2	79.08	1.4	77.4	3.49	76.07	5.15

Table (4-26): Compressive strength of mixtures after immersion in cycles wet and dry magnesium sulfate for 90 days.

Mix ID	Compressive Strength (MPa)						
	0% MgSO$_4$ at 120 days	5% MgSO$_4$	Loss %	10% MgSO$_4$	Loss %	20% MgSO$_4$	Loss %
Control Mix	77.1	74.8	3	72.24	6.3	70.7	8.3
SCC 2% NC	80.63	78.8	2.3	76.52	5.1	74.58	7.5
SCC 4% NC	83.25	81.9	1.6	79.84	4.1	77.92	6.4
SCC6% NC	91.31	90.1	1.3	88.11	3.5	86.79	4.95
SCC 50 QLP	70.79	67.9	4.1	65.69	7.2	63.99	9.6
SCC 75 QLP	74.94	72.3	3.5	69.84	6.8	67.97	9.3
SCC 100 QLP	80.83	78.7	2.65	76.14	5.8	74.28	8.1
SCC4%NC+50 QLP	78.8	76.7	2.7	74.47	5.5	72.73	7.7
SCC4%NC+75 QLP	80.9	79.4	1.9	77.02	4.8	74.99	7.3
SCC4%NC+100 QLP	81.97	80.5	1.8	78.28	4.5	76.4	6.8

الخلاصة

يهدف هذا البحث الى تحضير طين نانوي من طين الكاؤلين العراقي محليا من خلال حرقه بدرجة حرارة ٧٠٠ درجة مؤية لمدة ساعتين ثم طحنه لمدة ٤٠ ساعة باستخدام الطحن الدقيق المعروف بطحن الكرات (ball milling). تم استخدام العديد من التقنيات لتميز خواص الطين النانوي المحضر منها فحص الاشعة السينية المحايدة XRD وتحليل المساحة السطحية SSA وتوزيع حجم الحبيبات PSA والمسح المجهري الالكتروني SEM وفحص التحليل الكيميائي XRF و EDS.

اجريت هذه الدراسة باستخدام ثلاث نسب مختلفة من الطين النانوي المحضر (٢% و ٤% و ٦%) كبديل جزئي من وزن الاسمنت كذلك استخدام الجير الحي (QLP) Quicklime بوزن (٥٠و٧٥و١٠٠) كغم والذي تم تحضيره مختبريا من خلال حرق الحجر الجيري Limestone بدرجة حرارة ٧٠٠ لمدة ساعتين والجمع بين نسب الثلاث للجير الحي مع نسبة ٤% من الطين النانوي المختارة بالاعتماد على نتائج فحوصات قابلية التشغيل لخلطات الخرسانة المضغوطة ذاتيا SCC باستخدام الاسمنت المقاوم للاملاح.

تم إجراء دراسة تأثير الطين النانوي على خصائص الخرسانة ذاتية الرص SCC على أساس ثلاثة معايير. تضمن المعيار الاول خصائص التشغيل التي تتضمن (تدفق الركود ، وقت تدفق القمع V ، و L-box ، ومقاومة فصل الغربال والكثافة الطرية) . اما المعيار الثاني فقد تم فحص خصائص الصلبة للخرسانة ذاتية الانضغاط في عمر ٧ ، ٢٨ ، ٥٦ ، ٩٠ و ١٢٠ يومًا بما في ذلك الخواص الميكانيكية وتشمل (قوة الانضغاط ، قوة الشد ، قوة الانثناء ، معامل المرونة) ، والخصائص الفيزيائية التي تشمل (سرعة النبض الفائقة (UPV) ، الكثافة الصلبة ، حجم نفاذية المسام (الفراغات) و امتصاص الماء). اما المعيار الثالث فقد تم فحص خصائص المتانة من خلال اختبار تأثير الحرارة العالية بدرجات (٢٠٠ ، ٤٠٠، ٦٠٠ و٨٠٠) درجة مئوية على الخرسانة ذاتية الانضغاط عند عمر ٥٦ ، ٩٠ و ١٢٠ يوم ، وكذلك اختبار مقاومة هجوم الاملاح عن طريق الغمر في دورات متعاقبة من الترطيب والتجفيف لمحلول كبريتات المغنسيوم بتركيز ٥٪ و ١٠٪ و ٢٠٪ لمدة ٣٠ و ٦٠ و ٩٠ يوم ومقارنة النتائج مع العينات المخزونة في مياه المعالجة الاعتيادية للاعمار ٥٦ ، ٩٠ و ١٢٠ يوم .

أظهرت النتائج أن خصائص التشغيل تقل مع زيادة محتوى الطين النانوي .كما زادت خصائص الصلابة والمتانة تدريجياً مع زيادة محتوى الطين النانوي و الجير الحي في خلطات الخرسانة ذاتية الرص. علاوة على ذلك ، كان لإضافة الطين النانوي وحده تأثير أكثر أهمية على خصائص الصلابة والمتانة للعينات التي أنتجت قيمًا أعلى من الخرسانة المرجعية و عينات الجير الحي .

تم الحصول على افضل قيمة للطين النانوي وهي ٦ % . حيث اظهرت النتائج تحسنا ملحوظا للخصائص الصلبة حيث كانت الزيادة في نسب مقاومة الانضغاط عن مقاومة الانضغاط للخلطة المرجعية بحوالي ٢٨,٥%، ٢٣,٦%، ١٩,٥%، ١٩% و ١٨,٤% في الاعمار ٧، ٢٨، ٥٦، ٩٠و ١٢٠ يوم على التوالي. وكذلك زيادة في مقاومة الشد بنسب اعلى من الخلطة المرجعية بحوالي ١٦,٨%، ١٧,١%. ١٦% و ١٢,٤% في الاعمار ٢٨، ٥٦، ٩٠ و ١٢٠ يوم على التوالي .اما الزيادة في مقاومة الانثناء كانت اعلى ايضا من مقاومة الانثناء للخلطة المرجعية بنسب ٢٢,٦%، ٢٥,٤%، ٢٧,٤% و ٢٦,٥% للاعمار ٢٨، ٥٦، ٩٠ و ١٢٠ يوم .اما معامل المرونة فقد زاد بنسبة ٢٦,١% عن معامل المرونة للخلطة المرجعية في عمر ٩٠ يوم.

كذلك حققت الخلطة الحاوية على ٦% من الطين النانوي افضل الخصائص في مقاومة الحرارة العالية .حيث حققت اعلى قيمة في زيادة مقاومة الانضغاط بالنسبة للخلطة المرجعية تحت تاثير الحرق بدرجة حرارة ٢٠٠ درجة مؤية وكانت نسب الزيادة ٦,٢٣%، ٦,٤٩% و ٦,٣٤% بينما حققت اقل خسارة بمقاومة الانضغاط تحت تاثير اعلى درجة حرارة وهي ٨٠٠ درجة مؤية بنسب ٦٤,٣٩%، ٦١,٠٢% و ٥٥,٨% للاعمار ٥٦، ٩٠ و ١٢٠ يوم على التوالي .

ايضا اعطت نسبة ٦% من الطين النانوي المحضر افضل النتائج لمقاومة هجوم الاملاح الكبريتية حيث حققت اقل خسارة بمقاومة الانضغاط بالنسبة للخلطة المرجعية في فترات الغمر المتعاقبة . حيث كانت نسبة الخسارة بمقاومة الانضغاط عند فترة غمر ٣٠ يوم ٣٩,٤٣% ، ٣١,٤٣% و ٢٧,١% وعند فترة غمر ٦٠ يوم ٣٤,٦%، ٣٠%، و ٢٩,٥% وعند فترة غمر ٩٠ يوم ٥٦,٧% ، ٤٤,٥% و ٤٠,٤% عند التراكيز ٥% و ١٠% و ٢٠% من محلول كبريتات المغنيسيوم .

اضافة إلى ذلك ، فإن الجمع بين الطين النانوي والجير الحي له قيم ملحوظة لخصائص الصلابة والديمومة. حيث وجد أن استخدام ٤٪ من الطين النانوي مع ١٠٠ كغم من (QLP) الجير الحي يمكن أن يوفر تحسنًا مرضيًا في خصائص الصلابة والديمومة.

جمهورية العراق

وزارة التعليم العالي والبحث العلمي

جامعة الانبار

كلية الهندسة

قسم الهندسة المدنية

دراسة انتاج الطين النانوي وتاثيره على بعض خصائص الخرسانة ذاتية الرص

رسالة مقدمة إلى قسم الهندسة المدنية في كلية الهندسة بجامعة الانبار كجزء من

متطلبات نيل شهادة الماجستير في علوم الهندسة المدنية

من قبل :

نبراس يونس رشيد العاني

بكالوريوس هندسة مدنية ـ ٢٠٠١

بإشراف:

أ.د. ابراهيم احمد سرحان الجميلي   **أ.م.د. نهلة ناجي هلال**

نيسان   ٢٠٢١ م   شعبان ١٤٤٢ ه